

## **Distribution Agreement**

In presenting this thesis or dissertation as a partial fulfillment of the requirements for an advanced degree from Emory University, I hereby grant to Emory University and its agents the non-exclusive license to archive, make accessible, and display my thesis or dissertation in whole or in part in all forms of media, now or hereafter known, including display on the world wide web. I understand that I may select some access restrictions as part of the online submission of this thesis or dissertation. I retain all ownership rights to the copyright of the thesis or dissertation. I also retain the right to use in future works (such as articles or books) all or part of this thesis or dissertation.

Signature:

---

Brea Manuel

---

Date

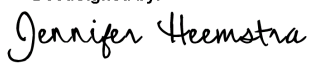
**Title** Building Nucleic Acid-Based Technologies for Biological Sensing and Modulation

**Author** Brea Manuel

**Degree** Doctor of Philosophy

**Program** Chemistry

**Approved by the Committee**

DocuSigned by:  
  
BF5C1F962DFC4A3...

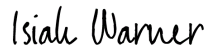
Jennifer Heemstra  
*Advisor*

DocuSigned by:  
  
8EA00928FE1F483...

William Wuest  
*Committee Member*

DocuSigned by:  
  
C5B292EAF764412...

Vincent Conticello  
*Committee Member*

DocuSigned by:  
  
6C492C31832D487...

Isiah Warner  
*Committee Member*

**Accepted by the Laney Graduate School**

Kimberly Jacob Arriola, PhD, MPH  
*Dean, James T. Laney School of Graduate Studies*

Building Nucleic Acid-Based Technologies for Biological Sensing and Modulation

By

Brea A. Manuel

B.S. Louisiana State University, 2018

Advisor: Jennifer M. Heemstra, PhD

An abstract of  
A dissertation submitted to the Faculty of the  
James T. Laney School of Graduate Studies of Emory University  
in partial fulfillment of the requirements for the degree of  
Doctor of Philosophy in Chemistry  
2022

## **Abstract**

Building Nucleic Acid-Based Technologies for Biological Sensing and Modulation

By Brea A. Manuel

Nucleic acids are historically known and studied for their natural functions of information storage. However, over the last few decades, functional nucleic acids have emerged in the fields of biotechnology, bioremediation, and biomedicine, as they possess the abilities to bind targets of interest and perform catalysis. Aptamers have been evolved to bind several targets, including proteins, heavy metals, and small molecules. As a result, many different aptamer-based applications have come to fruition. This dissertation aims to explore various applications of aptamers and develop different technologies for biological sensing and modulation, advancing the fields of biotechnology and biomedicine. Chapter 1 introduces the different functional nucleic acids, their uses, and the gaps in the field. In Chapter 2, we sought to address current challenges of modulating aptamers to produce stable nucleic acids that are capable of binding a range of targets with a range of affinities. We then use these aptamers in Chapter 3 in an attempt to study sequestration of small molecules, and the effects of this phenomenon on enzymes. Specifically, we use these aptamers to enhance enzyme activity with total control of the various kinetic parameters. In Chapter 4, we take an opposite turn and explore reversible control of enzymes and functional nucleic acids using a thermoreversible protecting/caging group. In Chapter 5, we then use the idea of aptamer evolution to explain the effects of the selection process on diversity, equity, and inclusion. Lastly, we summarize our findings and propose future explorations of aptamers and their applications in Chapter 6.



Building Nucleic Acid-Based Technologies for Biological Sensing and Modulation

By

Brea A. Manuel

B.S. Louisiana State University, 2018

Advisor: Jennifer M. Heemstra, PhD

A dissertation submitted to the Faculty of the  
James T. Laney School of Graduate Studies of Emory University  
in partial fulfillment of the requirements for the degree of  
Doctor of Philosophy in Chemistry  
2022

## Acknowledgments

Graduate school has been the hardest, most rewarding experience of my life thus far. From academic probation to a pandemic, to a leave of absence, to finishing my PhD with 5 papers in 4 years. It has been a journey for sure, and there's no way I could've done this without my amazing support system.

Firstly, I would like to thank my parents Sabrina Ratcliff-Lewis, Brian Lewis Sr., and Captain Tayhika Manuel, Sr. Momma, there were many times you were so hard on me, and I just couldn't understand why. The times as a kid that I got a B or C, I couldn't understand why it wasn't okay. You saw this potential in me that I clearly couldn't see. You knew that when I got those grades, I wasn't trying my hardest. As a Chemist, yourself, you knew what it took to be successful in the world, not only as a woman, but as a Black woman. You prepared me better than anyone else ever could. Thank you for your support, your encouragement, and for pushing me. Thank you for picking me up when I fell, for holding me when I wanted to quit, and for being my rock. I couldn't have done this without you. Daddy Brian, thank you for always putting a smile on my face. Thank you for always creating a safe space for me to be fully me. One of the hardest things about grad school as a POC is always having to codeswitch. Thank you for dancing to bounce music with me, licking your fingers with me when we enjoy that good ole BBQ you make, and for making our home such a fun environment to be in. Thank you so much for everything you've poured into me and J. Daddy, every time in grad school when I couldn't sleep at 2am, because I was stressed about an experiment, I'd text you and you'd call immediately. We would stay up for hours cracking jokes, gossiping, and telling old stories. Thank you for bringing so much laughter and joy in some of my toughest times in grad school. Thank you for also rubbing off on me, because I have a feeling that's why I make so many new friends. Your chill nature often reminds me that everything will be okay and "don't worry 'bout nothing."

Next, I'd like to thank my siblings, Brian Lewis, Jr. (aka BJ, aka J), A'Laysha Lewis, A'Rye Lewis, Ariane Bowie, Tayhika Manuel, Jr. (aka Scooty), and Tyra Manuel. J, you push me in ways you'll never begin to understand. When our mom told me I would be getting a new little brother, I was ecstatic, and I wanted to teach you literally everything. Maybe that's why you're such a genius now. Thank you for always encouraging me without being dismissive and invalidating when life and school got hard. While I know I could get a PhD without your support, you made this journey much, much, much easier. Thank you for always supporting me physically, mentally, and emotionally. I likely would've lost my sanity a long time ago had it not been for you. Laysh, thank you for being a big sister. Being the oldest sibling isn't always so fun, but you provided a space for me to actually be a younger sister. I appreciate all of your love and support over the years. Yannie, even though we are biologically cousins, it would be a great injustice to not add you to the sibling section of my dissertation. You, too, provided a space for me to be a little sister. Thank you so much for always accepting and loving me unconditionally. No matter what you have going on, you're always literally only a call away. You haven't missed a birthday, presentation, celebration, etc. Thank you for prioritizing me in some of your toughest, most hectic moments. Tyra, thank you for always bringing so much joy and your beautiful smile to our time spent together in person and on FaceTime. I honestly couldn't ask for a better sister. Thank you, also, for providing a space that I don't have to be perfect in. Scooty, you are literally one of my favorite little humans. Like our dad, you have such a laidback, carefree demeanor, and you'll never understand how much that has helped me. Like our sister, thank you also for providing a space that I could be wholeheartedly my childish self. Many times, I visited you I struggled with the mental aspects of grad school. You have no clue how many times playing Pokémon and VR with you helped me.

Next, I'd like to thank my grandparents Joyce Manuel-Williams, Mervin Williams, Nelson Manuel Sr., Adrian Ratcliff, Louis Revader Jr., and Betty Wilson. Nise, thank you for supporting

me all my life. When I look through all of my old pictures of old birthdays, grandparents' days, and big events, you've always been there. Thank you for your patience and understanding when I would miss events and phone calls. Thank you so much for your encouragement on some of my toughest days. I could never thank you enough for how much you've supported me my entire life. Paw Paw Merv, thank you for always making me laugh and encouraging me when I come to visit. Paw Paw Nel, I wish you could be here today to witness my being declared the first Dr. Manuel. Grandma Adrian, I don't even know where to begin with this. I think more than anything in the world, I wish you could be here to watch me become Dr. Brea Manuel. Thank you so much for being my first ever love and favorite person. I know my mom may be a little jealous reading that, but I'm sure she knows you were my favorite person in the entire universe. Grandma Adrian, thank you so much for raising my mom the way you did, because I don't know that I would be as successful had you not. Thank you so much for the values that you instilled in me so early in my life, because I still hold on to a lot of those. I know that you're looking down so proud. I promise to continue to make you proud. Paw Paw Pepa, I wish you could also be here to witness such a great accomplishment in my life and our family. Thank you for how much you encouraged me to be great. You always saw a superstar when you saw me, and you never ever, ever let me or anyone around me forget, and for that I will be forever grateful. Grandma Betty, wow, there's so much to say. Firstly, I am beyond appreciative that God has allowed you to be here to witness such an amazing accomplishment for me and our family. Grandma, you have been the glue that has held us all together. Thank you so much for your love, support, dedication, encouragement, and correcting for my last 26 years on this earth. We've had many deep and private talks during graduate school about my issues surrounding my race and gender in an environment that wasn't made for me. In those conversations you reminded me of my values and my reasoning for being in the position I was in. Grandma, thank you so much for always being so transparent about growing up in a time where even surviving as a Black woman was basically illegal, because it made me feel seen, heard, and understood. You reminded me and encouraged me that it would

all be okay. For that, I could never thank you enough. Talking to you always brought such a comforting feeling. I appreciate everything you've been to me.

Next, I'd also like to thank all my cousins, highlighting a few for sure. To all my cousins (Ariana Allen, Denzel Cameese, Nicholas Cameese, Niyanna Lopez, Daje Lopez, Evbu Obazuaye, Jasmine Wright, Sean Thompson Jr., Shamar Thompson, Aniyah Thompson, Aijah Thompson, Kendra Sumlin, Kendrick Sumlin Jr., Charmaine Stevenson, Jermesha Stevenson, Jasmine Sylvester, Jayshun Sylvester, Adrian Sumlin, and Johnny Sumlin, Donte Mitchell Jr., Madison Mitchell, Kadence Gallon) thank you for always loving and accepting me wholeheartedly. I'm a huge advocate for mental health and work/life balance. Man did y'all balance me out during grad school. Thank you all so much for being my safe space. I would like to extend my gratitude to my favorite cousin, Nelson Manuel III. Trae, you have seen and accepted me at my lowest. Thank you for always being a phone call away. Thank you for always being so understanding and validating. When you didn't understand the grad school struggles, you didn't just brush them off. You asked more questions to understand so that you could properly support me. Thank you so, so, so much for simply being you.

Next, I'd like to thank all my aunts and uncles, highlighting a few for sure. To all my aunts and uncles (Katama Manuel-Thompson, Natoya Manuel-Lopez, Tayanna Manuel-Mitchell, Nelson Manuel, Jr., Tramel Manuel, Varlencia Sumlin, Kendrick Sumlin, Sr., Willie Sumlin, Jessica Sumlin, Lisa Jackson, Lauren Jackson, Leanne Jackson, Kair Jackson, Zara Stipe, Tricia Gaudet, and Michelle Carter) thank you for your endless support throughout not only my graduate journey, but my entire academic journey. Thank you for showing genuine interest and trust in my work. I would like to extend my gratitude to my godmother, Michelle Carter. Nanny, thank you for always supporting me in life, and for always being so willing to look over all my statements for school.

I'd like to thank all my friends (Whitney Robertson, Dr. Sydney Mays, Sierra Sterling, Dr. Shakyra Richardson, Dr. Aimee Sanford, Kaelin Fort, Jaylyn Woods, Tamra Blue, Ayda Gonzales, Dr. Ordy Manuella, Kaitlyn Calais, Breanna Brown, Dr. Amber Scharnow, Diane Karloff, Timothy Holland, Natalie Khoury, Dante Jones, Tiffany Taylor, and Mrs. Charity Givens) for their endless support and encouragement.

I'd like to thank my partner, Dr. Devin Swiner for always supporting me and encouraging me to make the best decisions for me as it related to graduate school. Thank you for ensuring me that whatever I chose to do you'd support me. Thank you also for using your expertise in mass spectrometry to help me understand and interpret my data within my last year of graduate school.

Next, I'd like to thank my fur baby, Bruce, aka Bruce Wayne, aka Brucifer for all his emotional support in grad school. Even though he drove me insane at times, he made many bad days great by loving me unconditionally.

I'd also like to thank my mentors (Dr. Isiah Warner, Dr. Sandra Yancy-McGuire, Dr. Tyrslai Williams, Mrs. Melissa Crawford, Dr. Graca Vicente, Dr. Soumen Das, Dr. M.G. Finn, Ms. Annette Yancy, Dr. Gloria Thomas, Dr. Gretchen Schneider, Winter Foddrell, Clerissa Cooper, Dr. Mahalia Way, Dominique Harmon-Ware, Dr. Stephanie Vaughn, and Dr. Michael Summers) for all your mental, emotional, intellectual, and financial support. Specifically, to Dr. Warner, thank you for introducing me to research. I would not be getting a PhD in chemistry had I not met you. Thank you, also, for being the first person besides my mother to believe in.

I'd like to thank my committee members (Dr. Vince Conticello, Dr. Bill Wust, and Dr. Isiah Warner) for all of the feedback you all have provided throughout my PhD. The three of you have been an integral part of my growth as a scientist. Thank you for supporting me, writing recommendation letters, and most importantly, for advocating for me when I needed you most.

Next, I'd like to thank the Heemstra Lab both past and present for supporting me, providing feedback, and holding me accountable in our field. Thank you for the standard you held me to, because it really taught me to be a great scientist. Thank you, also for becoming my friends throughout this time. I'd like to specifically thank Shreyas Rajagopal, Kristen Patterson, and Alexandria Quillin for being fantastic mentees. I learned so much from the three of about leadership. Thank you for providing a space for me to fail, as well. I'd like to also thank my advisor Dr. Jennifer Heemstra. Thank you for introducing me to the world of chemical biology. Before joining the lab, I had no clue what chem bio was. Thank you for providing a space for me to grow as an independent scientist. I don't think I would've grown in this way had I joined another lab.

Next, I'd like to thank the most important being in my growth as a scientist and as an overall person, God. Lord, I would not have made it this far without you. Thank you for your unwavering and unconditional love and support as I've tackled tough journeys in and out of graduate school.

Lastly, I'd like to thank myself. I've become this successful with the support of everyone mentioned in this section of my dissertation. However, I chose to do the work. To myself, thank you for never giving up and for taking care of you. Thank you for reaching out for support when it was needed, and most importantly, thank you for sticking to all of your values and not losing yourself in these last four years.

## Table of Contents

<b>Chapter 1: Introduction</b> .....	<i>Error! Bookmark not defined.</i>
<b>1.1 Functional Nucleic Acids</b> .....	<i>Error! Bookmark not defined.</i>
<b>1.2 DNAzymes</b> .....	<i>Error! Bookmark not defined.</i>
<b>1.3 Aptamers</b> .....	<i>Error! Bookmark not defined.</i>
<b>1.4 Modulating Aptamer Recognition with Base Modifications</b> .....	<i>Error! Bookmark not defined.</i>
<b>1.6 Aptamer-Based Small Molecule Sequestration</b> .....	<i>Error! Bookmark not defined.</i>
<b>1.7 Summary and Conclusions of this Dissertation</b> .....	<i>Error! Bookmark not defined.</i>
<b>Chapter 2: Systematically Modulating Aptamer Affinity and Specificity by Guanosine-to-Inosine Substitution<sup>21</sup></b> .....	<i>Error! Bookmark not defined.</i>
<b>2.1 Abstract</b> .....	<i>Error! Bookmark not defined.</i>
<b>2.2 Introduction</b> .....	<i>Error! Bookmark not defined.</i>
<b>2.3 Results and Discussion</b> .....	<i>Error! Bookmark not defined.</i>
<b>2.4 Conclusion</b> .....	<i>Error! Bookmark not defined.</i>
<b>2.5 Materials and Methods</b> .....	<i>Error! Bookmark not defined.</i>
<b>Chapter 3: Modular Catalysis: Aptamer Enhancement of Enzyme Kinetics in a Nanoparticle Reactor</b> .....	<i>Error! Bookmark not defined.</i>
<b>3.1 Abstract</b> .....	<i>Error! Bookmark not defined.</i>
<b>3.2 Introduction</b> .....	<i>Error! Bookmark not defined.</i>



<b>3.3 Results and Discussion</b> .....	Error! Bookmark not defined.
<b>3.4 Conclusions</b> .....	Error! Bookmark not defined.
<b>3.5 Materials and Methods</b> .....	Error! Bookmark not defined.
<b>Chapter 4: Thermoreversible Control of Nucleic Acid Structure and Function with Glyoxal Caging</b> .....	Error! Bookmark not defined.
<b>4.1 Abstract</b> .....	Error! Bookmark not defined.
<b>4.2 Introduction</b> .....	Error! Bookmark not defined.
<b>4.3 Results and Discussion</b> .....	Error! Bookmark not defined.
<b>4.4 Conclusions</b> .....	Error! Bookmark not defined.
<b>4.5 Materials and Methods</b> .....	Error! Bookmark not defined.
<b><i>Chapter 5: Recruit and Retain a Diverse Workforce<sup>159</sup></i></b> .....	<i>Error! Bookmark not defined.</i>
<b>5.1 Abstract</b> .....	Error! Bookmark not defined.
<b>5.2 Introduction</b> .....	Error! Bookmark not defined.
<b>5.3 Assessing Candidates</b> .....	Error! Bookmark not defined.
<b>5.4 Origins of Exclusivity</b> .....	Error! Bookmark not defined.
<b>5.5 Cultivating Inclusion</b> .....	Error! Bookmark not defined.
<b>5.6 Outlook</b> .....	Error! Bookmark not defined.
<b>Chapter 6: Conclusions and Future Perspectives</b> .....	Error! Bookmark not defined.
<b><i>Appendix A: Omitted Data from Chapter 2<sup>21</sup></i></b> .....	<i>Error! Bookmark not defined.</i>
<b><i>Appendix B: Omitted Data from Chapter 3</i></b> .....	<i>Error! Bookmark not defined.</i>

**Appendix C: Omitted Data from Chapter 4** ..... *Error! Bookmark not defined.*

**References** ..... *Error! Bookmark not defined.*

## List of Tables and Figures

**Figure 1.1: Types of functional nucleic acids.....** Error! Bookmark not defined.

**Figure 1.2: Aptamer-based methods for sequestration of environmental contaminants... Error!**  
Bookmark not defined.

**Figure 1.3: Nucleic Acid-based Technologies. ....** Error! Bookmark not defined.

**Figure 2.1: Structures of parent aptamers MNS-4.1, 38-GC, and 38-GT with stems 1-3 labeled  
for MNS-4.1. ....** Error! Bookmark not defined.

**Table 2.1: Binding affinity for cocaine and analogues and melting temperature of parent  
aptamers and inosine-substituted variants. ....** Error! Bookmark not defined.

**Figure 2.2: (a) Cocaine (b) norcocaine and (e) cocaethylene binding of parent MNS-4.1  
aptamer in comparison to MNS-4.1 Inosine measured using MST. All MST experiments were  
performed in triplicate.....** Error! Bookmark not defined.

**Figure 2.3: Biosensor characterization for MNS-4.1 and MNS-4.1 Inosine... Error! Bookmark not  
defined.**

**Figure 3.1. ....** Error! Bookmark not defined.

**Figure 3.2. Characterization data for MS2@CocE-4.121 particles as a representative example  
.....** Error! Bookmark not defined.

**Table 3.1. Initial ratios and resulting average numbers of packaged enzymes and cocaine-  
binding aptamers. ....** Error! Bookmark not defined.

**Table 3.2. Kinetic Parameters of Free, Packaged, and Aptamer Co-packaged Enzymes. ... Error!**  
Bookmark not defined.

**Figure 3.3. Effect of co-encapsulation of aptamers and enzymes on enzyme kinetics. .... Error!**  
Bookmark not defined.

**Figure 3.4. Model of aptamer-assisted catalysis by packaged enzymes..... Error! Bookmark not defined.**

**Table 4.1: Temperature and pH dependent half-lives for glyoxal decaging. Error! Bookmark not defined.**

**Figure 4.1: Glyoxal caging imparts thermoresponsive fluorogenic activity in the broccoli RNA aptamer. .... Error! Bookmark not defined.**

**Figure 4.2: Reversible control of the RNA-cleaving 10-23 DNAzyme. .... Error! Bookmark not defined.**

**Figure 4.3: Glyoxal caging of a fully 2'-O-methylated RNA aptamer. .... Error! Bookmark not defined.**

**Figure 4.4: Glyoxal caging reversibly inactivates xenonucleic acid hybridization. .... Error! Bookmark not defined.**

**Figure 4.5: Reversible control of EcoRI. .... Error! Bookmark not defined.**

**Table 4.2: Glyoxalation reversibly modulates activity in several enzymes.. Error! Bookmark not defined.**

**Figure 4.6: Thermal reactivation of CRISPR-Cas9 function. .... Error! Bookmark not defined.**

**Figure 4.7: Thermal reactivation of antisense oligonucleotide (ASO) function in cellulose. .. Error!**  
*Bookmark not defined.*

**Figure A1: DNA sequences used in MST and biosensor experiments. .... Error! Bookmark not defined.**

**Figure A2: DNA sequences used in melting temperature experiments. .... Error! Bookmark not defined.**

**Figure A3: MST traces of all aptamers with cocaine. .... Error! Bookmark not defined.**

**Figure A4: MST traces of all aptamers with EME. .... Error! Bookmark not defined.**

**Figure A5: MST traces of all aptamers with BE. .... Error! Bookmark not defined.**

**Figure A6: MST traces of all aptamers with norcocaine. .... Error! Bookmark not defined.**

**Figure A7. MST traces of all aptamers with cocaethylene. .... Error! Bookmark not defined.**

**Figure A8. MST traces for MNS-4.1 and MNS-4.1 Inosine in saliva. Error! Bookmark not defined.**

**Figure A9: Melting temperature curves of all aptamers. .... Error! Bookmark not defined.**

**Figure A10. Biosensor characterizations..... Error! Bookmark not defined.**

**Figure B1. DNA sequences used in MST and kinetic. .... Error! Bookmark not defined.**

**Figure B2. Incubation concentrations and average numbers of packaged cocaine aptamers per VLP. .... Error! Bookmark not defined.**

**Figure B3. Kinetic parameters of packaged enzyme with free aptamer and co-packaged enzyme with scrambled DNA. .... Error! Bookmark not defined.**

**Figure B4. Characterization of MS2@CocE-4.122 particles ..... Error! Bookmark not defined.**

**Figure B5. Packaging of cocaine-binding aptamers in MS2 VLP confirmed by treatment with DNase-I..... Error! Bookmark not defined.**

**Figure B6. Determination of cocaine binding by aptamers by MST Error! Bookmark not defined.**

**Figure B7. Michaelis-Menten plots for (a) CocE-wt (b) MS2@CocE (c) MS2@CocE-4.13 (d) MS2@CocE-4.19 and (e) MS2@CocE-4.122. .... Error! Bookmark not defined.**

**Figure B8. Michaelis-Menten traces for (a) MS2@CocE-GC5 (b) MS2@CocE-GC11 (c) MS2@CocE-GC21..... Error! Bookmark not defined.**

**Figure B9. Michaelis-Menten traces for (a) MS2@CocE-IC4 (b) MS2@CocE-IC10 (c) MS2@CocE-IC20..... Error! Bookmark not defined.**

**Figure B10. .... Error! Bookmark not defined.**

**Figure C1: Decaging kinetics of a fully glyoxalated DNA strand at 95 °C with increasing pH. .... Error! Bookmark not defined.**

**Figure C2: Decaging kinetics of a fully glyoxalated DNA strand at 70 °C with increasing pH. .... Error! Bookmark not defined.**

**Figure C3: Decaging kinetics of a fully glyoxalated DNA strand at 50 °C with increasing pH. .... Error! Bookmark not defined.**

**Figure C4: Decaging kinetics of a fully glyoxalated DNA strand at 37 °C with increasing pH. .... Error! Bookmark not defined.**

**Figure C5: Room temperature stability of a glyoxalated DNA strand with increasing pH.** Error!  
Bookmark not defined.

**Figure C6: Fluorogenic performance of the broccoli RNA aptamer with increasing caging times.** ..... Error! Bookmark not defined.

**Figure C7: Restoration of fluorogenic activity in a caged broccoli RNA aptamer as a function of increasing decaging times.** ..... Error! Bookmark not defined.

**Figure C8: Glyoxalation disrupts 10-23 DNAzyme structure and target cleavage.** ..... Error!  
Bookmark not defined.

**Figure C9: DNAzyme decaging kinetics.**..... Error! Bookmark not defined.

**Figure C10. Glyoxal caging and decaging of a fully 2'-O-methylated RNA aptamer.** ..... Error!  
Bookmark not defined.

**Figure C11: Functional binding activity of increasingly caged ARC259.**..... Error! Bookmark not defined.

**Figure C12: Glyoxal caging of a TNA oligonucleotide.**..... Error! Bookmark not defined.

**Figure C13: Glyoxal caging of TNA disrupts hybridization to DNA.**.. Error! Bookmark not defined.

**Figure C14: Analytical characterization of synthesized model PNA strand.**.. Error! Bookmark not defined.

**Figure C15: Analytical characterization of glyoxal-treated PNA.** ... Error! Bookmark not defined.

**Figure C16: PAGE analysis of PNA caging and decaging.** ..... Error! Bookmark not defined.

**Figure C17: Proposed molecular mechanism of PNA mobility shifts..... Error! Bookmark not defined.**

**Figure C18: Glyoxal caging of PNA caging inhibits hybridization to DNA. ... Error! Bookmark not defined.**

**Figure C19: Reversible control of RNase H with glyoxal caging..... Error! Bookmark not defined.**

**Figure C20: One-pot activation of thermostable RNase H..... Error! Bookmark not defined.**

**Figure C21: Glyoxal does not inhibit RNase A. .... Error! Bookmark not defined.**

**Figure C22: Glyoxal does not inhibit Nuclease P1. .... Error! Bookmark not defined.**

**Figure C23: Reversible control of DNase I recognition and cleavage. .... Error! Bookmark not defined.**

**Figure C24: Reversible control of EcoRI..... Error! Bookmark not defined.**

**Figure C25: Glyoxal does not inhibit RNase T. .... Error! Bookmark not defined.**

**Figure C26: Glyoxal does not inhibit snake venom phosphodiesterase I..... Error! Bookmark not defined.**

**Figure C27: Glyoxalation disrupts sgRNA and Cas9 mediated target cleavage.. Error! Bookmark not defined.**

**Figure C28: Glyoxalation of sgRNA is reversible with rapid decaging. .... Error! Bookmark not defined.**

**Figure C29: Glyoxalation of sgRNA is reversible with slow decaging. .... Error! Bookmark not defined.**



**Figure C30: Amplification of  $\beta$ -actin from human genomic DNA using Taq and Hot Start Taq polymerases. .... Error! Bookmark not defined.**

**Figure C31: Forward primer glyoxal treatment and PCR specificity..... Error! Bookmark not defined.**

**Figure C32: Reverse primer glyoxal treatment and PCR specificity. Error! Bookmark not defined.**

**Figure C33: Primer decaging during PCR. .... Error! Bookmark not defined.**

**Figure C34: Confirming transfection efficiency and specificity. .... Error! Bookmark not defined.**

**Figure C35: Optimizing ASO concentration and confirming sequence specificity..... Error! Bookmark not defined.**

**Figure C36: Caging kinetics of an eGFP-targeting ASO as monitored by 20% PAGE gel illustrating an increase in apparent molecular weight. .... Error! Bookmark not defined.**

**Figure C37: Optimizing ASO glyoxal treatment time for inhibiting gene silencing..... Error! Bookmark not defined.**

**Figure C38: Untreated and glyoxal caged ASOs are cell permeable. .... Error! Bookmark not defined.**

**Figure C39: ASO glyoxalation is reversible with slow decaging..... Error! Bookmark not defined.**

**Figure C40: Increasingly caged ASO proportionally tunes the amount of GFP positive cells. .... Error! Bookmark not defined.**

**Figure C41: Representative live-cell fluorescence microscopy images during in cellulo ASO decaging..... Error! Bookmark not defined.**

**Figure C42: Caged ASOs do not affect cell viability. ....Error! Bookmark not defined.**



## Chapter 1: Introduction<sup>2†</sup>

### 1.1 Functional Nucleic Acids

Nucleic acids are historically known for their control of all cellular activity such as gene expression, recognition, and protein binding. However, nucleic acid function expands far beyond what nature intended. Functional nucleic acids are single-stranded nucleic acids capable of binding a specific target and capable of enzymatic activity (Figure 1.1). In 1990 Ellington et al. developed aptamers, single-stranded DNA or RNA capable of binding a target molecule, via Systemic Evolution of Ligands by Exponential Enrichment (SELEX).<sup>3</sup> Aptamers have been evolved over the last three decades to bind a variety of targets such as metals and proteins. There's been a shift in biotechnology with the emergence of small-molecule binding aptamers. Adjacent to aptamers, nucleic acid enzymes are DNA (DNAzymes) or RNA (ribozymes) that can perform catalysis.

### 1.2 DNAzymes

DNA enzymes, or DNAzymes, are a subset of functional DNAs that act as biocatalysts.<sup>4-6</sup> These catalytic DNAs offer similar advantages over protein-based enzymes as described for aptamers relative to protein-based affinity reagents. Through SELEX, DNAzymes have been generated for a variety of reactions, including RNA cleavage,<sup>7, 8</sup> RNA ligation,<sup>9, 10</sup> and even carbon-carbon bond forming reactions.<sup>11, 12</sup> DNAzyme SELEX is particularly challenging because the functional output is unique to every selection. Furthermore, the substrate molecule generally must be immobilized to the DNA library to maintain the genotype-phenotype link during isolation and

---

<sup>†</sup> Reproduced in part from ref. 2, <https://doi.org/10.1039/D2SC00117A>, under the terms of CC BY 3.0 license <https://creativecommons.org/licenses/by/3.0/>.

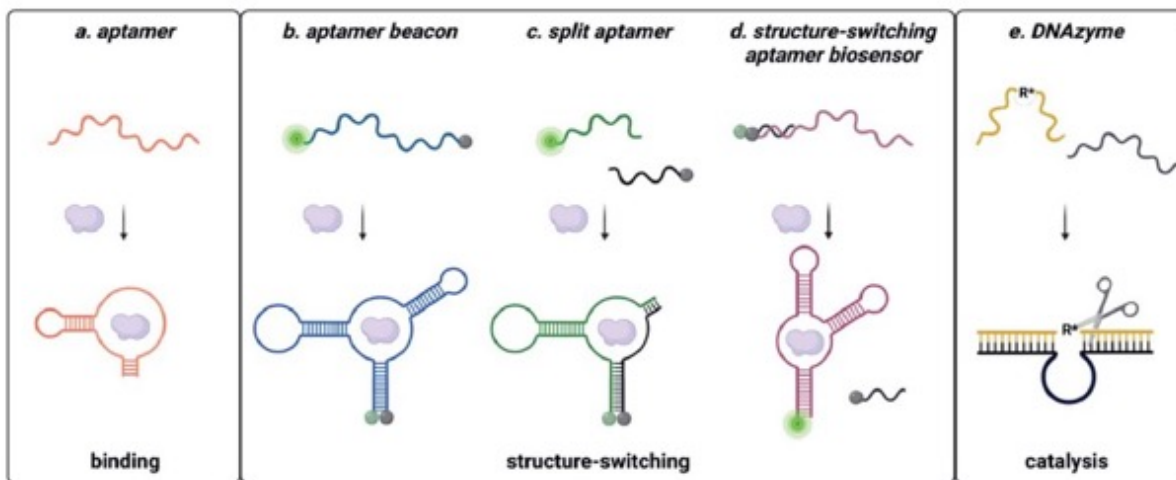


**Figure 1.1: Types of functional nucleic acids.** (a) Aptamers bind the small molecule. (b) Molecular beacon structure-switching biosensor. (c) Split aptamer structure-switching biosensor. (d) Structure-switching biosensor. Reprinted (adapted) with permission from B. A. Manuel, S. A. Sterling, A. A. Sanford and J. M. Heemstra, *Anal. Chem.*, 2022, 94(17) 6436–6440, <https://doi.org/10.1021/acs.analchem.2c00422>. Copyright 2022 American Chemical Society. (e) DNA catalysed reaction.

washing steps.<sup>12</sup> However, this can also offer an advantage as target specific affinity handles can then be used to isolate active sequences. For example, a zinc dependent DNAzyme capable of RNA cleavage activity was isolated by appending the target RNA strand with a biotin handle, which allowed for easy isolation using streptavidin-coated magnetic beads.<sup>13</sup>

While DNAzymes have found use in small molecule environmental contaminant detection, it is very rare that they are acting strictly as the biorecognition element. DNAzyme based biosensors instead are selected to rely on a specific heavy metal for an activity such as nucleic acid cleavage, and this metal-dependent activity is then coupled to a fluorescence readout or other amplification and sensing motif.<sup>14-17</sup> This format can make DNAzyme biosensors field deployable and cost effective, and in the next section we describe the use of reporter enzymes such as horseradish peroxidase (HRP) to amplify signal. A major limitation, however, is that the catalytic efficiency of DNAzymes remains poor compared to native enzymes. We suggest that this can be addressed by developing homogenous selection methods for DNAzymes, in which the substrate does not need to be tethered to the DNA library during the selection process. This would provide greater control over the stringency of the selection process and enable the direct selection of DNAzymes that function in trans with free substrate molecules. Selection in trans could also lead to improvements in selectivity, as sequences would be sorted based on their ability to produce a

specific reaction product rather than a general DNA cleavage or ligation event. A key hurdle to such selection methods is the ability to detect the desired products of the DNAzyme reaction, but we propose that other forms of DNA sensors such as those described below could be leveraged for such applications.

### **1.3 Aptamers**

Unlike DNAzymes, aptamers do not possess catalytic capabilities. However, over the years they have been evolved to bind small molecules, showing great promise in the fields of medicine, biosensing, and environmental remediation. Specifically, aptamers have been shown to be reusable, making them very affordable and environmental friendly as it relates to remediation.<sup>2, 18, 19</sup> In addition they have many advantages over chemical techniques, such as safety, and over other biological techniques such as antibodies due to their cost and easier generation.<sup>2, 20</sup> In addition, aptamers are far more tunable by simply modifying bases via error prone PCR, stem truncations, and changing the environment of the aptamer.<sup>21-23</sup> On the other hand, other affinity reagents such as peptides, proteins, and antibodies are tuned via longer and less cost effective methods. In addition, These biomolecules are much larger, resulting in limitations when using them in biological settings. While aptamers tend to be less stable than their amino acid-based counterparts, they are able to be tuned to be nuclease-resistant, and more recently, it has been shown that encapsulation allows for nuclease-resistance without a perturbation of function.<sup>24-29</sup>

### **1.4 Modulating Aptamer Recognition with Nucleotide Modifications**

Modifying nucleic acid bases and nucleotides have many benefits including nuclease resistance, catalytic ability (nucleic acid enzymes), and recognition tunability.<sup>2, 21</sup> Specifically, unnatural nucleotides are incorporated, yielding xenonucleic acids (XNAs), and we specifically

explore natural bases that are not typically found in DNA.<sup>30-32</sup> There are many different forms of modified nucleotides, such as peptide nucleic acids (PNA), threose nucleic acids (TNA), and 2'OMe RNA to name a few. PNA replaces the phosphate backbone with a peptide moiety.<sup>30-32</sup> These biomolecules have shown great stability and nuclease resistance. TNA replaces the ribose sugar backbone of RNA with a threose sugar backbone, making them also resistant to nuclease digestion. A huge limitation of using these unnatural bases, however, is that for further generation and certain applications, polymerases are not promiscuous enough for efficient replication of these molecules. Therefore, generating aptamers from them is rather challenging. Therefore, we focus on using natural bases, not found in DNA, to tune recognition, and in chapter 4, we explore glyoxal-based modifications to control nucleic acid function altogether.

As an initial model system for aptamer recognition tuning, we chose a well-studied and well-characterized anti-cocaine aptamer reported by Stojanovic et al.<sup>33</sup> Stojanovic and others have explored multiple modifications to this sequence, most of which result in decreased binding affinity.<sup>33-35</sup> Due to this perturbation, others explored other methods to more efficiently tune binding. Because improving the binding affinity improves the LOD of aptasensors, various base mutations were explored, leading to both slight increases and decreases in cocaine binding affinity.<sup>35</sup> Truncations were also explored, and it was shown that not only did this decrease the binding affinity for cocaine but it also increased the affinity to off-target analytes.<sup>34</sup> From these studies, they concluded that cocaine binding relies on structure as opposed to specific sequence, further leading us to explore more natural base modifications and in chapter 4, reversible base modification.

## 1.5 Aptamer-Based Small Molecule Detection

Aptamers form secondary structures upon binding of their targets. Therefore, over time, their 5' and/or 3' termini have been functionalized to produce a readout upon binding of targets. Aptamer-based sensors, or aptasensors, have been developed for a number of targets and applications, and there are three different types: molecular beacons, split aptamers, and structure-switching. Molecular beacons consist of one end being functionalized with a fluorophore and the other with a quencher. Upon binding, the two ends come together, and there is a quenching of fluorescence. Split aptamer-based sensors consists of a parent aptamer that is strategically cut at a specific site to create two separate strands. One strand is functionalized with a fluorophore and the other, with a quencher. In the presence of the target, the strands hybridize to bind the target, resulting in FRET between the fluorophore and quencher. Lastly, structure-switching aptasensors consist of an aptamer functionalized with a fluorophore prehybridized to a quencher-functionalized partial complement, also called a capture strand. Upon hybridization, the signal is quenched. In the presence of the target, the capture strand is displaced, resulting in a restoration in fluorescence. Aptasensors show great promise, as they are safe to use in a variety of different settings. For example, aptasensors have been used to detect BPA in water<sup>18</sup> and on the other hand have been used in living systems for metal detection.<sup>36</sup>

In this dissertation, we specifically explore work with DNA aptamers that bind cocaine. The anti-cocaine aptamer has been extensively utilized in biosensor development for drug monitoring and remediation. In addition, much effort has been taken to modulate this aptamer in an attempt to tune target recognition, and thus improve aptasensor LOD.<sup>37</sup> These efforts include truncations and crucial base modifications near binding sites. However, both of these methods lead to diminished binding, and thus poorer biosensing activity.<sup>23, 38, 39</sup> In addition to improving affinity, generating aptamers having a range of binding affinities is a crucial component of the work presented.



Altering aptamer structure can also lead to a change in selectivity,<sup>40</sup> and thus, modulating aptamer affinities to generate a range can enable full control over detection and sequestration of analyte mixtures containing structurally similar molecules, which we explore in chapters 2 and 3.

## 1.6 Aptamer-Based Small Molecule Sequestration

While functional nucleic acids have mainly been developed for detection of small molecules, the new emerging field of small molecule sequestration has found great promise. Because aptamers are easily tunable and functionalizable, there are many methods that have been explored for aptamers to be used as sequestering agents, such as scaffolds, solid supports, and membranes for a variety of applications, including removal from soil, water, and food (Figure 1.2).<sup>18-20, 41</sup> Specifically, many of these methods sequester via dispersion in the sample, and they typically work to sequester and remove. For example, Huang, et al. explore sequestration of *E. coli* using TiO<sub>2</sub> particles, coupled to DNA aptamers. Upon UV irradiation, TiO<sub>2</sub> produces reactive oxygen species, killing the *E. Coli*.<sup>42</sup> Another example is the use of these biomolecules in hydrogels and liposomes. Specifically, BPA has been sequestered and removed from water using both methods, and oxytetracycline has been removed using liposomes.<sup>43, 44</sup> Lastly, our group has shown the beneficial effects of functionalizing membranes with BPA aptamers in order to purify water.<sup>18</sup>

While sequestration has been scarcely studied, and specifically for removal of toxins, in this dissertation, we specifically explore the effects of co-encapsulating aptamers with enzymes. Encapsulation of nucleic acids in a wide variety of nanocompartments, including lipid vesicles, liposomes, and virus-like particles (VLPs) has been explored.<sup>25-29, 45, 46</sup> Specifically, encapsulation of nucleic acids, including aptamers, have been explored greatly in therapeutics as liposomes,

lipid vesicles, and VLPs have all been shown to protect their cargo for nucleases.<sup>25-29, 45, 46</sup> While nucleic acid encapsulation has been utilized widely for protection, we take a more unorthodox approach in Chapter 3 and explore sequestration to improve enzyme enhancement, specifically

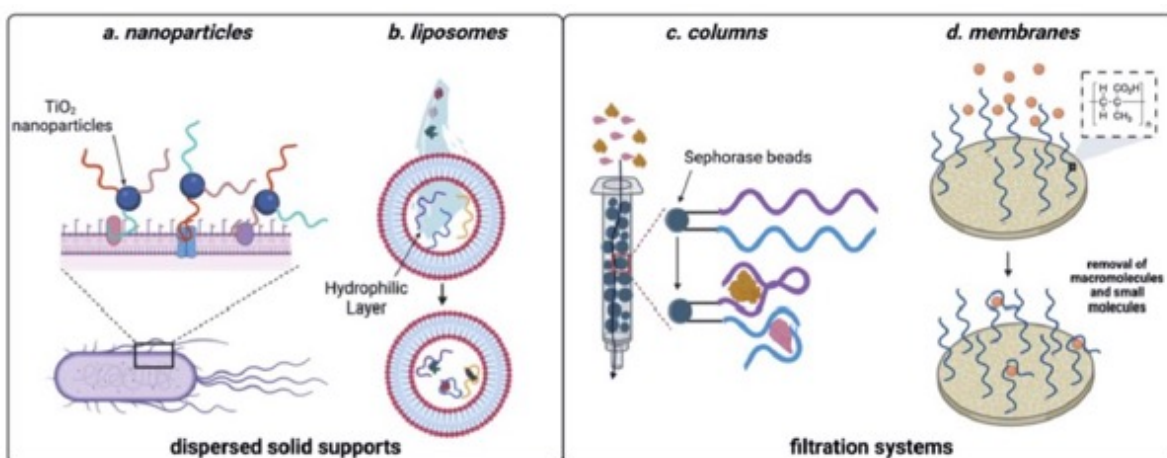


**Figure 1.2: Aptamer-based methods for sequestration of environmental contaminants.** (a) Nanoparticle-based aptamer support. (b) Liposome-based aptamer support. (c) Aptamer column filtration. Reproduced from ref. 147, <https://doi.org/10.1155/2017/3712070>, under the terms of CC BY 4.0 license. (d) Aptamer membrane filtration.

by controlling the degree of saturation, in turn, controlling  $K_M$ .

## 1.7 Summary and Conclusions of this Dissertation

Because aptamers are small, easily tunable, and cost effective, they show great promise in bioremediation, therapeutics, and biotechnology. As a result, modulating them allows for great control of their function, and further, great control over biological systems overall. The primary research goal of this dissertation was to develop and modulate aptamers for control in biological systems. Here, we describe four major applications involving aptamer and nucleic acid modulation: recognition tuning, biosensing, enzyme enhancement, and enzyme inhibition (Figure 1.3).

In the areas of recognition tuning and biosensing, we first sought to modulate aptamer affinity and specificity to generate aptamers with ranges of binding affinities for both their intended target and their off targets using guanosine-to-inosine substitutions (Chapter 2). This was the first demonstration of an inosine-driven range of affinities. We then sought to generate structure-switching biosensors from these new aptamers. Excited with this newfound control over recognition, we then sought to study the effects of these affinity reagents and their affinities on enzyme enhancement driven by sequestration (Chapter 3). This was accomplished by co-encapsulating anti-cocaine aptamers of varying affinities with the cocaine-hydrolyzing enzyme cocaine esterase. After successfully controlling aptamer  $K_D$ , we aimed to control enzyme  $K_M$  separate from enzyme  $k_{cat}$  by controlling the degree of sequestration using the aptamers of ranging affinities. In Chapter 4, we investigate the effects of nucleic acid modulation on enzyme, aptamer, and nucleic acid enzyme inhibition. Specifically, we are the first to demonstrate thermoreversible control of nucleic acids and its role in reversible enzyme inhibition. In Chapter 5, we discuss the analogy between aptamer selection and the selection process of graduate school as underrepresented students are often weeded out during every round of selection, along with ways that diversity, equity, and

inclusion can be improved in graduate school. Finally, I summarize these works and their contribution to the field, and I propose future directions (Chapter 6).

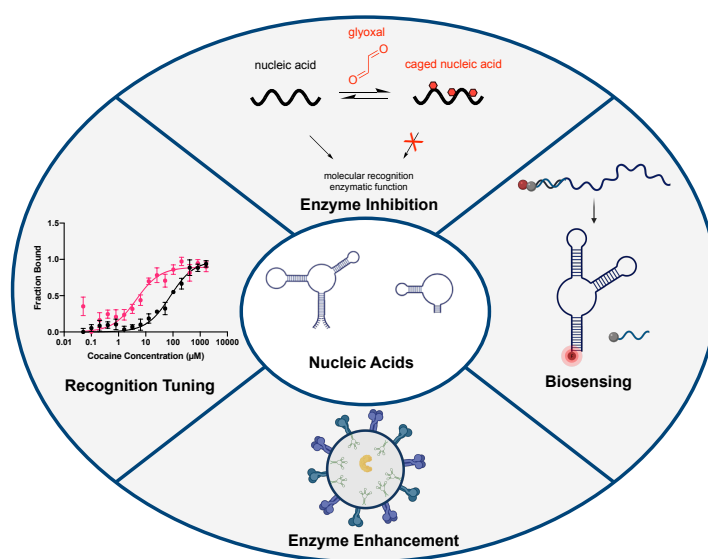


**Figure 1.3: Nucleic Acid-based Technologies.** Nucleic acid-mediated biosensing, enzyme enhancement, and enzyme inhibition. Figure made with Biorender.

## Chapter 2: Systematically Modulating Aptamer Affinity and Specificity by Guanosine-to-Inosine Substitution<sup>21‡</sup>

<sup>‡</sup> Reproduced from Ref. 21 with permission from Manuel, B. A.; Sterling, S. A.; Sanford, A. A.; Heemstra, J. M., Systematically Modulating Aptamer Affinity and Specificity by Guanosine-to-Inosine Substitution. *Analytical Chemistry* **2022**, 94 (17), 6436-6440. Copyright 2022 American Chemical Society.

## 2.1 Abstract

Aptamers are widely used in small molecule detection applications due to their specificity, stability, and cost effectiveness. One key challenge in utilizing aptamers in sensors is matching the binding affinity of the aptamer to the desired concentration range for analyte detection. The most common methods for modulating affinity have inherent limitations, such as the likelihood of drastic changes in aptamer folding. Here, we propose that substituting guanine for inosine at specific locations in the aptamer sequence provides a less perturbative approach to modulating affinity. Inosine is a naturally occurring nucleotide that results from hydrolytic deamination of adenosine, and like guanine, it base pairs with cytosine. Using the well-studied cocaine binding aptamer, we systematically replaced guanosine with inosine and were able to generate sequences having a range of binding affinities from 230 nM to 80  $\mu$ M. Interestingly, we found that these substitutions could also modulate the specificity of the aptamers, leading to a range of binding affinities for structurally-related analytes. Analysis of folding stability via melting temperature shows that, as expected, aptamer structure is impacted by guanosine-to-inosine substitutions. The ability to tune binding affinity and specificity through guanosine-to-inosine substitution provides a convenient and reliable approach for rapidly generating aptamers for diverse biosensing applications.

## 2.2 Introduction

Aptamers are single-stranded oligonucleotides that selectively recognize and bind to a target analyte through non-covalent interactions. Their specificity, stability, and cost-effectiveness have made them attractive for use as affinity reagents in small-molecule detection applications, and a large number of DNA aptamer-based sensor designs have been described.<sup>47-52</sup> In particular,

the cocaine aptamer has been extensively utilized in biosensor development for drug monitoring,<sup>53</sup> and significant effort has been directed toward improving aptamer affinity through truncations and base modifications. However, aptamer truncations and drastic base modifications often compromise stability, leading to diminished selectivity and binding affinity.<sup>37-39</sup> In addition to improving affinity, generating aptamers having a range of binding affinities can yield biosensors having a wide dynamic range. Altering aptamer structure can also lead to a change in selectivity,<sup>22</sup> and thus using combinations of aptamer analogues can enable more efficient detection or sequestration of analyte mixtures containing structurally related molecules.

We recognized that guanosine-to-inosine substitution could provide a convenient approach to modulating aptamer affinity and selectivity, as this substitution changes the number of hydrogen bonds involved in base pairing, but should not affect folding to the same extent as other non-synonymous mutations.<sup>40, 54</sup> While guanosine-to-inosine substitution has been explored in aptamers, these studies have focused on single mutations of key binding residues in order to study aptamer folding and binding as opposed to modulating affinity.<sup>55</sup> Additionally, these substitutions are predominantly studied in G-quadruplex aptamer sequences.<sup>56-58</sup>

As an initial model system, we chose the MNS-4.1 anti-cocaine aptamer reported by Stojanovic and coworkers.<sup>59</sup> Stojanovic and others have explored multiple modifications to this sequence, most of which result in decreased binding affinity.<sup>1, 34, 59</sup> Due to this perturbed binding, other efforts were sought after to improve binding by modifying the MNS-4.1 aptamer. Roncancio et al. tested the parent MNS-4.1 aptamer in their dye displacement cocaine biosensor.<sup>1</sup> Because improving the binding affinity improves the LOD of aptamer-based biosensors, they performed various base mutations, leading to both slight increases and decreases in cocaine binding affinity.<sup>1</sup> Like Stojanovic and coworkers, Sachan et al. reported that truncations of their modified MNS-

4.1 sequence or substituting key adenosines in stems 1 and 2 with 2-aminopurine not only decreased the binding affinity for cocaine, but also increased the affinity to off-target analytes.<sup>34</sup> From these studies, they concluded that cocaine binding relies on structure as opposed to specific sequence.

Starting from the MNS-4.1 and related 38-GC and 38-GT parent aptamer sequences; we explore systematic replacement of guanine with inosine in strategic locations known to impact structure or target binding. Using microscale thermophoresis (MST) to quantify the binding affinity of these aptamers to cocaine and structurally similar analytes, we find that guanosine-to-inosine substitution can be used to dramatically alter both binding affinity and specificity. Whereas the parent aptamer has a  $K_d$  value of  $\sim 80 \mu\text{M}$ , we are able to generate aptamers having a range of  $K_d$  values of 230 nM– $80 \mu\text{M}$ . Additionally, we found that guanosine-to-inosine substitution could have a surprisingly large impact on binding specificity. Together, these data demonstrate that guanosine-to-inosine substitution serves as a convenient method for rapidly generating aptamer

analogues having varying binding properties, and thus is well-suited for use in diverse biosensing applications.

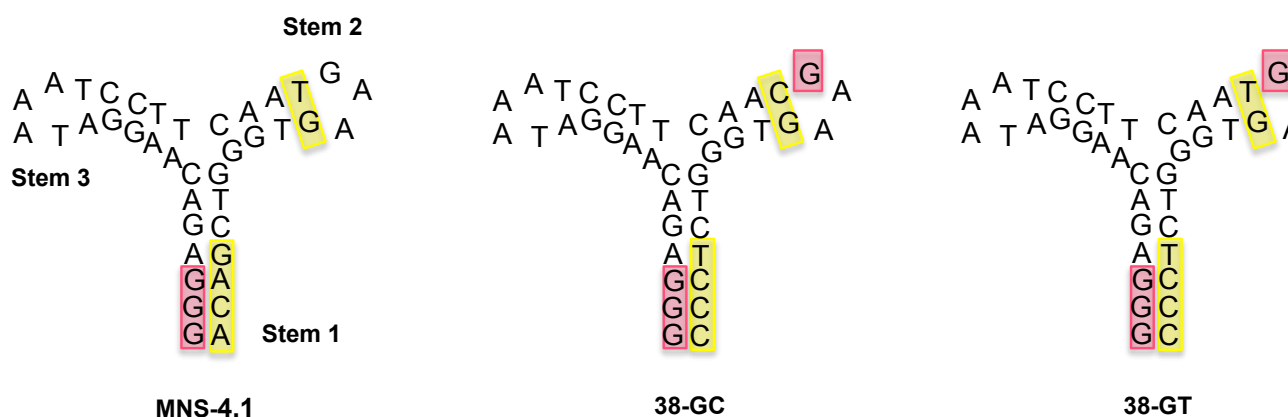


**Figure 2.1: Structures of parent aptamers MNS-4.1, 38-GC, and 38-GT with stems 1-3 labeled for MNS-4.1.** Stems 1-3 are the same for all aptamers. Magenta boxes indicate positions of guanine-to-inosine substitutions. Yellow boxes indicate key differences between parent aptamers implemented by Roncancio et al. in an attempt to increase aptamer stability.<sup>1</sup> Inosine substitutions were formed at positions G1-3 for all aptamers and G25 of 38-GT and 38-GC.

## 2.3 Results and Discussion

### 2.3.1 Binding affinity of aptamers to cocaine

The cocaine aptamer has been subjected to many sequence truncations and mutations, and we based our investigation on the parent aptamer sequences MNS-4.1, 38-GC, and 38-GT.<sup>1</sup>

Because it has been shown that changes made to stem 1 affect binding affinity, we substituted G<sub>1-3</sub> of all aptamers to inosine to yield MNS-4.1 Inosine, 38-GC Inosine, and 38-GT Inosine.<sup>1, 34,</sup>

<sup>59</sup> In addition, we substituted G<sub>25</sub> of 38-GC and 38-GT to inosine to yield 38-IC and 38-IT respectively (Figure 2.1). G<sub>25</sub> is near, but not in, the binding pocket therefore we did not suspect that changing this base would severely alter the binding pocket.<sup>23, 34, 60, 61</sup>



Using fluorescently labeled DNA strands, we employed microscale thermophoresis (MST) to measure the binding affinities of all eight aptamer sequences for cocaine. MST is a highly sensitive method based on changes in thermophoretic mobility upon target binding. Unlike surface plasmon resonance and many other analytical methods, MST does not require that the target or aptamer be immobilized on a surface. In addition, compared to isothermal titration calorimetry, MST requires only small amounts of sample. Thus, MST offers an accurate and convenient method for quantifying aptamer binding affinity.<sup>62, 63</sup> MST analyses indicated that most inosine-containing aptamers bound cocaine with a higher affinity than their unmodified counterparts (Table 2.1, Figure 2.2a). The  $K_d$  value of the MNS-4.1 Inosine aptamer having substitutions at  $G_{1-3}$  improved 17-fold in comparison to the parent MNS-4.1 aptamer. In addition, 38-GT Inosine bound cocaine with a ~2.5-fold improvement in comparison to the parent 38-GT aptamer. However, 38-GC Inosine bound with a  $K_d$  of 18.7  $\mu$ M, which is comparable to the 38-GC parent aptamer. In the case of the  $G_{25}$  substitution, 38-IT only bound with a ~1.5-fold improvement in comparison to the 38-GT aptamer. Finally, the 38-GC  $G_{25}$  substitution, 38-IC, showed an impressive 63-fold increase in affinity compared to the parent 38-GC aptamer. We were very excited about these results, as

most modifications to the cocaine-binding aptamer have resulted in a decrease in binding affinity for the target, and achieving an increase in affinity is significantly more challenging.

### 2.3.2 Melting temperature of aptamers

To investigate the relationship between folding stability and cocaine binding affinity, we purchased non-labeled aptamer strands and used UV absorbance to determine the melting temperature ( $T_m$ ) of each aptamer (Table 2.1, Figure A9). We found that substituting  $G_{1-3}$  for inosine had a large effect on the  $T_m$  of the 38-GT and 38-GC parent sequences, decreasing  $T_m$  by 13.7 and 9.6 °C, respectively. This is not unexpected, as I-C base pairs have one fewer hydrogen bond than G-C base pairs.<sup>64, 65</sup> However, the  $G_{1-3}$  substitutions interestingly had a slightly stabilizing effect on the MNS-4.1 aptamer. Given that where  $G_{1-3}$  are located in the  $S_1$  stem has been noted to be crucial for cocaine binding,<sup>23, 34, 60</sup> we found it interesting that we did not observe a distinct correlation between binding affinity and melting temperature. We also found that changing  $G_{25}$  of

**Table 2.1: Binding affinity for cocaine and analogues and melting temperature of parent aptamers and inosine-substituted variants.**

Aptamer	Positions	Cocaine $K_d$ ( $\mu$ M)	Norcocaine $K_d$ ( $\mu$ M)	Cocaethylene $K_d$ ( $\mu$ M)	$T_m$ (°C)
MNS-4.1	-	79.6 $\pm$ 14.0	15.1 $\pm$ 2.6	22.2 $\pm$ 4.9	41.5 $\pm$ 0.1
MNS-4.1 Inosine	$G_{1-3}$	4.5 $\pm$ 1.2	159 $\pm$ 69	3.8 $\pm$ 1.8	42.9 $\pm$ 0.1
38-GT	-	20.3 $\pm$ 2.8	15.1 $\pm$ 4.2	25.6 $\pm$ 2.5	45.6 $\pm$ 0.8
38-GT Inosine	$G_{1-3}$	6.2 $\pm$ 2.6	111 $\pm$ 24	1.4 $\pm$ 0.5	31.9 $\pm$ 0.2
38-IT	$G_{25}$	13.7 $\pm$ 3.8	23.2 $\pm$ 13.0	128 $\pm$ 33	45.0 $\pm$ 0.7
38-GC	-	14.5 $\pm$ 8.8	N.D.	15.5 $\pm$ 7.6	51.4 $\pm$ 0.7
38-GC Inosine	$G_{1-3}$	18.7 $\pm$ 3.9	N.D.	35 $\pm$ 14	41.8 $\pm$ 0.3
38-IC	$G_{25}$	0.23 $\pm$ 0.10	13.1 $\pm$ 3.8	15.2 $\pm$ 4.6	48.9 $\pm$ 0.1

38-GT and 38-GC only slightly affected the  $T_m$  values of the aptamers indicating that the changes in affinity for these inosine-substituted aptamers are likely a result of much more subtle changes in fold or structure as opposed to overall stability

### 2.3.3 Binding affinity of aptamers to cocaine-like analogues

Next, we were curious to investigate the effect of inosine substitution on binding selectivity against structurally related analytes. Cocaine is primarily hydrolyzed to benzoyl ecgonine (BE) by human choline esterase 1 and to ecgonine methyl ester (EME) by butyrylcholinesterase, human cholinesterase 2, and cocaine esterase.<sup>66-68</sup> Therefore, binding to these metabolites is of significant interest in biosensing applications. We performed MST with each of the parent and inosine-substituted aptamers and found no detectable binding of any of the aptamers to BE or EME (Figure A4 and A5). This indicates that the change in aptamer structure arising from inosine substitution does not decrease specificity against EME and BE.

We were also curious to test the binding affinity of the aptamers with norcocaine and co-caethylene, as the parent MNS-4.1 aptamer has been reported to bind these metabolites.<sup>34</sup> Interestingly; norcocaine is also the only known metabolite of cocaine to be biologically active.<sup>69</sup> As expected, we found that the parent MNS-4.1 aptamer binds norcocaine (Figure 2.2b, Table 2.1). However, inosine substitution at  $G_{1-3}$  resulted in 11-fold weaker binding, demonstrating that this substitution can dramatically impact selectivity. Similarly, we found that inosine substitution at  $G_{1-3}$  of the 38-GT aptamer resulted in 7.4-fold weaker binding however, inosine substitution at  $G_{25}$  of the 38-GT aptamer did not have a significant impact on norcocaine binding affinity. Interestingly, the parent 38-GC aptamer shows no affinity for norcocaine, and this selectivity was retained with inosine substitution at  $G_{1-3}$ . However, substitution of the 38-GC aptamer at the  $G_{25}$  position

restored norcocaine binding, and in fact, this sequence had the highest affinity for norcocaine of all of those tested. In the case of cocaethylene, we also found that the parent MNS-4.1 aptamer binds with an affinity of 22  $\mu\text{M}$ , which is not unexpected given previous reports and the similarity between cocaethylene and cocaine.<sup>34</sup> In a similar trend, our MNS-4.1 Inosine aptamer bound with a higher affinity to cocaethylene than MNS-4.1 and with a higher affinity to cocaethylene than cocaine (Figure 2.2c, Table 2.1). Inosine substitution at the  $G_{1-3}$  positions of the 38-GT and 38-GC aptamers produced similar changes in cocaethylene binding as observed for cocaine. However, while 38-IC bound cocaethylene with the same affinity as its parent 38-GC aptamer, 38-IT bound with a 5-fold lower affinity than its parent 38-GT aptamer. Together, these data demonstrate that inosine substitution not only impacts binding for the target substrate, but can also dramatically impact selectivity by modulating the affinity of aptamers for off-target analytes. For cocaethylene, substitutions made to either  $G_{1-3}$  and  $G_{25}$  resulted in an increase in affinity in most cases. However, norcocaine showed a nearly opposite trend, with the exception of 38-IC.

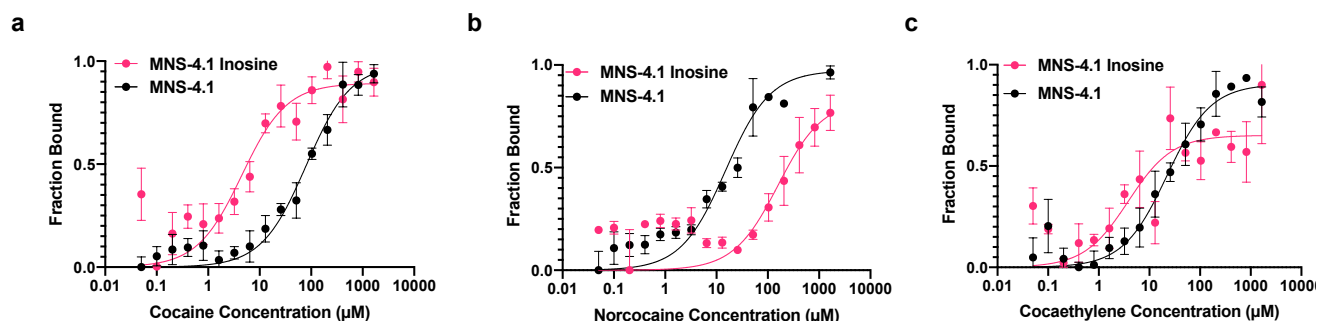


**Figure 2.2:** (a) Cocaine (b) norcocaine and (e) cocaethylene binding of parent MNS-4.1 aptamer in comparison to MNS-4.1 Inosine measured using MST. All MST experiments were performed in triplicate.

### 2.3.4 Binding affinity of aptamers to cocaine in biological fluid

MNS-4.1 has been shown to have salt-dependent affinity for cocaine, and thus we sought to also test binding in a biological fluid.<sup>22, 34</sup> We performed MST analysis with MNS-4.1 and MNS-4.1 Inosine in 2.5% artificial saliva, which has higher KCl concentration than the standard binding buffer used for the aptamer. Interestingly, we observed a ~10-fold increase in binding affinity in the case of MNS-4.1, but observed no change in affinity in the case of MNS-4.1 Inosine (Figure A8).

### 2.3.5 Generation of cocaine structure-switching biosensors

Cocaine-binding aptamers have found wide use in structure-switching biosensors, and thus we sought to test MNS-4.1 and its inosine counterpart, MNS-4.1 Inosine in this context. We functionalized our aptamers with Cy5 and hybridized each to a BHQ3-functionalized complementary strand.<sup>70, 71</sup> In the absence of cocaine, the two sequences hybridize, resulting in quenching of the Cy5 fluorescence. In the presence of cocaine, however, the capture strand (CS) is displaced, resulting in an enhancement in fluorescence (Figure 2.3a). We observed dose-dependent

curves with  $K_{\text{sens}}$  values of  $11.4 \pm 4.6 \mu\text{M}$  and  $20.9 \pm 6.6 \mu\text{M}$  for MNS-4.1 and MNS-4.1 Inosine, respectively (Figure 2.3b). Using a previously reported method, we combined these measurements with the  $K_d$  of each aptamer for the complementary strand in order to independently calculate the  $K_d$  of each aptamer for cocaine.<sup>71, 72</sup> This resulted in  $K_d$  values of  $41.2 \mu\text{M}$  for MNS-4.1 and  $13.9 \mu\text{M}$  for MNS-4.1 Inosine, which are consistent with our MST data. These data further support our earlier observations and demonstrate that inosine modification can also be used to modulate the dynamic range of aptamer sensors.

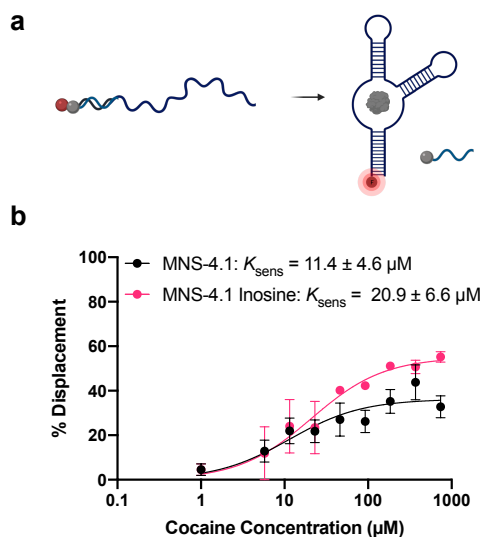


**Figure 2.3: Biosensor characterization for MNS-4.1 and MNS-4.1 Inosine.** (a) Schematic of our structure-switching biosensing method. The red circle represents our fluorophore, and the grey represents our quencher. (b) Dose-dependent curves for MNS-4.1 and MNS-4.1 Inosine biosensors with cocaine.

## 2.4 Conclusion

Here we explore guanosine-to-inosine substitution as a method to modulate the affinity and specificity of DNA aptamers. Using the well-studied cocaine-binding aptamer, we designed and analyzed five inosine-containing sequences based on the parent aptamers MNS-4.1 38-GT

and 38-GC.<sup>1, 59</sup> Using MST, we found that inosine substitution at G<sub>1-3</sub> and G<sub>25</sub> resulted in sequences having a wide range of binding affinities. Excitingly, in some cases, we observed improved affinity with one aptamer showing 63-fold stronger binding as a result of a single inosine substitution. Melting temperature studies showed that inosine substitution also dramatically impacts thermal stability, but we did not observe a strong correlation between changes in  $T_m$  value and changes in binding affinity for cocaine. Thus, we hypothesize that inosine impacts cocaine binding through more subtle structural changes to the aptamer that are not necessarily reflected in thermal stability.

A survey of aptamer binding to cocaine metabolites demonstrated that inosine substitution does not impact selectivity against EME and BE as no binding was detected for the parent aptamers or their inosine-containing analogues. However, we did find that selectivity for norcocaine and cocaethylene could be modulated by inosine substitution with G<sub>1-3</sub> modification resulting in up to 10-fold increase in selectivity compared to the parent aptamer. We also demonstrated that inosine substitution could be used to modulate the dynamic range of aptamer sensors.

While at times we observe dramatic changes to analyte binding upon inosine substitution, we have not yet been able to elucidate clear trends that would predict how inosine substitution could be used to strategically tune affinity. We envision that future studies harnessing a greater number of analogues in tandem with machine learning approaches could provide insight into this interesting question. We also look forward to exploring inosine substitution with other aptamer sequences. We envision that this approach will provide a facile, rapid, and cost-efficient method for obtaining aptamers having a range of binding affinities, not only for the desired target, but also for off-target analytes. We anticipate that this will significantly advance the use of DNA aptamers in

biosensing applications by enabling researchers to carefully tune binding affinity to match the desired dynamic range for analyte detection.

## **2.5 Materials and Methods**

### 2.5.1 Chemicals

Cocaine, benzoylecgonine, ecgonine methyl ester, cocaethylene, and norcocaine were purchased from Sigma-Aldrich. All stock solutions were prepared in water and stored at 4 °C. For biological samples, artificial saliva was purchased from Sigma-Aldrich.

### 2.5.2 Generation of aptamers

Oligonucleotides were purchased from the University of Utah DNA/Peptide Synthesis Core Facility or Integrated DNA Technologies (Table A1 and A2). All oligonucleotides were purified by 10% denaturing polyacrylamide gel electrophoresis prior to use. Gel bands were excised and incubated in 300 mM sodium acetate, 1 mM EDTA (pH 8.0) at 37 °C for 24 h. The DNA was then separated from the gel pieces using cellulose acetate membrane filters (ThermoFisher) and concentrated using 10K Amicon Ultra-0.5 centrifugal unit with Ultracel 10 membrane (EMD Millipore). DNA concentrations were measured on a NanoDrop 2000 (Thermo Scientific).

### 2.5.3 Generation of binding curves using microscale thermophoresis (MST)

MST experiments were performed using a Monolith NT.115 (NanoTemper Technology). All measurements were performed in 10 mM Tris buffer (pH 7.4), 0.01 mM MgCl<sub>2</sub> and 5% DMSO or with with 2.5% artificial saliva at 25 °C. The aptamer concentration was kept constant at 5 nM, while the titrant (cocaine, EME, BE, cocaethylene, or norcocaine) concentrations ranged from 50 μM to 1.65 mM. We introduced 16 Monolith capillaries (NanoTemper) of 5 μL each at N=3 for



cocaine, cocaethylene, and norcocaine and  $N=1$  for EME and BE. Data were fitted using Prism 8 analysis software to determine the aptamer  $K_D$  values.

#### 2.5.4 Determination of melting temperatures

Samples were prepared at a concentration of 3  $\mu\text{M}$ . All measurements were performed in 10 mM Tris buffer (pH 7.4), 0.01 mM  $\text{MgCl}_2$  and 5% DMSO at 25  $^\circ\text{C}$  in 8-well cuvettes and run on a Shimadzu UV-1800 spectrophotometer to monitor absorbance at  $N=3$ . Measurements were taken from 20-95  $^\circ\text{C}$  at a ramping rate of 0.5  $^\circ\text{C}$  per minute. Melting temperatures were determined by the first derivate method.

#### 2.5.5 Generation of structure-switching biosensors

Cy5-labeled aptamer stock solutions were diluted in 2X tris buffer as used in MST. Biosensors were prepared by combining Cy5-labeled aptamer (2.5  $\mu\text{M}$ ) and BHQ3-labeled capture strand (2.5  $\mu\text{M}$ ) in 2X tris buffer used in MST. This solution was heated to 95  $^\circ\text{C}$  and slow-cooled to 25  $^\circ\text{C}$  over 30 minutes in a thermal cycler. Biosensor solutions were stored at 4  $^\circ\text{C}$  until use. The biosensor was equilibrated to room temperature and 20  $\mu\text{L}$  added to 384-well black plates (Corning, #3573). In triplicate, increasing concentrations of cocaine (30  $\mu\text{L}$ ) was added to the wells and the solutions incubated for 40 minutes at 25  $^\circ\text{C}$  while protected from light. Displacement was quantified by measuring the fluorescence intensity on a Cytation 5 multi-mode plate reader (BioTek) using excitation at 650 nm and emission at 670 nm (bandwidth 9, read height 10.5 mm). All samples were normalized to wells containing Cy5-labeled aptamer alone. Percent displacement was calculated and plotted using GraphPad Prism.

## Chapter 3: Modular Catalysis: Aptamer Enhancement of Enzyme Kinetics in a Nanoparticle Reactor<sup>§</sup>

### 3.1 Abstract

Enzymes are widely used in commercial processes and therapeutic applications due to their efficient catalytic turnover, environmental sustainability, and high biocompatibility. While directed evolution and random mutagenesis are common methods for improving enzyme activity, these methods can be costly and time-consuming, and do not allow for independent control of  $K_M$  and  $k_{cat}$ . To achieve such control, we envisioned that co-encapsulation of aptamer affinity reagents with enzymes could increase catalytic efficiency through pre-concentration of substrate. We explored this concept with cocaine esterase and anti-cocaine aptamers of varying affinities, co-encapsulated in MS2 virus-like particles. Rate enhancements were observed, with magnitudes dependent on both aptamer  $K_D$  and aptamer:enzyme stoichiometry. Peak performance was obtained when aptamer binding affinity and enzyme  $K_M$  were roughly equivalent; the beneficial effects of substrate-binding aptamers was lost either when aptamer binding was too tight or the aptamers were not co-localized with the catalyst.

### 3.2 Introduction

Enzymes have demonstrated great promise in biomedicine, bioremediation, and chemical synthesis due to favorable properties of bioavailability, catalytic turnover, and selectivity.<sup>73-75</sup> Enzymatic catalysis encompasses substrate binding, bond-breaking or bond-making (termed “chemistry” for the purposes of this discussion), and product binding (release). These steps are often

---

<sup>§</sup> Unpublished work.

conceptualized separately, such as in the common (and incomplete) association of the Michaelis-Menten parameter  $K_M$  with substrate binding affinity and  $k_{cat}$  with the rate of the bond-altering step. However, the modification of enzyme sequence, whether by rational design<sup>76, 77</sup> or laboratory selection/evolution,<sup>78-80</sup> necessarily changes all functional steps at the same time.

While natural evolution often achieves advantageous levels of enzymatic reactivity by striking a balance between binding and chemistry, there are situations in which these functions are spatially separated. One striking example is ribosomal translation, in which the catalyst provides a general compartment for substrate binding and localized bond-making, the specificities of which are entirely controlled by the substrates. In parallel, non-ribosomal peptide synthesis offers a system in which substrate binding is mediated by thioester handoffs, thereby escaping problems of substrate recognition and product release that would otherwise occur if each intermediate were freely diffusible.

We sought to explore whether the substrate binding and chemistry functions of an enzymatic reaction could be partially separated by co-localization of a substrate-binding DNA aptamer and a substrate-converting enzyme inside the confines of a stable virus-like particle (VLP) shell. Encapsulation of enzymes in a wide variety of nanocompartments, including liposomes, polymersomes, nucleic acid cages, carbohydrates, hydrogels, mineral capsules, and VLPs, has been described, mostly to aid in enzyme stabilization.<sup>81, 82</sup> In many of these cases, no or only modest decreases in enzyme activity (often defined as  $k_{cat}/K_M$ ) are observed while stability is enhanced.<sup>81, 83-108</sup> However, few examples of rate improvement upon encapsulation have been reported, including the use of a DNA nanocages<sup>109</sup> and alginate or carboxymethylcellulose-coated silica.<sup>110</sup>

It has been suggested that encapsulation increases the probability of collision between enzyme and substrate, leading to an improvement in catalytic activity.<sup>111, 112</sup> Peeples et al. investigated this phenomenon in biomolecular droplet condensates and showed that the degree of saturation was increased by high local concentrations of the substrate (mass action) and proximity of substrate to target, leading to a decrease in  $K_M$ .<sup>113</sup> In a separate study, Gao et al. also explored this phenomenon in enzyme-DNA nanostructures, emphasizing the role of proximity of substrate and catalyst.<sup>114</sup>

To test our hypothesis that co-encapsulation enables tuning of substrate binding separate from catalytic turnover, we explored VLPs as the container. VLPs are sufficiently porous to allow free diffusion of small molecules through the capsid shell while excluding large molecules and proteins,<sup>25</sup> and so they provide an excellent way to test the role of a separate substrate-binding additive on enzyme activity. VLP packaging of enzymes imparts resistance to denaturation by heat, organic solvents, and chaotropic agents.<sup>27, 28</sup> Additionally, kinetic parameters are insensitive to the number of enzymes entrained per particle, suggesting that the packaged proteins are not sterically crowded.<sup>25, 27, 28</sup> Because encapsulation is achieved through noncovalent interactions, minimal redesign is needed to swap out components, providing helpful modularity.

In the simplest terms, we envisioned that co-packaging of aptamers and enzyme would provide a boost to  $k_{cat}/K_M$  by pre-concentrating substrate in close proximity to the enzyme using binding agents (aptamers) of varying substrate affinity. Co-encapsulation of stabilizing agents,<sup>90</sup> small-molecule cofactors,<sup>115</sup> and (most often) other enzymes for cascade-reaction systems<sup>28, 115, 116</sup> have all received attention in the literature. Co-localization of sequential enzymes in a cascade inside nanoparticles usually results in modest advantages, often no more than a doubling of activity but occasionally a much more substantial enhancement (in one case as much as a 24-fold

increase<sup>82, 117</sup>). To our knowledge, the pairing of an independent affinity reagent with an enzyme has not been previously investigated. Aptamers are well suited to this role<sup>2, 3, 118</sup> due to their specificity, size, cost-effectiveness, and, particularly useful in our case, their polyanionic nature which makes them natural substrates for VLP packaging. Using co-encapsulation as illustrated in Figure 3.1, we demonstrate the ability of aptamers to modulate enzyme activity and show that this can be tuned by varying the stoichiometry and affinity of the aptamer reagents.

### 3.3 Results and Discussion

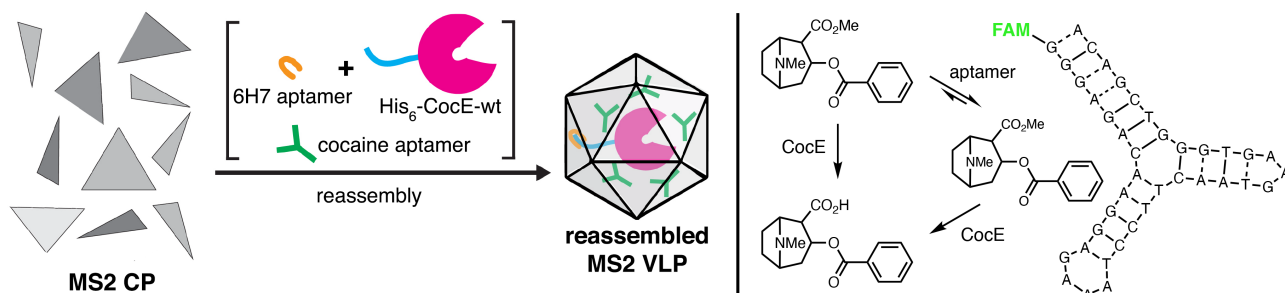


**Figure 3.1.** (left) Co-encapsulation of His<sub>6</sub>-CocE-wt and cocaine-aptamers inside MS2 VLPs. Assembly of purified MS2 CP was initiated with His<sub>6</sub>-binding aptamer 6H7 driving the packaging of His<sub>6</sub>-CocE-wt; anti-cocaine aptamers were simultaneously packaged by electrostatic interaction with the positively charged inner wall of MS2 CP. (right) Enzyme-catalyzed hydrolysis of cocaine and acceleration via aptamer pre-concentration; the cocaine-binding aptamer sequence shown is that of MNS-4.1.

#### 3.3.1 Production and characterization of MS2-packaged enzymes and aptamers

The icosahedral capsid of bacteriophage MS2 is composed of 180 subunits (T = 3 symmetry) with a diameter of 28 nm.<sup>119</sup> When MS2 capsid protein is heterologously expressed, the subunits only assemble into VLPs without nucleic acid or scaffolding proteins at higher protein concentrations. Consequently, *in vitro* assembly of VLPs from isolated MS2 coat proteins can be controlled and used to capture a variety of molecular cargos for nanotechnology applications.<sup>120-</sup>  
<sup>126</sup> The cargo molecules can be encapsulated randomly, or in the case of negatively charged cargo molecules, packaging is favored by electrostatic interactions with the interior-facing positively charged N-terminal sequence of the MS2 CP.

To test the inherent aptamer-packaging ability of the MS2 capsid, we employed the 38-GC variant<sup>35</sup> of the Landry cocaine-binding aptamer MNS4.1<sup>33</sup>. Different concentrations of fluorescein-labeled aptamer were incubated with a standard concentration of MS2 coat protein in reassembly buffer, followed by sucrose gradient purification. VLPs appeared in a bright green band at the standard density in these gradients, consistent with the expected entrainment of the aptamers, with a maximum of approximately 75 aptamers packaged per particle (Figure B2, assessed by UV-vis absorbance of the dye relative to protein concentration determined by repeat Bradford assay). However, the relatively large (approx. 70 kDa) His<sub>6</sub>-CocE-wt enzyme was not captured in significant amounts by a similar approach; a maximum average of only one enzyme for every 10 particles (0.1 CocE per VLP) was found despite testing a number of different component concentrations, and no enzyme at all could be co-packaged with aptamer. (Protein encapsidation efficiency was determined by the relative intensities of electrophoretic bands of denatured MS2 CP and CocE, correcting for the respective protein molecular weights; Figure 3.2c).

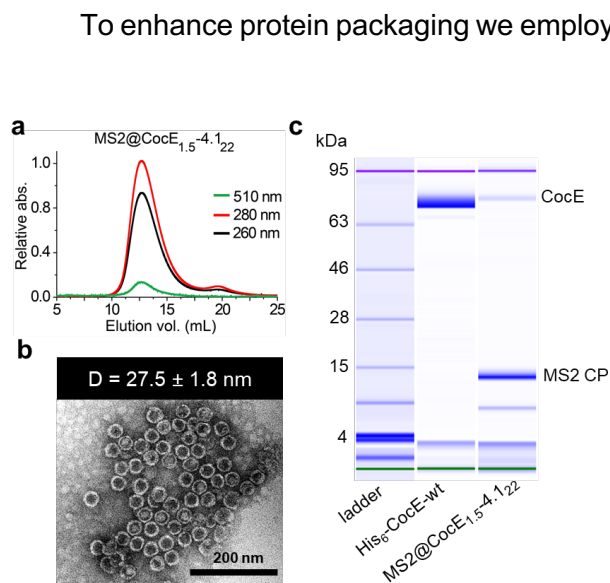


**Figure 3.2. Characterization data for MS2@CocE-4.121 particles as a representative example.** a) size-exclusion FPLC; b) negative-stain (uranyl acetate) transmission electron microscopy; c) denaturing microfluidic electrophoresis (Agilent Bioanalyzer).

per VLP. Presumably, this arises from the effective conversion of the positively-charged His<sub>6</sub>-tagged N-terminus to a negatively charged aptamer-bound handle. Co-packaging of enzyme and cocaine-binding aptamer was explored by initial incubation of His<sub>6</sub>-CocE-wt with 6H7 aptamers followed by addition of cocaine aptamer and purified MS2 CP in varying ratios. Conditions were thereby identified which provided encapsulation of a consistent range of 1.5-2.1 CocE enzymes and varying amounts of cocaine-binding aptamers (from 4 to 21) per VLP (Table 3.1). The particle recoveries, determined by Bradford assay, were 55-65%, typical for these types of manipulations. Further, the encapsulation efficiency of enzyme and aptamers remained consistent for different aptamer sequences of similar lengths, as expected for an assembly process controlled primarily by electrostatic interactions.

To enhance protein packaging we employed the His<sub>6</sub>-binding DNA aptamer 6H7 that binds to the hexahistidine peptide with nM affinity<sup>127</sup> and can simultaneously bind to the MS2 coat protein through electrostatic interactions. Therefore, the 40-mer 6H7 aptamer (2 equivalents with respect to enzyme, in DI water) was pre-mixed with His<sub>6</sub>-CocE-wt then introduced into the MS2 reassembly reaction. Presence of this aptamer in the assembly mixture enhanced the protein packaging efficiency by approximately 20-fold, to a maximum average of 2.5 His<sub>6</sub>-CocE-wt molecules

VLPs having only enzyme are designated as MS2@CocE and VLPs having both enzyme and aptamer are denoted MS2@CocE<sub>n</sub>-aptamer<sub>m</sub> where n is the average number of enzymes per VLP and m is the average number of aptamers per VLP. As evidence that packaging does not impact the VLP architecture, we note that all particles were found to elute at the same retention time on size-exclusion chromatography (SEC, example in Figure 3.2a), appear essentially identical by TEM (example in Figure 3.2b), and do not have significant difference in hydrodynamic radius by dynamic light scattering (Figure B4). Aptamer packaging on the inside of the particles was confirmed by correlation of dye (510 nm) and nucleoprotein (280 nm) absorbance on SEC and by incubation with DNase-I (Figure B5). Such treatment induced no change in aptamer-associated dye signal for aptamer-containing VLPs but a rapid loss of signal for a physical mixture of MS2 VLPs and aptamer.

**Table 3.1. Initial ratios and resulting average numbers of packaged enzymes and cocaine-binding aptamers.** Error represents standard deviation for at least three independent replicates.

MS2-CP	6H7	His <sub>6</sub> -CocE-wt		cocaine aptamers	
		used	found per VLP	used	found per VLP
50	2	1	2.5	-	-
50	2	1	2.1	1	4 ± 1



50	2	1	1.8	5	10 ± 1
50	2	1	1.5	15	21 ± 1

### 3.3.2 Anti-cocaine aptamer binding

In the expected interplay of affinity reagents and catalysts, the relative values of aptamer  $K_D$  and enzyme  $K_M$  should impact the level of cooperativity that can be achieved between these two components. Thus, we used aptamer variants having similar length and structure but varying affinities bracketing the  $K_M$  of CocE (10  $\mu\text{M}$ ): the parent MNS-4.1 aptamer (cocaine  $K_D = 100 \mu\text{M}$ ), 38-GC ( $K_D = 9 \mu\text{M}$ ), and 38-IC ( $K_D = 0.3 \mu\text{M}$ ), as determined by microscale thermophoresis (MST) at 30 °C (the same temperature as the rate measurements described below; Figure S3, Table 3.2). These values were similar to reported aptamer-cocaine dissociation constants measured at room temperature (80  $\mu\text{M}$ , 15  $\mu\text{M}$ , and 0.23  $\mu\text{M}$ , respectively).<sup>21</sup> A scrambled 38-GC sequence (Scr) exhibited no binding to cocaine by MST (Figure B6).

### 3.3.3 Catalytic activities of free and MS2-packaged enzymes and aptamers

Measurements of enzyme kinetics were performed under standard conditions as described in the Materials and Methods and Supporting Information (Figure B7). Data for each of the free, packaged, and co-packaged enzyme systems provided a good fit to the single-site Michaelis–Menten equation ( $R^2 > 0.9$ ). Table 2 and Figure 3 summarize the resulting kinetic parameters. The packaged enzyme alone (without co-packaged aptamer) exhibited increased catalytic rate ( $k_{\text{cat}}$ ) but also a higher value of  $K_M$ , making for a slight diminution in catalytic efficiency ( $k_{\text{cat}}/K_M$ ) relative to free enzyme. As a control, inclusion of 10 or 20 copies of the scrambled (nonfunctional)

DNA aptamer per particle made little difference in the kinetic parameters, consistent with our prior findings that the presence or absence of randomly packaged bacterial RNA has no effect on the catalytic properties of enzymes packaged in the related Q VLP.<sup>25</sup>

**Table 3.2. Kinetic Parameters of Free, Packaged, and Aptamer Co-packaged Enzymes.**

Particle/enzyme	Aptamer	Aptamer $K_D$ ( $\mu\text{M}$ )	Average ap-tamer/VLP	$K_M$ ( $\mu\text{M}$ )	$k_{\text{cat}}$ ( $\text{min}^{-1}$ )	$k_{\text{cat}}/K_M$ ( $\mu\text{M}^{-1} \text{min}^{-1}$ )
CocE-wt	-	-	-	$10.3 \pm 1.0$	$281 \pm 4$	$27.4 \pm 1.9$
MS2@CocE <sub>2.5</sub>	-	-	-	$19.9 \pm 1.0$	$403 \pm 8$	$20.3 \pm 1.0$
MS2@CocE <sub>2.1-4.13</sub>	MNS-4.1	98.3	3	$9.7 \pm 0.9$	$237 \pm 4$	$24.5 \pm 1.5$
MS2@CocE <sub>1.8-4.19</sub>			9	$4.1 \pm 0.2$	$201 \pm 2$	$49.2 \pm 2.4$
MS2@CocE <sub>1.5-4.122</sub>			22	$6.9 \pm 0.6$	$197 \pm 5$	$28.8 \pm 2.5$
MS2@CocE <sub>2.1-GC5</sub>	38-GC	8.5	5	$6.4 \pm 0.9$	$216 \pm 9$	$34.3 \pm 4.0$
MS2@CocE <sub>1.8-GC11</sub>			11	$3.9 \pm 0.3$	$227 \pm 5$	$57.7 \pm 3.5$
MS2@CocE <sub>1.5-GC21</sub>			21	$9.7 \pm 0.8$	$244 \pm 3$	$25.5 \pm 2.4$
MS2@CocE <sub>2.1-IC4</sub>	38-IC	0.3	4	$14.2 \pm 3.8$	$239 \pm 13$	$17.1 \pm 4.5$
MS2@CocE <sub>1.8-IC10</sub>			10	$14.6 \pm 2.8$	$235 \pm 9$	$16.2 \pm 2.5$
MS2@CocE <sub>1.5-IC22</sub>			22	$11.1 \pm 2.4$	$220 \pm 9$	$19.9 \pm 1.6$
MS2@CocE <sub>1.8-Scr10</sub>	Scrambled	-	10	$13.6 \pm 5.3$	$309 \pm 34$	$22.8 \pm 1.2$
MS2@CocE <sub>1.5-Scr20</sub>			20	$23.0 \pm 6.6$	$363 \pm 34$	$15.8 \pm 2.4$

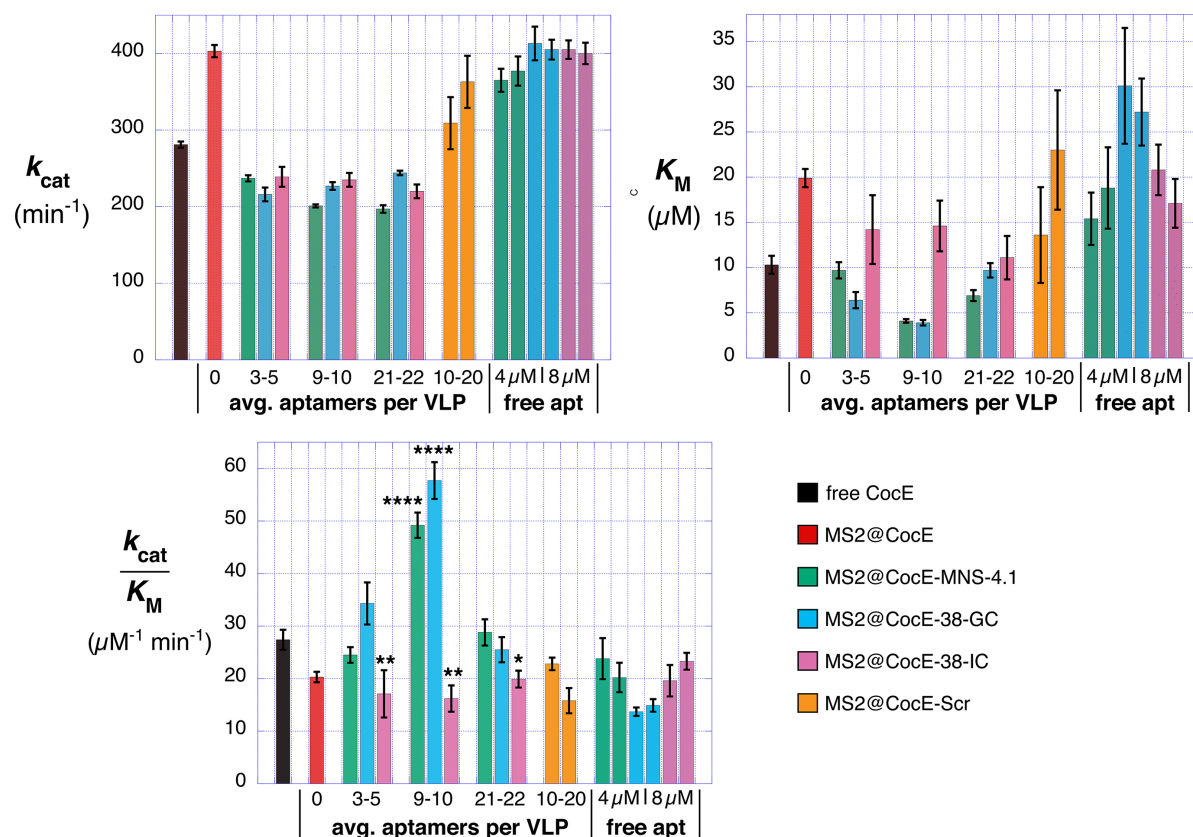


**Figure 3.3. Effect of co-encapsulation of aptamers and enzymes on enzyme kinetics.** Error bars represent the standard deviation of three independent trials. Statistical significance was evaluated by One-way ANOVA with Dunnett's multiple comparisons test at  $p^* < 0.01$ ,  $p^{**} < 0.001$ , and  $p^{****} < 0.0001$ . All data compared to WT CocE.

In contrast, the presence of the co-packaged substrate-binding aptamer had a consistent deleterious effect on  $k_{cat}$  (Figure 3.3a) diminishing that parameter by 30-40% (7-15% relative to  $k_{cat}$  of the free enzyme) regardless of the amount of aptamer present in the particle. The response of  $K_M$ , however, was much more nuanced, decreasing by at least a factor of 2 (with respect to the

packaged enzyme alone) when the enzyme was entrained with the weak (MNS-4.1) and moderate-binding (38-GC) aptamers, but not the high-affinity 38-IC aptamer. Furthermore, the beneficial effects of aptamer binding to catalysis (low  $K_M$ ) were maximized in the presence of a moderate number of aptamers (9-10 per VLP, Figure 3.3b). This gave rise to an approximately 2-fold increase of in catalytic efficiency relative to free enzyme and approximately 2.5-fold enhancement relative to the packaged enzyme in the absence of aptamer. Aptamers are unable to transit the capsid shell, and so as expected, their presence in solution outside the particles made little difference to overall catalytic efficiency. Indeed, only the moderately-binding 38-GC aptamer induced significant differences in any kinetic parameter compared to the packaged enzyme alone when present outside the particle, giving rise to an increase in  $K_M$ , and therefore a modest decrease in catalytic efficiency (Fig. 3.3, Figure B3, Figure B10).

A model of the relevant interactions in this system is shown in Figure 3.4. Diffusion of the small-molecule substrate and products through the capsid protein is assumed to be essentially unconstrained, as we have shown in a different context.<sup>29</sup> Since the effect of packaged aptamer is sequence-dependent, relying on sequences having specific affinity for the cocaine substrate, the aptamer can only improve enzyme performance if it increases the local substrate concentration but releases the substrate easily enough to be processed by the enzyme. Thus, the binding constant added to the system by the presence of the aptamer ( $K_{A-S}$ ) can neither be too large (insufficiently able to capture enough substrate in the particle to make a difference) nor too small (unable to release enough substrate in the vicinity of the enzyme).

Such a phenomenon is demonstrated here, in which the low- and medium-affinity aptamers improve  $k_{cat}/K_M$ , but only when present in moderate amounts. Weaker-binding aptamers have a greater effect when present in higher numbers in the VLPs, whereas the moderate-binding

aptamer exerts its influence at lower copy numbers. In contrast, aptamer 38-IC, with  $K_D$  much lower than  $K_M$ , has little effect on catalysis, as more than enough substrate is present to saturate the aptamer and render it innocuous. In these cases, the concentration of substrate is much greater than that of aptamer, and thus the loss of substrate to aptamer binding is negligible. As expected, the beneficial effect with low and moderate binding aptamers occurs by modulation of  $K_M$ , not  $k_{cat}$ , and location is important: only when the aptamer is held close to the enzyme can its substrate-binding ability help. (The interior volume of the MS2 VLP is approximately 7 zeptoliters; 10 aptamer molecules in such a volume represents a concentration of approximately 2 mM).

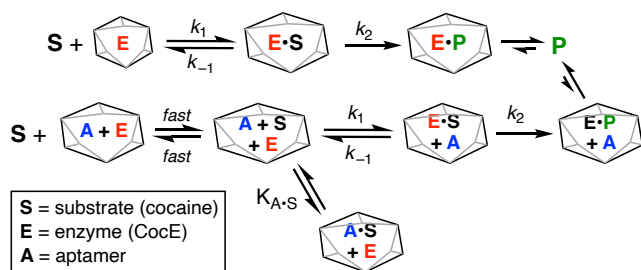


**Figure 3.4. Model of aptamer-assisted catalysis by packaged enzymes.**

### 3.4 Conclusions

The use of substrate-binding moieties outside of the active site of an enzyme is demonstrated most elegantly by natural systems such as non-ribosomal peptide synthesis. Here, the substrate is passed from enzyme to enzyme in the cascade by reversible covalent (thioester) linkages. This highly evolved mechanism has inspired many attempts to immobilize multiple enzymes in close proximity to each other to allow the product of one catalyst to be passed along as

the substrate of another. We describe here a system in which substrate-binding affinity reagents can act in cooperation with enzymes in order to enhance the rate of catalysis.

Co-packaging of aptamers with enzymes gave rise to a maximum improvement in catalytic efficiency of 2.5-fold. While perhaps a bit disappointing in magnitude, we were gratified to see that the reaction enhancement required the right balance of affinity and enzyme  $K_M$ , as predicted: too strong or too weak recruitment of the substrate were both ineffective. The former scenario is similar in some respects to substrate competition in a multi-enzyme system.<sup>128</sup>

These studies also provide some clues about strategies to improve performance further. For example, an aptamer that was 10-fold weaker in substrate affinity was able to give very similar improvements by being packaged at only 3-fold higher concentration. This suggests that faster off-rates may be an important factor that we have yet to explore. Overall, while enzyme evolution has the advantage of simultaneous adjustment of the steps of substrate binding and transformation, such a complex interplay is often beyond our predictive capabilities. The conceptual reductionism demonstrated here certainly makes it easier to change these functions independently, with potential advantages for the understanding and enhancement of biomolecular catalysis.

## **3.5 Materials and Methods**

### **3.5.1 Chemicals**

Cocaine, benzoylecgonine, and ecgonine methyl ester were purchased from Sigma-Aldrich. All stock solutions were prepared in water and stored at 4 °C.

### **3.5.2 Aptamer Generation**

Oligonucleotides were purchased from the University of Utah DNA/Peptide Synthesis Core Facility or from Integrated DNA Technologies. A list of oligonucleotides is provided in Table S1. All oligonucleotides were purified by 10% denaturing polyacrylamide gel electrophoresis prior to use. Gel bands were excised and incubated in 300 mM sodium acetate, 1 mM EDTA (pH 8.0) at 37 °C for 24 h. The DNA was then separated from the gel pieces using cellulose acetate membrane filters (ThermoFisher) and concentrated using 10K Amicon Ultra-0.5 centrifugal unit with Ultracel 10 membrane (EMD Millipore). DNA concentrations were measured on a NanoDrop 2000 (Thermo Scientific).

### 3.5.3 Microscale Thermophoresis (MST)

MST experiments were performed using a Monolith NT.115 (NanoTemper Technology) instrument. All measurements were performed in 10 mM Tris buffer (pH 7.4) and 0.01 mM MgCl<sub>2</sub> at 30°C. The aptamer concentration was kept constant at 5 nM, while the titrant (cocaine or EME) concentrations ranged from 50 nM to 412.5 μM. We introduced 16 Monolith capillaries (NanoTemper) of 5 μL each at N=1. Data were fitted using Prism 8 analysis software to determine the aptamer K<sub>D</sub> values.

### 3.5.4 Cloning, Production, and Purification of MS2-wt VLPs

We used plasmids coding for MS2 CP in the pCDF-1b parent vector as previously described.<sup>26</sup> Sequences were verified before expression. *E. coli* BL21 (DE3) (Biogen) cells harboring the appropriate plasmids were grown in SOB (Amresco) supplemented with 20 mM magnesium sulfate and 50 μg/mL streptomycin. Starter cultures were grown overnight at 37 °C and used to inoculate larger expression cultures. Expression was induced with 1 mM IPTG when OD<sub>600</sub> reached approximately 1.0, and the induced culture was kept at room temperature overnight for

expression. Cells were then harvested by centrifugation in a JA-10 rotor at 6000 rpm, and the pellets were either processed immediately or stored at  $-80\text{ }^{\circ}\text{C}$ . The cell lysate was prepared by re-suspending the cell pellet with 100 mL of 20 mM HEPES buffer (pH 7.4) and sonicating at 50 W for 10 min with 5 s bursts and 5 s intervals. Cell debris was pelleted in a JA-17 rotor at 14000 rpm, and 0.265 gm/mL ammonium sulfate was added to the supernatant to precipitate the VLPs. The crude VLP pellet from precipitation was re-suspended in 3 mL of 20 mM HEPES (pH 7.4). Organic extraction with 1:1 *n*-butanol:chloroform was performed to remove lipids and other cellular debris. The aqueous layer containing VLPs was further purified by sucrose density ultracentrifugation (10–40% w/v). Particles were pelleted out by ultracentrifugation in a 70Ti rotor (Beckman) at 68000 rpm for 2 hours.

### 3.5.5 Production and purification of His<sub>6</sub>-CocE-wt enzyme

Free (unpackaged) enzymes were expressed as C-terminal His<sub>6</sub> fusions as above, but protein expression was done at  $18\text{ }^{\circ}\text{C}$  instead of room temperature. The cleared *E. coli* cell lysate was passed through a cobalt-NTA Talon resin column (0.5 mL bed volume), and the column was washed and eluted according to the manufacturer's instructions at  $4\text{ }^{\circ}\text{C}$ . The fractions containing free enzyme were pooled and dialyzed against three changes of 1 L of 10 mM Tris buffer (pH 7.4) and concentrated with an Amicon Ultra centrifugal filtration unit (30 kDa MWCO, Millipore). Purity was assayed by chip-based electrophoresis.

### 3.5.6 Packaging of His<sub>6</sub>-CocE-wt enzyme and aptamers using disassembly-reassembly of MS2 VLPs

Packaging of enzymes and aptamers was performed by the method of Stockley and coworkers (Figure 3.1).<sup>120, 121</sup> In brief, 1.0 mL of glacial acetic acid was slowly added to 0.5 mL of



the MS2 CP (10 mg/mL in 20 mM HEPES, pH 7.4) and mixed by flipping the tube twice. The reaction mixture was kept on ice for 30 min before centrifugation at 6600g at 4 °C for 10 min. The supernatant was desalted into 1 mM acetic acid by passage over a NAP-25 column pre-equilibrated with 1 mM acetic acid. The fractions containing disassembled MS2 coat protein were combined and protein concentration was determined by Bradford assay. This MS2 CP solution (5 mg/mL, 365  $\mu$ M in MS2 CP monomer), enzyme (7.3  $\mu$ M in 10 mM Tris, pH 7.4), and aptamer (varying concentrations in DI water) in separate eppendorf tube was treated with 1/10th volume of 10x TMK buffer (10x TMK = 100 mM Tris, 10 mM MgCl<sub>2</sub>, and 80 mM KCl) respectively on ice. After a min of incubation, the resulting solutions were mixed to a different molar ratio of MS2 coat protein: enzyme: aptamers on ice. Then the reaction mixture was removed from ice and incubated at room temperature for 3 h followed by storage at 4 °C for overnight. The assembled MS2 particles were purified by sucrose density ultracentrifugation (10–40% w/v) and isolated by ultracentrifugation in a 70Ti rotor (Beckman) at 68000 rpm for 2 hours.

### 3.5.7 Characterization of enzyme and aptamers packaged VLPs

The purity of assembled VLPs was assessed by isocratic size exclusion FPLC chromatography (Superose 6 column). Non-aggregated MS2 particles were eluted at approximately 12.5 mL after the void volume. Dynamic light scattering (DLS) was used to measure hydrodynamic radius, and a Bioanalyzer 2100 Protein 80 microfluidics chip was used to analyze the average number of enzymes packaged inside the particles. The latter value was determined by normalizing the integrated intensities of coat protein and cargo protein peaks to their respective molecular weights to estimate the molar ratio of cargo protein to coat protein, assuming that equal molar amounts of the two proteins gives the same intensity in the staining and detection in the microfluidic Bioanalyzer instrument. This ratio was divided by 180 to obtain the loading of cargo proteins

per VLP, as each VLP is composed of 180 CP subunits. The overall protein concentration was determined with Coomassie Plus Protein Reagent (Pierce) according to the manufacturer's instructions. The average number of aptamers entrained per particle was determined from UV-Vis absorbance measurements using the molar absorptivity of FAM molecule attached to the aptamer.

### 3.5.8 Transmission Electron Microscopy (TEM)

TEM was performed by applying the VLP sample (0.1 mg/mL; 6  $\mu$  L) onto a 300-mesh Lacey Formvar/Carbon-coated copper grid for 90 s followed by removal of the solvent with filter paper. Negative staining of the particles was done using freshly filtered uranyl acetate solution [2% (w/v); 3  $\mu$  L] for 45 s followed by removal of the solvent with filter paper. The grids were viewed (Hitachi HT-7700) at an accelerating voltage of 120 kV with magnification between 4,000-600,000.

### 3.5.9 Enzyme activity assay

Cocaine esterase (CocE) activity was measured by monitoring the loss of cocaine by tracking the UV absorbance at 240 nm using a Shimadzu UV-1800 spectrophotometer. For determinations of kinetic parameters, 3  $\mu$  L of a 1  $\mu$ M enzyme solution of unpackaged, packaged, or co-packaged CocE was added to 147  $\mu$  L of solution containing 0–330  $\mu$ M substrate in 10 mM Tris buffer (pH 7.4), 0.01 mM MgCl<sub>2</sub> and read at 30 °C every 40 seconds for 20 minutes. (Note: a solution of 1.06 mg/mL of VLP containing an average of 2.5 CocE molecules per particle establishes a total enzyme concentration of 1  $\mu$ M.) A Michaelis–Menten nonlinear fit was used to obtain  $K_M$  and  $k_{cat}$  values.

## Chapter 4: Thermoreversible Control of Nucleic Acid Structure and Function with Glyoxal Caging<sup>24\*\*</sup>

### 4.1 Abstract

Controlling nucleic acid structure and function expands their applicability of these biomolecules in biomedicine, nanotechnology, and biosensing. Many chemical and light-based methods have been employed to achieve this goal. However, these stimuli often come with costly limitations. One field that has not been extensively studied, however, is heat-triggered control of nucleic acids. Here we show that glyoxal, a chemical denaturant of nucleic acids, addresses several of these limitations by thermoreversibly controlling the structure and activity of any nucleic acid scaffold. Using DNA and RNA constructs, we show that glyoxal-modified nucleic acids can temporarily and reversibly be inhibited from forming secondary structures. With this, we show that we can have reversible control over functional nucleic acids, XNAs, nuclease function, CRISPR-Cas9, and gene expression in live cells. Together, this demonstrates that thermoreversible glyoxal caging can be easily applied for reversible inhibition of nucleic acid function in a multiple different applications, establishing a straightforward and effective framework for use in a variety of potential biomedical applications.

---

\*\* Reproduced in part from Ref. 24 with permission from Knutson, S. D.\*; Sanford, A. A\*.; Swenson, C. S.; Korn, M. K.; Manuel, B. A.; Heemstra, J. M. *Journal of the American Chemical Society*. **2020**, 142(41), 17766–17781. Copyright 2020 American Chemical Society.

## 4.2 Introduction

Nucleic acids have been studied for over a century as they control all cellular activity such as gene expression, recognition, and protein binding. Therefore, understanding the structures and functions of these biopolymers has opened doors to many different applications, including biosensing, therapeutics, and biotechnology. Externally controlling these biomolecules can further expand the field, allowing for better characterization of these molecules, leading to better biosensors, therapeutics, and biotechnology. One method that has been put into place to control nucleic acids externally is using chemical stimuli. Bases have been modified by incorporating compounds such as trichloroethyl (TCE), which inhibit duplex formation.<sup>129</sup> This interaction is reversible by reacting these sequences with reducing agents in order to remove TCE.<sup>129</sup> However, this method can only be used for shorter DNA and RNA sequences. Another method involves reacting sequences with an azide-functionalized acylating agent. These agents react with the 2' hydroxyls of RNA, and the interaction is reversible by using triphosphine derivatives. However, this method can only be applied to RNA. Another method that has been put into place to control nucleic acids is using light stimuli. Nucleobases are functionalized with protecting groups that are light sensitive at their respective wavelengths.<sup>130</sup> Therefore, this interaction is easily reversed by irradiating these protected sequences with light at the respective wavelength, causing the protective groups to “fall off.”<sup>130</sup> However, these protecting groups have to be synthesized into the nucleobases, which becomes time consuming and costly.<sup>131</sup> In addition, because some of these groups require UV-irradiation for long periods of time, using these in cellular settings is not ideal.

Glyoxal reacts with the Watson-Crick-Franklin face of nucleobases, inhibiting duplex formation in nucleic acids.<sup>132</sup> In particular glyoxal preferentially interacts with guanosine, and at high concentrations, it interacts with cytosine and adenosine.<sup>132</sup> Because glyoxal does not have to be

chemically synthesized into the bases, we aimed to explore it further for caging properties. In addition, the reversibility of this compound in nucleic acids has never been studied.

Because DNA and RNA contain important structural and functional properties in gene regulation, storage, and transport, being able to “turn on” and “turn off” the function of these biopolymers is very beneficial.<sup>133-135</sup> We envisioned the use of glyoxal to “cage” these nucleic acids by reacting with guanosine, cytosine, and adenine. Our group is broadly exploring the caging and decaging of a variety of biomolecules. My role in the project focused on exploring the ability of glyoxal to inhibit the activity of EcoRI, a restriction endonuclease, on double stranded DNA. Further, I tested the thermoreversibility of this activity by heat activation to restore full enzymatic activity. Together, using glyoxal as a caging group allows for further application in the biomedical sciences as it is thermally reversible and is non-toxic.

## **4.3 Results and Discussion**

### *4.3.1 Caging and decaging kinetics of glyoxal*

Partial decaging and/or caging may produce false negatives and positives in downstream applications, and thus it is crucial that we are able to fully cage and decage the DNA. Therefore, we sought out to determine the caging and decaging kinetics of glyoxal at different temperatures and pH's. In our initial conditions (1.3 M glyoxal in 50:50 DMSO:H<sub>2</sub>O, 50°C), we determined a half-life of 9 minutes with full caging in 30-40 minutes. We then decaged in pH 7.5 PBS at 70°C,

and observed a half-life of 11 minutes with full decaging at 30 minutes. We then observed decaging at different pH's and temperatures. We observed that decaging rates increased as the temperature and pH increased (Table 4.1).

**Table 4.1: Temperature and pH dependent half-lives for glyoxal decaging**

	pH 6.5	pH 7.0	pH 7.5	pH 8.0
95 °C	1.4 ± 0.34 minutes	1.1 ± 0.24 minutes	<1 minute	<<1 minute
70 °C	52 ± 7.7 minutes	14 ± 2.7 minutes	11 ± 2.4 minutes	3.8 ± 1.6 minutes
50 °C	14 ± 1.8 hours	8.0 ± 1.7 hours	4.6 ± 1.1 hours	3.1 ± 0.70 hours
37 °C	14 ± 4.2 days	6.6 ± 1.4 days	3.0 ± 0.5 days	2.0 ± 0.33 days

#### 4.3.2 Thermoreversible control of functional nucleic acids

Because glyoxal binds nucleic acids, we decided to begin our studies with the broccoli aptamer, 10-23 DNAzyme, and modified nucleic acids. We chose these targets, because they are well characterized. The broccoli aptamer is an RNA oligonucleotide that binds the fluorogenic dye 3,5-difluoro-4-hydroxybenzylidene imidazolinone (DFHBI) (Figure 4.1a).<sup>136</sup> Aptamers must adopt a secondary structure to function properly and bind their target. Therefore, we hypothesize that by disrupting this secondary structure; the aptamer will not be capable of binding the dye, resulting in no fluorescence. Upon decaging, this activity should be restored, leading to a gain in fluorescent signal. Using our determined caging time of 10 minutes and our rapid decaging conditions of 95°C and pH 7.5 for 2 minutes, we were able to observe a loss in fluorescence and a regain in signal (Figure 4.1b-f).

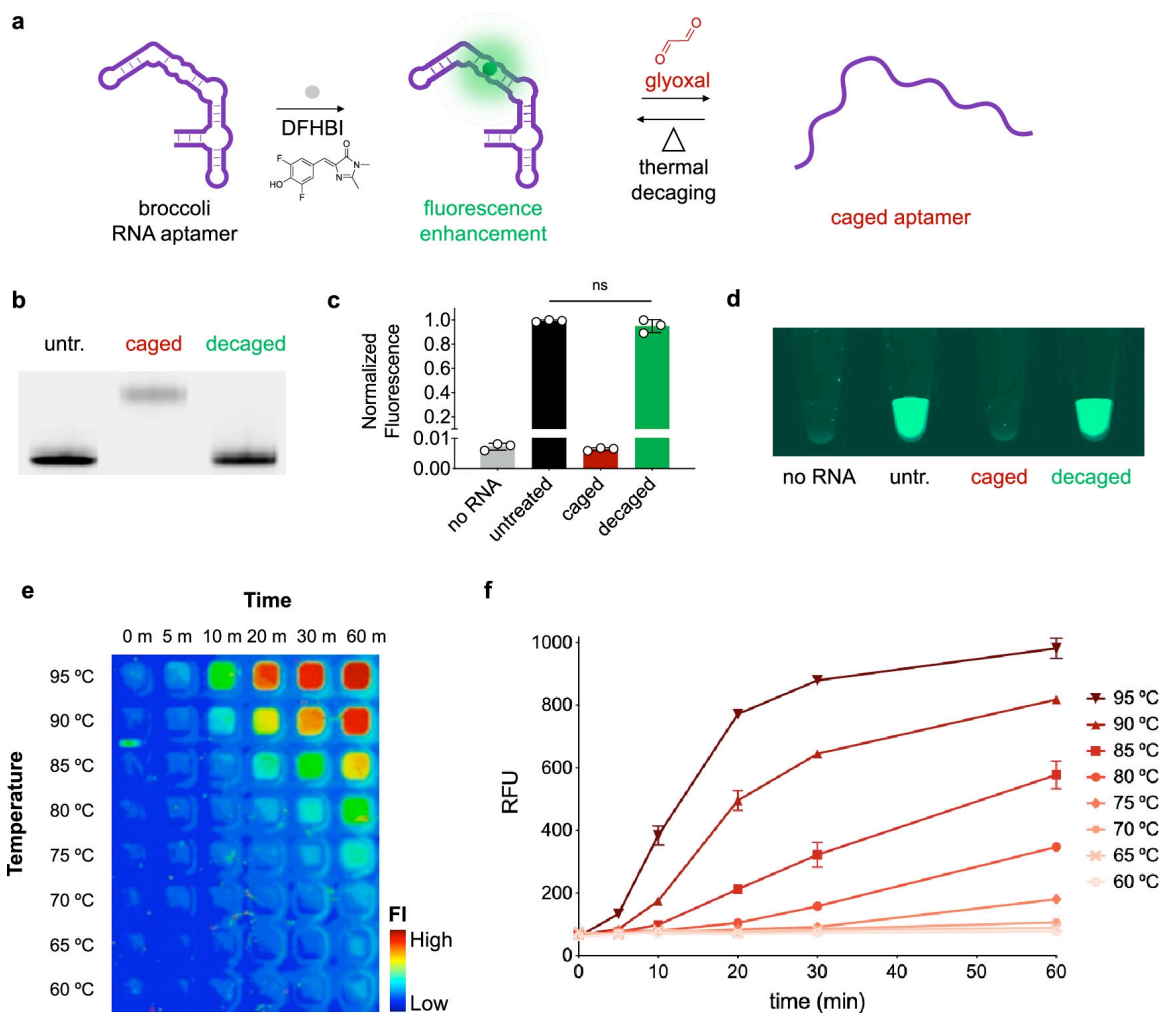


**Figure 4.1: Glyoxal caging imparts thermoresponsive fluorogenic activity in the broccoli RNA aptamer.** A+) Schematic of the fluorogenic broccoli RNA aptamer. Glyoxal caging reversibly denatures and cages the aptamer, preventing fluorescent signal generation. b) 20% denaturing PAGE analysis of untreated (untr.), caged, and decaged RNA aptamers. 60 pmol (2  $\mu$ g) of RNA aptamer was first treated with 1.3 M glyoxal in 50:50 DMSO:H<sub>2</sub>O, 50 °C for 10 minutes. To decage the aptamer, 20 pmol of caged RNA (10 minutes glyoxal treatment time) was incubated at 95 °C, pH 7.5 for 2 minutes. c) Quantified fluorescence enhancement of untreated (untr.), caged, and decaged broccoli aptamers. 20 pmol of untreated, minimally caged (10 minute glyoxal treatment time), or decaged aptamer (2 minutes at 95 °C, pH 7.5) was combined with 2  $\mu$ M 3,5-difluoro-4-hydroxybenzylidene imidazolinone (DFHBI), 40 mM HEPES, 100 mM KCl, and 1 mM MgCl<sub>2</sub>, pH 7.4 and incubated for 30 minutes at 37 °C prior to fluorescent measurement. Bars represent mean and S.D. from triplicate binding reactions. Unpaired t-test was performed between untreated and decaged samples. “ns” indicates no significant difference. d) Fluorescence enhancement reactions visualized with a typhoon gel imager. e) Minimally caged broccoli (10 minutes glyoxal treatment time) was combined with 2  $\mu$ M DFHBI in 40 mM HEPES, 100 mM KCl, and 1 mM MgCl<sub>2</sub>, pH 7.4 and incubated at various temperatures for increasing times. Reactions in 384-well plates were then visualized using a Typhoon gel imager. Heat map values represent fluorescent intensity generated using the acquisition software (FI = fluorescent intensity). f) Quantified broccoli aptamer fluorescence plotted against temperature and incubation time. Values represent mean and S.D. of 2 independent trials.

Next, we explored the effects of glyoxal caging on DNAzyme function. The 10-23 DNAzyme is the first ever developed DNAzyme. It hybridizes a ssDNA target and cleaves at an internal ribonucleotide (Figure 4.2a).<sup>137</sup> Upon caging for 20 minutes, we began to notice reduced activity from our DNAzyme, and after 1 hour, we see a full reduction in activity. Upon decaging at 95°C and pH 7.5 for 10 minutes, we notice full restoration of DNAzyme activity (Figure 4.2).



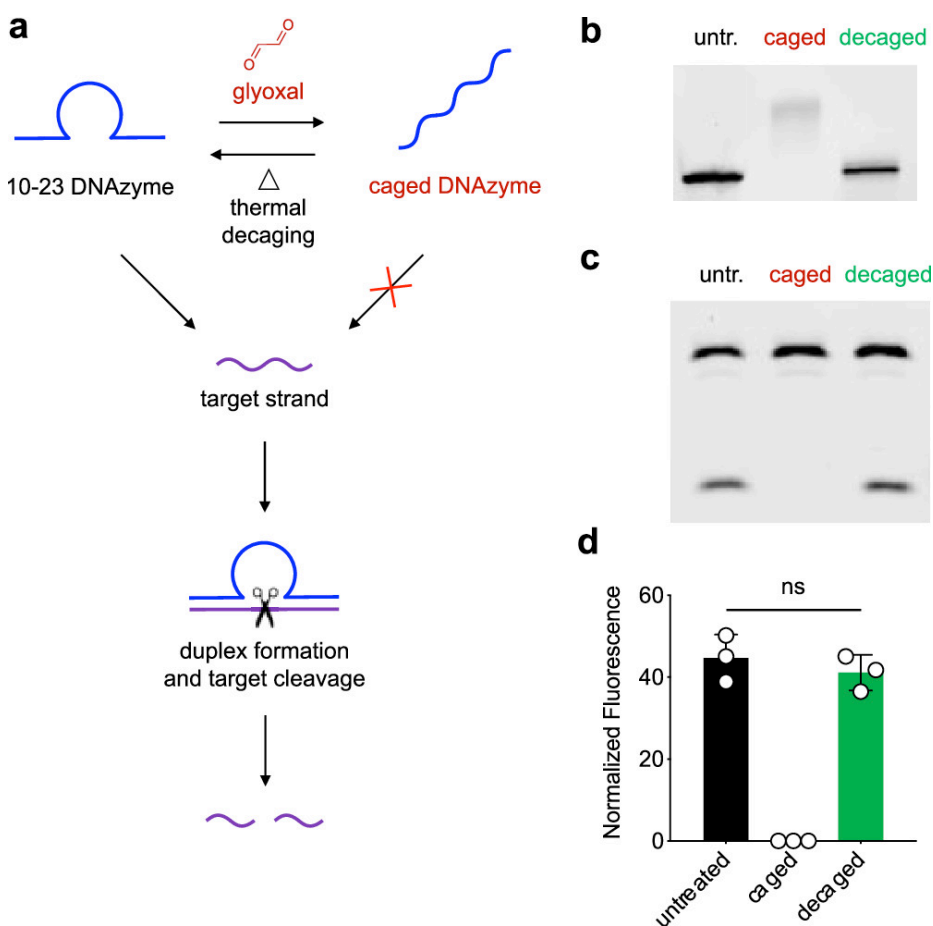


**Figure 4.2: Reversible control of the RNA-cleaving 10-23 DNAzyme.** a) Schematic of the 10-23 DNAzyme-mediated cleavage of the target strand following hybridization. Glyoxal reversibly inhibits hybridization and catalytic activity. b) 20% denaturing PAGE analysis of untreated (untr.), caged, and decaged 10-23 DNAzyme. 100 pmol of DNAzyme was first treated with 1.3 M glyoxal in 50:50 DMSO: H<sub>2</sub>O, 50 °C for 1 hour. To decage the DNAzyme, 10 pmol of caged DNA (1 hour glyoxal treatment time) was incubated at 95 °C, pH 7.5 for 10 minutes. c,d) Functional activity of untreated (untr.), caged, and decaged 10-23 DNAzyme was tested by combining 15 pmol of untreated, caged, or decaged 10-23 DNAzyme with 1.5 pmol of a target DNA strand in 10 mM MgCl<sub>2</sub>, 150 mM NaCl, 50 mM Tris-HCl, pH 7.5. Reactions were incubated for one hour at 37 °C, quenched with EDTA, and then analyzed with 12% denaturing PAGE. Percent target strand cleavage (n = 2) was quantified using band densitometry. Values represent mean and S.D. of 2 independent trials. Unpaired t-test was performed between untreated and decaged samples. “ns” indicates no significant difference.

Many functional nucleic acids benefit greatly from containing modified bases that aid in both thermal stability and nuclease resistance. Therefore, we sought to explore the effects of glyoxal on the function of these XNAs. We first tested this with the VEGF aptamer, ARC259, which is a 2'-OMe containing RNA aptamer (Figure 4.3a). To begin, we first validated caging and decaging kinetics with the new backbone. We found that there was no significant change to caging and decaging kinetics of the VEGF aptamer (Figure 4.3b). Using fluorescence polarization (FP), we observed binding of the untreated ARC259 to its VEGF target. Upon increasing caging times, we noticed a gradual decrease in binding, with binding being fully diminished after ~40 minutes. We then sought to determine the reversibility of the system. Using FP, we, again, tested the binding of the now decaged ARC259 to VEGF. We found that both the untreated and decaged aptamers exhibited similar  $K_D$ s of  $3.27 \pm 0.59$  nM and  $3.36 \pm 0.55$  nM respectively (Figure 4.3c).

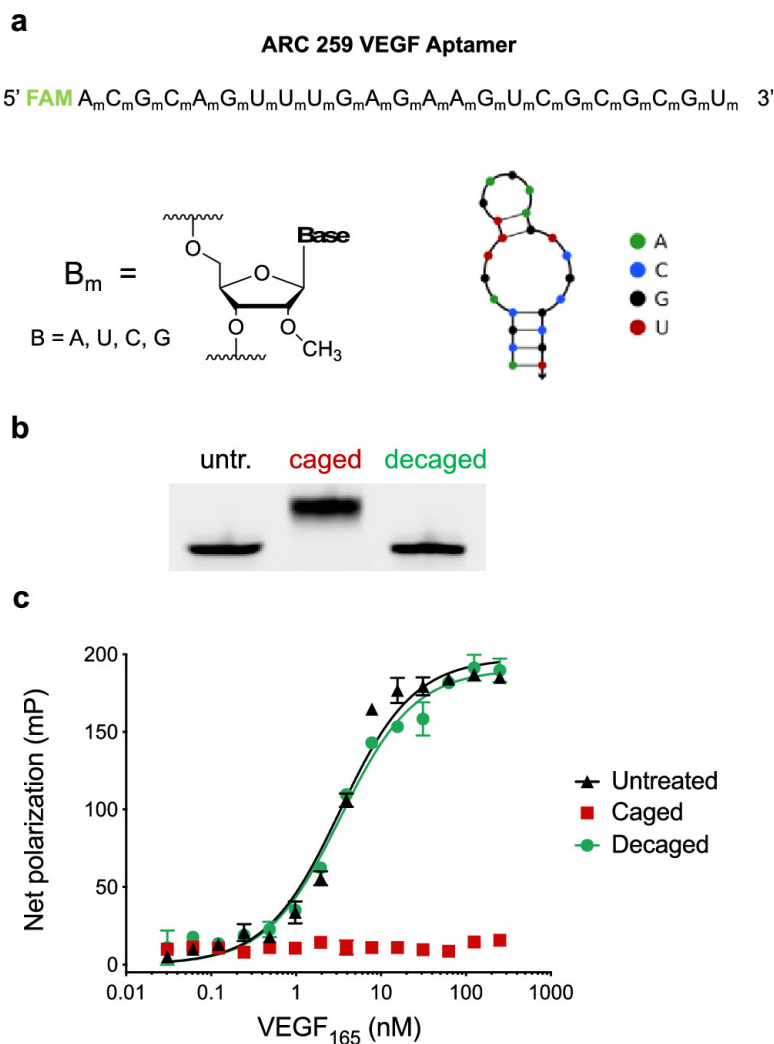


**Figure 4.3: Glyoxal caging of a fully 2'-O-methylated RNA aptamer.** a) Sequence and NUPACK fold analysis of 2'-O-methylated ARC259 RNA aptamer. b) 20% PAGE analysis of untreated (untr.), caged and decaged ARC259 aptamer. 60 pmol of RNA aptamer was first treated with 1.3 M glyoxal in 50:50 DMSO: H<sub>2</sub>O, 50 °C for 40 minutes. To decage the aptamer, 20 pmol of caged ARC259 (40 minutes glyoxal treatment time) was incubated at 95 °C, pH 7.5 for 5 minutes. c) Fluorescence polarization (FP) binding curves of untreated, caged, and decaged aptamer towards VEGF<sub>165</sub>. A 10 nM solution of untreated, caged (40 minutes glyoxal treatment time), or decaged (5 minutes at 95 °C, pH 7.5) ARC259 aptamer was combined with increasing amounts of recombinant human VEGF<sub>165</sub> and allowed to incubate at room temperature for 30 minutes. Binding reactions were then transferred to a 384-well black plate and fluorescence polarization was measured using Cytation 5 multi-mode plate reader. All values were normalized to a buffer blank and represent mean and S.D. of independent replicates (n = 3).

Encouraged by the versatility of our approach, we next tested our approach with threose nucleic acid (TNA) and peptide nucleic acid (PNA). TNA's backbone consists of repeating threose sugars connected with alternating 2' to 3' phosphodiester bonds,<sup>30</sup> and PNA consists of a peptide backbone versus a phosphodiester backbone (Figure 4.4a).<sup>31</sup> For TNA, we first determined the caging and decaging kinetics of glyoxal, and we observed comparable kinetics to that of DNA. We then evaluated the effect of caging on hybridization between TNA and a DNA complement or scrambled sequence (Figure 4.4b). Using MST to observe duplex formation, we found that as we increased caging times, we gradually notice a disruption in the duplex, with full disruption at ~40 minutes. We then decaged the TNA and observed full duplex formation (Figure 4.4c-d). To apply these experiments to PNA, we synthesized the "Nielsen decamer" sequence as a model strand.<sup>32</sup> Interestingly when characterizing caging kinetics of PNA, we noticed a decrease in molecular weight on 20% denaturing PAGE as the caging times increased (Figure 4.4e). We originally hypothesized that this was due to degradation or hydrolysis. However, we did confirm an increase in mass via mass spectrometry. We also were able to decage our PNA using heat. We hypothesize that the glyoxal may lead to a partial negative charge on the strand, leading to the opposite effect on gel electrophoresis. We then tested hybridization of the caged PNA. We observed duplex disruption as caging times increased, with full disruption occurring at 20 minutes. We then compared untreated, caged, and decaged (Figure 4.4f). We noticed full duplex formation for the decaged species. Together, these results show that glyoxal is a robust and universal method for reversibly modulating nucleic acids of all types.

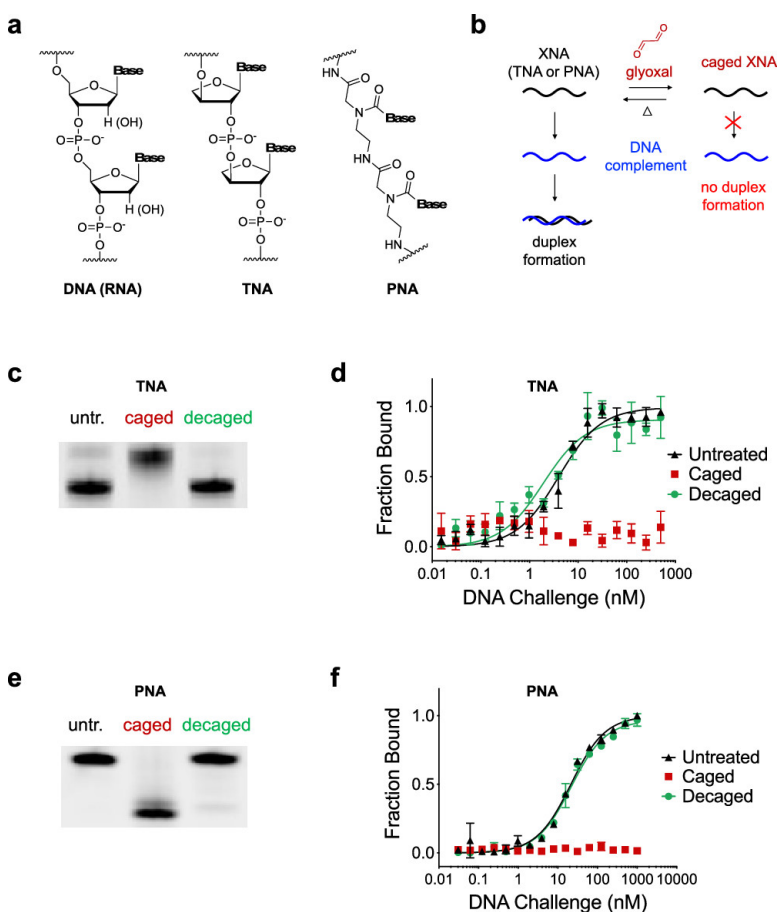


**Figure 4.4: Glyoxal caging reversibly inactivates xenonucleic acid hybridization.** a) Chemical structures of DNA/RNA alongside threose nucleic acid (TNA) and peptide nucleic acid (PNA) scaffolds. b) Heteroduplex formation between XNA strands and a DNA complement. Glyoxal caging reversibly inhibits duplex formation. c) 20% denaturing PAGE analysis of untreated (untr.), caged, and decaged TNA strands. 250 pmol of TNA strand was first treated with 1.3 M glyoxal in 50:50 DMSO: H<sub>2</sub>O, 50 °C for 40 minutes. To decage the TNA substrate, 20 pmol of caged strand (40 minutes glyoxal treatment time) was incubated at 95 °C, pH 7.5 for 5 minutes. d) MST binding curves of untreated, caged (40 minutes glyoxal treatment time), and decaged (5 minutes at 95 °C, pH 7.5) TNA strands when challenged with increasing amounts of DNA complement. Bars represent mean and S.E. from triplicate binding titration curves. e) 20% denaturing PAGE analysis of untreated (untr.), caged, and decaged PNA strands. 1 nmol of PNA was first treated with 1.3 M glyoxal in 50:50 DMSO: H<sub>2</sub>O, 50 °C for 20 minutes. To decage the PNA substrate, 20 pmol of caged strand (20 minutes glyoxal treatment time) was incubated at 95 °C, pH 7.5 for 5 minutes. f) MST binding curves of untreated, caged, and decaged PNA strands when challenged with increasing amounts of DNA complement. Bars represent mean and S.E. from triplicate binding titration curves.

### 4.3.3 Determining EcoRI efficiency

Our EcoRI enzyme must be able to fully cleave the decaged dsDNA. In this aim, we tested the efficiency of our EcoRI enzyme and our caging and decaging ability. EcoRI cleaves after the G in the recognition sequence (GAATTC) in dsDNA.<sup>132</sup> Therefore, we needed to ensure that we can hybridize the complement to the FAM labeled ssDNA. We also needed to validate that our enzyme cleaves with high efficiency. To test for this, we incubated or ssDNA alone with EcoRI. We then hybridized our ssDNA with its partial complement to produce dsDNA, which we also incubated with EcoRI. We then ran the samples on a native polyacrylamide gel with ssDNA and dsDNA alone to serve as controls. We observed no cleavage for the ssDNA sample that was incubated with EcoRI (Figure 4.5), which was expected as EcoRI only cleaves dsDNA. There was partial cleavage of the dsDNA with EcoRI, which we attributed to not having the full complementary strand as opposed to reduced efficiency of EcoRI. The dsDNA and ssDNA controls showed no difference, which we also attributed to not having the full complementary strand. We needed to ensure that we were able to fully cage and fully decage as partial caging and decaging can result in false positives and negatives. To cage the DNA, we took our ssDNA and incubated it with glyoxal for one hour. To decage, an aliquot of this sample was heated for three minutes at 95°C. These were then run on native polyacrylamide gel along with the ssDNA as a template (Figure 4.5). We observed no shift between the ssDNA and the decaged sample, indicating that we fully decaged the DNA. We did observe a complete shift for the caged sample indicating full caging.

### 4.3.2 EcoRI digestion of caged and decaged DNA

Once we validated and optimized all steps, we tested our hypothesis that by caging ssDNA using glyoxal, we can inhibit EcoRI. We first incubated ssDNA with EcoRI for one hour and two

hours separately. We also incubated ssDNA without EcoRI. We also did this for caged and decaged samples. We then ran these on a polyacrylamide native gel as seen in Figure 4.5. We observed no cleavage for the caged DNA, as expected. We also confirmed that there was hybridization. Lastly, we observed cleavage of the decaged DNA, as expected. These data supported our hypothesis that caging ssDNA with glyoxal inhibits EcoRI activity.

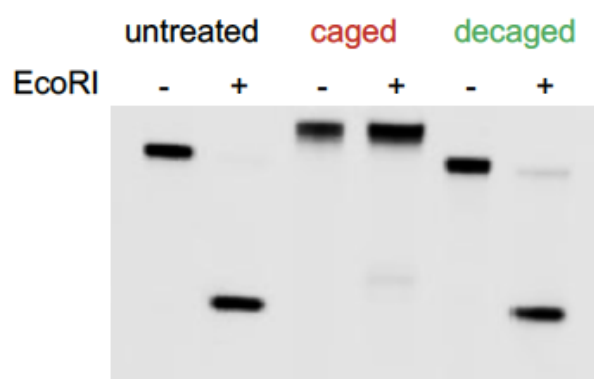


**Figure 4.5: Reversible control of EcoRI.** 12% PAGE gel of EcoRI mediated target cleavage by untreated, caged, and decaged DNA.

#### 4.3.4 Thermoreversible control of other enzymes

After exploring how glyoxal affects duplex formation and secondary structure, we were curious how caging nucleic acids would affect restriction enzyme function. RNase T1 is known to be inhibited by glyoxalation, as it cleaves after both guanosine and inosine.<sup>138, 139</sup> Taking inspiration from this, we first tested RNase H, which cleaves RNA/DNA duplexes.<sup>140</sup> We began by incubating the RNA strand with or without glyoxal. We then hybridized the target RNA to a complementary DNA strand, and exposed the sample to RNase H. As expected, we observed cleavage of untreated duplexes, while the caged ssRNA showed no cleavage. Upon thermal decaging, we

observed full cleavage activity due to RNase H. We were then curious to observe the effects of glyoxal caging on thermostable RNase H.<sup>141</sup> To test this, we combined caged target RNA, complementary DNA, and thermostable RNase H in 1X reaction buffer (50 mM Tris-HCl, 75 mM KCl, 3 mM MgCl<sub>2</sub>, 10 mM DTT, pH 8.3) in a “one pot” reaction. Reactions were then separately heated to 95°C for increasing time points, followed by 1 h at 37°C. We observed an increase in RNase H cleavage approaching 100% over 10 minutes as the target RNA strand degraded.

Next, we wanted to study the effects of glyoxal caging on RNase A, as it cleaves ssRNA and dsRNA after cytidine and uridine nucleotides.<sup>142</sup> However, we did not observe any activity inhibition in the presence of caged RNA. We observed similar results with nuclease P1, which hydrolyzes phosphodiester bonds in the 3' → 5' direction<sup>143</sup>, where we noticed no inhibition. We next tested DNase I, which cleaves dsDNA after pyrimidine nucleotides.<sup>144</sup> Similar to the other enzymes, we first treated the ssDNA with glyoxal, followed by hybridization to a complementary DNA strand. We then introduced DNase I. We noticed full inhibition upon glyoxal caging, and upon decaging, we observed full cleavage of the target DNA.

Lastly, we wanted to observe the effects of glyoxal on exonuclease activity. We first used RNase T, which cleaves both ssRNA and ssDNA from 3' to 5'.<sup>145, 146</sup> However, we noticed full hybridization even in the presence of glyoxal and no inhibition of RNase T. We observed similar results in the case of snake venom phosphodiesterase I, which hydrolyzes ssDNA and ssRNA in the 5' to 3' direction.<sup>147</sup> While these data were disappointing, exonuclease activity isn't typically sequence specific, and they typically interact with the phosphate backbone, which is not affected by glyoxal.



As seen in Table 4.2, glyoxal caging is most effective where nucleic acid secondary structure is required for enzyme recognition. Specifically, RNase H, DNase I, and EcoRI all prefer duplex formation for cleavage. Therefore, glyoxal introduction inhibits this activity by inhibiting duplex formation. With the exception of RNase T1, all other enzymes appeared to be unaffected by glyoxal, likely due to their preference for ssRNA.

**Table 4.2: Glyoxalation reversibly modulates activity in several enzymes.**

Name	Type	Target	Inhibition?
RNase T1	Endonuclease	ssRNA after G residues	Partial
RNase H	Endonuclease	RNA: DNA heteroduplexes	Yes
RNase A	Endonuclease	ssRNA, dsRNA	No
Nuclease P1	Endonuclease	ssRNA, ssDNA	No
DNase I	Endonuclease	ssDNA, dsDNA (preferred)	Yes
EcoRI	Endonuclease	dsDNA at 5' GAATTC 3'	Yes
RNase T	Exonuclease	3' exonuclease	No
Phosphodiesterase I	Exonuclease	5' exonuclease	No

#### 4.3.5 Thermoreversible control of CRISPR-Cas9

Because we analyzed the effects of glyoxal on restriction enzymes, we hypothesized that we could likely control CRISPR-Cas9 activity, as it relies on a single guide RNA (sgRNA). The

sgRNA acts as both an aptamer toward Cas9 to bind the nuclease and a sequence-specific probe to bind the ribonucleoprotein (RNP) complex to the genetic locus of interest for cleavage (Figure 4.6a).<sup>148, 149</sup> Similar to restriction enzymes, many have tried to control the CRISPR-Cas9 system. Given the control we have over nucleic acids, we first characterized the caging and decaging of the sgRNA. Over 30 minutes of caging, we only observed minimal inhibition. However, we observed a drastic decrease in cleavage after ~40 minutes - 1 hour, and full inhibition after 2 hours of caging (Figure 4.6b-d). We hypothesized that this is likely due to uridine-rich nature of the sgRNAs, which is not known to react with glyoxal. Based on our previous experiments with the aptamers, it is likely that partially caged sgRNAs are still active with Cas9. However, we observed full inhibition after 2 hours of caging and full activity after 2 minutes of decaging (Figure 4.6e-f). When compared to untreated sgRNA, there was also no significant difference in Cas9 cleavage activity when paired with a decaged sgRNA.

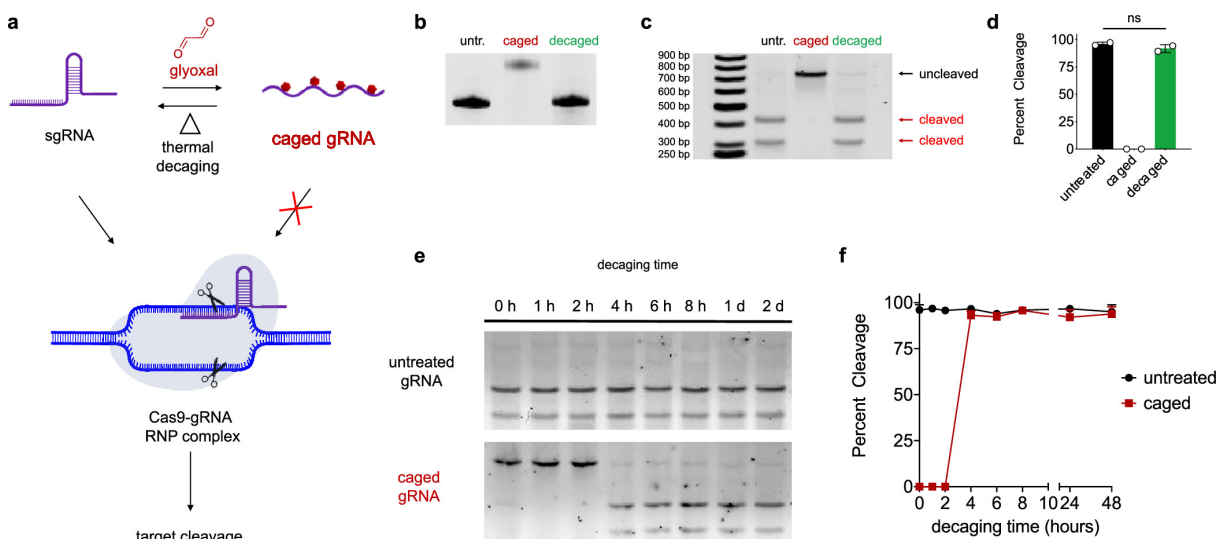


**Figure 4.6: Thermal reactivation of CRISPR-Cas9 function.** a) Schematic of reversible modulation of CRISPR-Cas9 cleavage. Glyoxal caging reversibly denatures and cages the sgRNA, preventing RNP complex formation and target cleavage. b) 20% denaturing PAGE analysis of untreated (untr.), caged, and decaged sgRNAs. 2  $\mu$ g of sgRNA was first treated with 1.3 M glyoxal in 50:50 DMSO: H<sub>2</sub>O, 50 °C for 2 hours. To decage the substrate, 2  $\mu$ g of caged sgRNA (2 hours glyoxal treatment time) was incubated at 95 °C, pH 7.5 for 5 minutes. c) Functional Cas9 target cleavage with untreated (untr.), caged, and decaged sgRNAs visualized by 1% agarose gel and d) quantified using densitometry. Bars represent mean and S.D. from 2 independent trials. Unpaired t-test was performed between untreated and decaged samples. "ns" indicates no significant difference. e) Caged sgRNAs (2 hours glyoxal treatment time) were decaged at 37 °C for increasing times and combined with Cas9 and dsDNA target followed by 1% agarose gel analysis and f) quantified using densitometry. Values represent mean and S.D. of 2 independent trials.

#### 4.3.6 Thermoreversible control in cells

After exploring decaging kinetics and a wide range of *in vitro* applications, we were interested in exploring caged nucleic acids *in cellulo*. We decided to continue forward with our studies using an antisense oligonucleotide (ASO). Controlling gene expression is emerging as a powerful strategy in cellular processes and cancer research.<sup>150, 151</sup> Therefore, we curious whether caging an ASO would allow us to explore tunable control over gene expression in living cells. To begin,

we identified an ASO optimized to silence eGFP expression by degrading its mRNA via a RNase H-mediated decay pathway (Figure 4.7a).<sup>152, 153</sup> This class of ASOs is composed of locked nucleic acid (LNA) nucleotides at both the 3' and 5' ends and contains phosphorothioate linkages throughout the strand, making these oligonucleotides highly stable and resistant to endonucleases.<sup>154-156</sup> Using glyoxal, we hypothesize that we could inhibit hybridization of the ASO to its target mRNA, thus blocking expression of eGFP (Figure 4.7b). Our previous kinetic experiments show that decaging is possible for RNA constructs at 37°C (Table 4.1). We also hypothesize that this expression could be restored upon full decaging. We were concerned that the high stability of GFP would hinder the detection of ASO activity. To circumvent this, we appended a C-terminal degron tag (supp.).

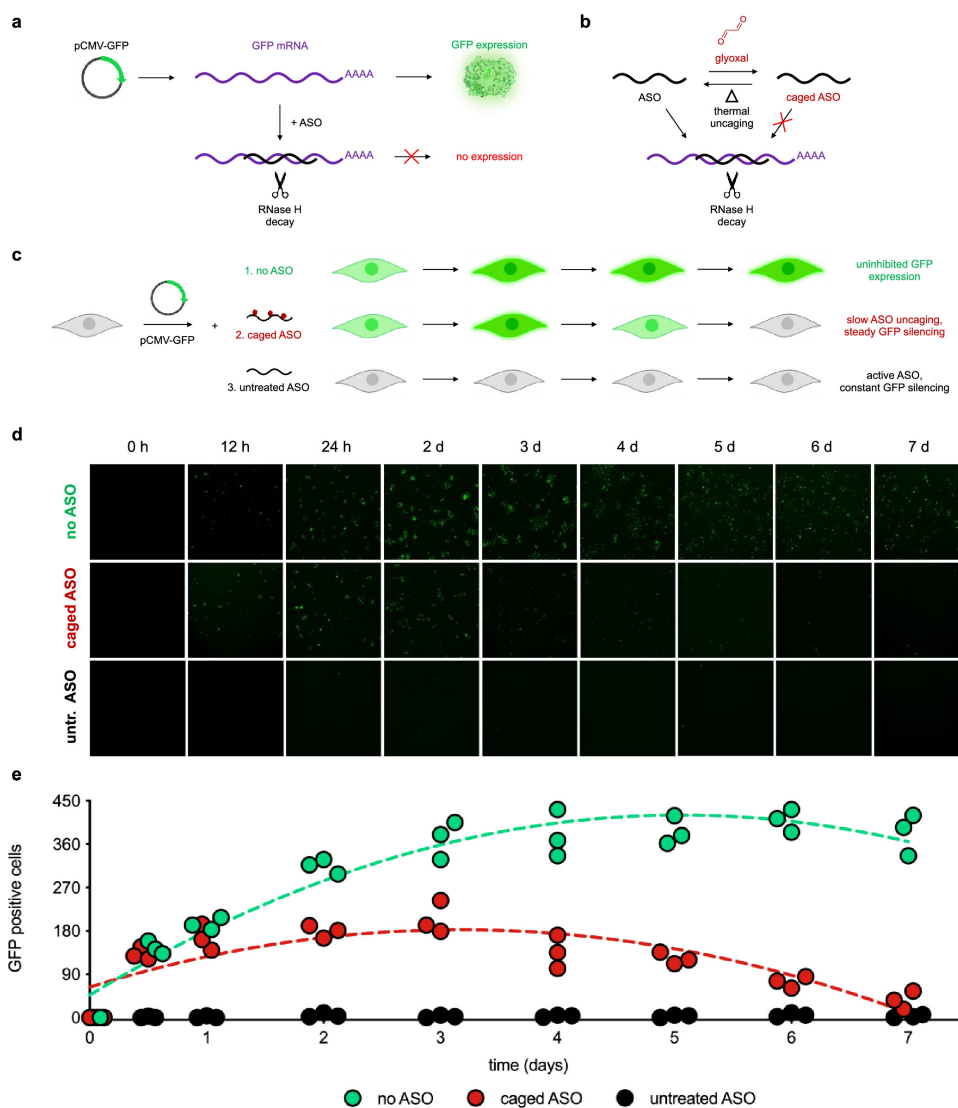


**Figure 4.7: Thermal reactivation of antisense oligonucleotide (ASO) function in cellulo.**

a) Schematic of ASO gene silencing mechanism through antisense mRNA hybridization and RNase H-mediated decay. b) Glyoxal caging reversibly blocks ASO hybridization, preventing silencing complex formation and target cleavage. c) Experimental workflow for in cellulo time-release ASO decaging. At  $t = 0$ , HEK293T cells were transfected with a pCMV-GFP plasmid as well as 250 nM glyoxal caged ASO (8 hours glyoxal treatment time, red), untreated (untr.) ASO (black) or no ASO (green). Cells receiving no ASO exhibit uninhibited GFP expression throughout the experiment, while cells given untreated (untr.) ASO produce no detectable GFP due to constant gene silencing. Cells treated with caged ASO (8 hours glyoxal treatment time) exhibit initial increase in fluorescence due to GFP expression followed by a delayed suppression of GFP signal due to time-release reactivation of glyoxalated ASO. d) Representative live-cell fluorescence microscopy images (4X magnification) taken throughout the course of the experiment. e) Quantification of GFP-positive cells in each field across treatment groups during the experimental time course. Circles represent individual wells ( $n = 3$ ) from a 96-well plate. Curves are overlaid with a second-order polynomial fit (dashed lines).

We inserted this construct into a cytomegalovirus (CMV) mammalian expression plasmid (Figure 4.7c). We then evaluated the GFP expression efficiency in HEK293T cells using fluorescence microscopy. Next, we aimed to identify an optimal ASO concentration for silencing GFP expression. At 250-500 nM of ASO, we observed no detectable GFP signal, and a scrambled sequence produced no GFP expression across all concentrations. Using these optimal conditions (250 nM ASO), we next created a library of increasingly caged ASO samples and observed the impact of glyoxal caging on GFP silencing by cotransfecting HEK293T cells with both the pCMV-GFP vector and respective ASOs. We then imaged the cells and noticed that 6-8 hours of glyoxal treatment completely inhibited ASO function. We then thought that it could be possible that glyoxal treatment could inhibit cellular uptake. However, using Cy5-labeled ASOs showed similar uptake to untreated ASOs.

Next, we explored the ability of gene expression to be restored upon decaging of the ASOs *in cellulo*. Therefore, we performed a time-course experiment to monitor GFP expression in HEK293T cells. On day 0, cells received either (1) GFP plasmid alone, (2) plasmid and a fully caged ASO (8 h glyoxal treatment time), or (3) plasmid and an untreated active ASO (Figure 4.7c). We imaged the samples over the course of 7 days (Figure 4.7d-e). We noticed that cells receiving fully caged ASO showed similar GFP increases throughout the first 24 hours as the untreated, which suggests full inhibition. However, our control cells showed increased GFP expression throughout days 2-7, and cells treated with caged ASO showed a decrease in GFP expression (Figure 4.7d-e). Lastly, cells receiving untreated ASO showed no GFP expression for the entire experiment, confirming that 250 nM ASO was sufficient for gene silencing. We then wanted to compare decaging in these conditions. Therefore, we prepared several caged ASO samples in DMEM and monitored decaging at 37°C using denaturing PAGE. We determined that

full decaging took 1-2 days. Next we decided to test the viability of our cells using a tetrazolium assay,<sup>157</sup> and we observed that no matter the degree of caging, there was no significant decrease in viability. We also tested the cytotoxicity of glyoxal alone, and we observed that glyoxal was cytotoxic at higher concentrations ( $IC_{50} = 310 \pm 83 \mu\text{M}$ ).

#### **4.4 Conclusions**

Nucleic acids are versatile and attractive materials for nanotechnology, biomedicine, and biosensing. Therefore, the ability to control their structure and function is essential in advancing the field of bioscience. However, many of the efforts for controlling nucleic acids reversibly involve chemical or light-based stimuli, which is often harmful to nucleobases and cells. In addition, many of these methods are not compatible with XNAs. Heat, however, remains unexplored as nucleic acid cages. Here, we explore glyoxal, a chemical denaturant, as a thermal cage. We show that it can impart thermoreversible inhibition of both the structure and activity of nucleic acids. We first show that glyoxal is able to cage and decage effectively from unmodified RNA and DNA over a range of different pH's, temperatures, and incubation times. We then went on to demonstrate the thermoreversibility of glyoxal with functional nucleic acids, aptamers and DNAzymes. In addition, we show that thermoreversible caging can be applied towards noncanonical XNAs as well. We also explore the reversible control of many endonucleases, as well as the CRISPR-Cas9 system. Lastly, we demonstrate that glyoxal still imparts thermoreversible gene expression in live cells. Together, this demonstrates that thermoreversible glyoxal caging can be easily applied for reversible inhibition of nucleic acid function in a multiple different applications, establishing a straightforward and effective framework for use in a variety of potential biomedical applications.

#### **4.5 Materials and Methods**

#### 4.5.1 Caging Kinetic Assays

For visualization and quantification of caging kinetics, a custom designed DNA oligonucleotide was purchased from Integrated DNA Technologies (IDT), containing a 6-FAM (Fluorescein) label at the 5' terminus as shown below.

5' FAM TGCCAAGACTGTTGAGGAAGATGAGAGAAT 3'

In triplicate, 0.2 nmol of the test DNA strand was mixed with 14.5  $\mu$ L of a 40% glyoxal solution (Sigma Aldrich) and 50  $\mu$ L DMSO. Reactions were brought to a final volume of 100  $\mu$ L with nuclease-free water, and incubated at 50  $^{\circ}$ C for 0, 5, 10, 20, 30, 40, 50, and 60 minutes. At each time point, reactions were ethanol precipitated and reconstituted in 60  $\mu$ L of nuclease-free water. 10 pmol of each purified reaction was then mixed with 2X RNA loading dye (New England Biolabs) and then separated with 20% PAGE and imaged with a GE Amersham Typhoon RGB scanner using a 488 nm excitation laser and the Cy2 525BP20 emission filter. Fiji (ImageJ) was used to calculate densitometric intensity of each reaction and normalizing to the fully caged DNA band at 60 min to estimate percent conversion. Caging half-times was estimated based on pseudo-first order rate kinetics using a nonlinear curve fit in GraphPad Prism.

#### 4.5.2 Decaging Kinetic Assays

In duplicate, 20 pmol of a fully caged (1 hour treatment) test DNA strand was incubated in a final volume of 50  $\mu$ L of phosphate buffered saline (137 mM NaCl, 2.7 mM KCl, 8 mM Na<sub>2</sub>HPO<sub>4</sub>, and 2 mM KH<sub>2</sub>PO<sub>4</sub>) adjusted to pH 6.5, 7.0, 7.5, or 8.0 where appropriate. Samples were incubated at various temperatures (25  $^{\circ}$ C, 37  $^{\circ}$ C, 50  $^{\circ}$ C, 70  $^{\circ}$ C, 95  $^{\circ}$ C) in a thermal cycler, and 3  $\mu$ L samples were taken at the indicated time points and mixed with 2X RNA loading dye (New England Biolabs) and then separated with 20% PAGE and imaged with a GE Amersham Typhoon



RGB scanner using a 488 nm excitation laser and the Cy2 525BP20 emission filter. Fiji (ImageJ) was used to calculate densitometric intensity of each reaction and normalizing to an untreated DNA band to estimate percent fully degraded. For stability at 25 °C, percent remaining was calculated using the band intensity of each reaction normalized to the fully caged DNA strand at T = 0 hours. Decaging half-times were estimated based on pseudo-first order rate kinetics using a non-linear curve fit in GraphPad Prism.

#### 4.5.3 Broccoli Aptamer Preparation

A dsDNA template gBlock containing a T7 RNA polymerase promoter (underlined) was purchased from Integrated DNA Technologies (IDT) as shown below.

5' GCTAGTAATACGACTCACTATAGTTGCCATGTGTATGTGGGAGACGGTCCGGTCCAGATATTCGTATCTGTTCGAGTAGAGTGTGGGCTCCCACATACTCTGATGATCCTTCGGGATCATTCA TGGC 3'

Template was then amplified with a forward primer (5'GCTAGTAATACGACTCACTATA GGGTTGCC 3') and reverse primer 5' GCCATGAATGATCCCGAAGGATCATCA 3') using HotStart Taq DNA polymerase (New England Biolabs) according to the manufacturer's instructions, using the following PCR program: 94 °C for 3 min, followed by 30 cycles of (94 °C for 1 m, 57 °C for 45 s, 68 °C for 1 m), 68 °C for 5 min. PCR reactions were then purified using the Monarch PCR & DNA Cleanup Kit (New England Biolabs). RNA was then synthesized and purified using the HiScribe T7 High Yield RNA Synthesis Kit and Monarch RNA Cleanup Kit (New England Biolabs).

#### 4.5.4 Broccoli Aptamer Caging and Functional Fluorogenic Analysis

60pmol (~2 µg) of broccoli RNA aptamer was mixed with 14.5 µL of a 40% glyoxal solution (Sigma Aldrich) and 50 µL DMSO. Reactions were brought to a final volume of 100 µL with

nuclease-free water and reacted at 50 °C for 0 min, 30 sec, 5 min, 10 min, 15 min, 20 min, 25 min, 30 min, and 1 hour. At each time point, reactions were ethanol precipitated and reconstituted in 25 µL of nuclease-free water. 10 pmol of each purified reaction was then mixed with 2X RNA loading dye (New England Biolabs) and then separated with 10% denaturing PAGE. Gels were then stained with 1X SYBR Gold solution (Thermo Fisher Scientific) for 20 minutes, and visualized with the Typhoon RGB scanner. Functional fluoregenic activity of the broccoli RNA aptamer was performed by mixing 20 pmol of untreated, caged, or decaged aptamer with 2 µM 3,5-difluoro-4-hydroxybenzylidene imidazolinone (DFHBI, Sigma Aldrich), 40 mM HEPES, 100 mM KCl, 1 mM MgCl<sub>2</sub>, pH 7.4 in a final volume of 20 µL. Reactions were incubated for 30 minutes at 37 °C. Reaction tubes were imaged with the GE Amersham Typhoon RGB scanner using a 488 nm excitation laser and the Cy2 525BP20 emission filter. Fluorescence was also quantified by transferring the reactions to 384-well black plates (Greiner) and measuring intensity on a Cytation 5 multi-mode plate reader (BioTek) using excitation at 447 nm and emission at 501 nm.

#### *4.5.5 Broccoli Aptamer Decaging*

To remove glyoxal adducts, 20 pmol of minimally caged (10 minute glyoxal treatment) broccoli RNA aptamer was added to a final volume of 50 µL of phosphate buffered saline (137 mM NaCl, 2.7 mM KCl, 8 mM Na<sub>2</sub>HPO<sub>4</sub>, 2 mM KH<sub>2</sub>PO<sub>4</sub>, pH 7.5). Samples were incubated in a thermal cycler at 95 °C for indicated times and purified by ethanol precipitation. 10 pmol of the collected RNAs were then combined with DFHBI and analyzed as described above.

#### *4.5.6 In Situ Broccoli Aptamer Decaging*

20 pmol of minimally caged broccoli RNA aptamer was combined with 2 µM DFHBI, 40 mM HEPES, 100 mM KCl, 1 mM MgCl<sub>2</sub>, pH 7.4 in a final volume of 20 µL. Reactions were

incubated in a thermal cycler set at 60 °C, 65 °C, 70 °C, 75 °C, 80 °C, 85 °C, 90 °C, and 95 °C and allowed to react for 0, 5, 10, 20, 30 and 60 minutes. Reactions were quenched by freezing at -80 °C. Reactions were then thawed at room temperature and transferred to a 384-well black plate with a clear bottom (Greiner) and imaged and analyzed as described earlier. Heatmap image was obtained using the Typhoon acquisition software and reflects relative fluorescent intensities.

#### *4.5.7 10-23 DNAzyme Caging and Functional Assay*

The 10-23 DNAzyme oligonucleotide was purchased from IDT as shown below:

5' - AGGACGGGAGGCTAGCTACAACGAGTGGTTGCC- 3'

100 pmol of DNAzyme was mixed with 14.5  $\mu$ L of a 40% glyoxal solution (Sigma Aldrich) and 50  $\mu$ L DMSO. Reactions were brought to a final volume of 100  $\mu$ L with nuclease-free water and reacted at 50 °C for 0 min, 1 min, 5 min, 10 min, 20 min, 30 min, 40 min, and 1 hour. At each time point, reactions were ethanol precipitated and reconstituted nuclease-free water at a final concentration of 1  $\mu$ M. 10 pmol of each purified reaction was then mixed with 2X RNA loading dye (New England Biolabs) and then separated with 20% denaturing PAGE. Gels were then stained with 1X SYBR Gold solution (Thermo Fisher Scientific) for 20 minutes and visualized with the Typhoon RGB scanner. To test functional cleavage activity, 15 pmol of untreated or caged 10-23 DNAzyme were added to 1.5 pmol of target strand: (5' FAM GGCAACCACrGTCCCGTCCT BHQ1 3', rG indicates ribonucleotide guanosine) in DNAzyme buffer (10 mM MgCl<sub>2</sub>, 150 mM NaCl, 50 mM Tris-HCl, pH 7.5) at a total volume of 50  $\mu$ L. The reaction was incubated in a thermocycler for one hour at 37 °C and quenched with addition of 1  $\mu$ L of 125 mM EDTA. All samples were then analyzed with 12% denaturing PAGE, stained with 1X SYBR Gold solution (Thermo Fisher

Scientific) for 20 minutes and visualized with the Typhoon RGB scanner. Percent cleavage was calculated by densitometry analysis of the cleaved band/sum using ImageJ software.

#### 4.5.8 10-23 DNAzyme Decaging

To decage the 10-23 DNAzyme, we first determined the minimum amount of thermal decaging time required for the gel shift to return to the original size. 10 pmol DNAzyme was suspended in 1X PBS and incubated at 95 °C for 30 seconds, 1 min, 2 min, 3 min, 5 min, 8 min, and 10 mins. The samples were ethanol precipitated and resuspended at a concentration of 1 µM. The size shift from glyoxal removal was monitored by 20% denaturing PAGE. Optimal timepoints for caging (1 h) and decaging (10 minute) were then analyzed for size shift with untreated 10-23 DNAzyme on 20% denaturing PAGE. For full tuning of activity, we performed the cleavage assay with untreated, caged, and decaged 10-23 DNAzyme. 15 pmol of untreated, caged, or decaged 10-23 DNAzyme were added to 1.5 pmol of target strand in DNAzyme buffer in a total volume of 50 µL. The reaction was incubated for one hour at 37 °C and quenched with the addition of 1 µL of EDTA at 125 mM. All samples were then analyzed on 12% denaturing PAGE. Densitometry analysis was performed using ImageJ software. Percent cleavage was calculated by dividing the band intensity of the cleaved product by the sum of all band intensities in that lane.

#### 4.5.9 ARC259 Aptamer Caging

ARC259 2'-O-Methylated RNA aptamer was purchased from Integrated DNA Technologies, containing a 6-FAM (Fluorescein) label at the 5' terminus as shown below (m indicates 2'-O-Methylated modification).

5' FAM mAmCmGmCmAmGmUmUmUmGmAmGmAmAmGmUmCmGmCmGmCmGmU 3'

60pmol (~2 µg) of ARC259 aptamer was mixed with 14.5 µL of a 40% glyoxal solution (Sigma Aldrich) and 50 µL DMSO. Reactions were brought to a final volume of 100 µL with nuclease-free water and reacted at 50 °C for 0 min, 30 sec, 5 min, 10 min, 15 min, 20 min, 25 min, 30 min, and 1 hour. At each time point, reactions were ethanol precipitated and reconstituted in 25 µL of nuclease-free water. 5 pmol of each reaction was analyzed by 20% denaturing PAGE.

#### *4.5.10 ARC259 Aptamer Decaging*

20 pmol of minimally caged (40 minute glyoxal treatment) ARC259 aptamer was added to a final volume of 50 µL of phosphate buffered saline (137 mM NaCl, 2.7 mM KCl, 8 mM Na<sub>2</sub>HPO<sub>4</sub>, 2 mM KH<sub>2</sub>PO<sub>4</sub>, pH 7.5). Samples were incubated in a thermal cycler at 95 °C for indicated times and purified by ethanol precipitation. 10 pmol of the collected RNAs were then analyzed by 20% denaturing PAGE as described above.

#### *4.5.11 VEGF Fluorescence Polarization Binding Assay*

A 20 nM solution of untreated, caged, or decaged ARC259 aptamer was prepared in 1X binding buffer (phosphate buffered saline 137 mM NaCl, 2.7 mM KCl, 8 mM Na<sub>2</sub>HPO<sub>4</sub>, 2 mM KH<sub>2</sub>PO<sub>4</sub>, pH 7.5 with 0.05% Tween 20). A 30 µM solution of recombinant human VEGF165 (Peprotech) or bovine serum albumin (BSA, Sigma Aldrich) was prepared in 1X binding buffer and serially diluted 1:1 several times. Dilutions were combined with an equal volume of 20 nM ARC259 to yield final conditions in all samples of 10 nM ARC259, 1X binding buffer, and protein (VEGF or BSA) ranging from ~30 pM to 250 nM in a final volume of 40 µL. Binding reactions were allowed to incubate at room temperature for at least 30 minutes, and then transferred to a 384-well black plate. Fluorescence polarization was measured using Cytation 5 multi-mode plate reader (BioTek) equipped with a Blue/UV FP filter cube. All measurements were performed using

a 360/40 excitation and 460/40 emission filter set in combination with a 400 nm cut off dichroic mirror. Net values were computed by subtracting FP values calculated from blank (buffer) wells.

#### *4.5.12 TNA Oligonucleotide Synthesis and Labeling*

TNA phosphoramidites were synthesized according to previously published methods for solid phase synthesis of TNA oligonucleotides.<sup>158</sup> A custom TNA oligonucleotide was synthesized and purchased from the University of Utah DNA/Peptide Synthesis Core Facility as shown below:

3' CATGACATGAGCTAACCAGACAG 2'

TNA was fluorescently labeled with Cyanine 5 (Cy5) using the Label IT® Tracker™ Intracellular Nucleic Acid Localization Kit (Mirus Bio) according to the manufacturer's instructions. The oligonucleotide was ethanol precipitated and analyzed by UV/Vis spectrophotometry to measure degree of labeling, confirming approximately 2 dye molecules per strand.

#### *4.5.13 TNA Caging*

250 pmol of TNA oligonucleotide was mixed with 14.5  $\mu$ L of a 40% glyoxal solution (Sigma Aldrich) and 50  $\mu$ L DMSO. Reactions were brought to a final volume of 100  $\mu$ L with nuclease-free water and reacted at 50 °C for 0 minutes, 5 minutes, 10 minutes, 20 minutes, 30 minutes, 40 minutes, 50 minutes, and 1 hour. At each time point, reactions were ethanol precipitated and reconstituted in 25  $\mu$ L of nuclease-free water. 5 pmol of each reaction was analyzed by 20% denaturing PAGE and imaged with a GE Amersham Typhoon RGB scanner using a 635 nm excitation laser and the Cy5 670BP30 emission filter.

#### *4.5.14 TNA Decaging*

20 pmol of minimally caged (40 minute glyoxal treatment) TNA oligonucleotide was added to a final volume of 50  $\mu$ L of phosphate buffered saline (137 mM NaCl, 2.7 mM KCl, 8 mM  $\text{Na}_2\text{HPO}_4$ , 2 mM  $\text{KH}_2\text{PO}_4$ , pH 7.5). Samples were incubated in a thermal cycler at 95  $^\circ\text{C}$  for 5 minutes and purified by ethanol precipitation. 5 pmol of collected TNA was then analyzed by 20% denaturing PAGE as described above.

#### 4.5.15 TNA Hybridization Assays

To test hybridization, a full complement and scrambled DNA oligonucleotide was purchased from Integrated DNA Technologies as shown below.

TNA complement: 5' CTGTCTGGTTAGCTCATGTCATG 3'

TNA scrambled: 5' ACTCTGTTCCGGTACTGGTCTTG 3'

For each hybridization test, a 10 nM solution of untreated, caged, or decaged Cy5-labeled TNA strand was prepared in 1X binding buffer (40 mM HEPES, 100 mM KCl, 1 mM  $\text{MgCl}_2$ , 0.05% Tween 20, pH 7.4). A 1  $\mu$ M solution of complement and scrambled DNA was prepared in 1X binding buffer and serially diluted 1:1 several times. Dilutions were combined with an equal volume of 10 nM TNA solution to yield final conditions in all samples of 5 nM TNA strand, 1X binding buffer, and DNA challenge (complement or scramble) ranging from ~152 pM to 500 nM in a final volume of 100  $\mu$ L. Samples were incubated at room temperature for 30 minutes and then loaded into NT.115 standard glass capillaries. MST experiments were performed using a Nanotemper Monolith NT.115 Pico instrument. All measurements were analyzed using the Pico-RED filter with 20% LED intensity and low laser power.

#### 4.5.16 PNA Oligomer Synthesis

A fluorescently labeled PNA strand was synthesized using a standard solid-phase synthesis protocol on a Biotage SP wave semi-automatic synthesizer. Sequence is shown below. FAM denotes fluorescein, and E denotes a single glutamate residue (structure shown in Figure S14a).

N - FAM GTAGATCACT E - C

Synthesis began by loading 69.1 mg of a rink amide MBHA resin (0.52 mmol/g) with 5  $\mu$ mol of Fmoc-L-glutamic acid  $\gamma$ -*tert*-butyl ester using 1.5 eq. HATU, 1.5 eq. DIPEA, and 1.5 eq. 2,6-lutidine in 200  $\mu$ L dry NMP for 1 hour followed by a 1 hour capping step using a solution of 9% acetic anhydride and 13% 2,6-lutidine in DMF. The resin was then deprotected with a solution of 25% piperidine in DMF. For monomer couplings, 5 eq. of monomer was pre-activated for 10 minutes with 5 eq. HATU, 5 eq. DIPEA, and 5 eq. 2,6-lutidine in 400  $\mu$ L NMP before addition to the resin. Coupling proceeded with microwave-assistance at 75°C for 6 min. The resin was then washed (5x1 mL DMF), capped using the capping solution (2x5 min with 1 mL each), washed (5x1 mL DMF, 3x1 mL DCM, 3x1 mL DMF), deprotected with deprotection solution (3x2 min with 1mL each), and washed (5x1 mL DMF, 3x1 mL DCM, 3x1 mL DMF) to complete a coupling cycle. Upon completion of synthesis, the resin was washed with DCM and dried before cleavage using a solution of 2.5% H<sub>2</sub>O and 2.5% TIS in TFA. The crude oligomer was ether precipitated, washed with ether, and dried for purification. Purification was performed by reverse-phase HPLC using an Agilent Eclipse XDB-C18 5  $\mu$ m, 9.4x250 mm column at 60°C with a flow rate of 2 mL/min, monitored at 260 nm using a linear gradient (10%-40% in 15 min) of 0.1% TFA/acetonitrile in 0.1% TFA/H<sub>2</sub>O. Identity of pure oligomer was confirmed using an Agilent 6230 electrospray ionization time-of-flight (ESI-TOF) mass spectrometer.



#### Abbreviations:

Fmoc, fluorenylmethyloxycarbonyl; HATU, 1- [Bis(dimethylamino)methylene]-1*H*-1,2,3-triazolo[4,5-*b*]pyridinium 3-oxid hexafluorophosphate; DIPEA, diisopropylethylamine; NMP, N-methyl-2-pyrrolidone; DCM, dichloromethane; TIS, triisopropylsilane; TFA, trifluoroacetic acid.

#### 4.5.17 PNA Caging

1 nmol of PNA oligonucleotide was mixed with 14.5  $\mu$ L of a 40% glyoxal solution (Sigma Aldrich) and brought to a final volume of 100  $\mu$ L with nuclease-free water. Samples were reacted at 50 °C for 0 minutes, 5 minutes, 10 minutes, 20 minutes, 30 minutes, 1 hour, 2 hours, and 4 hours. At each time point, reactions were purified with reverse-phase HPLC using an Agilent Eclipse Plus C18 3.5  $\mu$ m, 4.6x150 mm column at 60°C with a flow rate of 1 mL/min, monitored at 260 nm using a linear gradient (10% - 50% in 20 min) of 0.1% TFA/acetonitrile in 0.1% TFA/H<sub>2</sub>O. Collected fractions were dried under vacuum and then resuspended in 50  $\mu$ l phosphate buffered saline (137 mM NaCl, 2.7 mM KCl, 8 mM Na<sub>2</sub>HPO<sub>4</sub>, 2 mM KH<sub>2</sub>PO<sub>4</sub>, pH 7.5). 10 pmol of each reaction was analyzed by 20% denaturing PAGE as described earlier.

#### 4.5.18 PNA Decaging

250 pmol of caged (2 h glyoxal treatment) PNA strand was added to a final volume of 50  $\mu$ L of phosphate buffered saline (137 mM NaCl, 2.7 mM KCl, 8 mM Na<sub>2</sub>HPO<sub>4</sub>, 2 mM KH<sub>2</sub>PO<sub>4</sub>, pH 7.5). Samples were incubated in a thermal cycler at 95 °C for 0 minutes, 1 minutes, 2 minutes, 5 minutes, 10 minutes and 20 minutes. 5 pmol of each reaction was then analyzed by 20% denaturing PAGE as described above.

#### 4.5.19 PNA Hybridization Assays

To test hybridization, a full complement and scrambled DNA oligonucleotide was purchased from Integrated DNA Technologies as shown below.

PNA complement: 5' AGTGATCTAC 3'

PNA scrambled: 5' CTATGGTACA 3'

For each hybridization test, a 20 nM solution of untreated, caged, or decaged Cy5-labeled PNA strand was prepared in 1X binding buffer (40 mM HEPES, 100 mM KCl, 1 mM MgCl<sub>2</sub>, 0.05% Tween 20, pH 7.4). A 1 μM solution of complement and scrambled DNA was prepared in 1X binding buffer and serially diluted 1:1 several times. Dilutions were combined with an equal volume of 10 nM PNA solution to yield final conditions in all samples of 5 nM PNA strand, 1X binding buffer, and DNA challenge (complement or scramble) ranging from ~152 pM to 500 nM in a final volume of 100 μL. Samples were incubated at room temperature for 30 minutes and then loaded into NT.115 standard glass capillaries. MST experiments were performed using a Nanotemper Monolith NT.115 Pico instrument. All measurements were analyzed using the Pico-RED filter with 20% LED intensity and low laser power.

#### 4.5.20 RNase H assays

An RNA oligonucleotide containing a 6-FAM modifier was purchased from IDT as shown below:

5' FAM rArArGrCrArGrCrArGrGrCrUrArUrGrUrUrArGrArArCrArArU 3'

To demonstrate duplex requirement for activity, 5 pmols of this RNA was then hybridized to 5 pmols of complementary DNA (5'- ATTGTTCTAACATAGCCTGCTGCTT -3') in 1X RNase H buffer (New England Biolabs) in a total volume of 50 μL for 30 minutes at 37 °C. After

hybridization, 5 units of RNase H (New England Biolabs) were added to 10  $\mu$ L of each sample. Reactions were incubated for one hour at 37 °C and halted with addition of 1  $\mu$ L of 125 mM EDTA. Samples were then analyzed with 12 % non-denaturing native PAGE.

To inhibit RNase H activity through caging, 100 pmol of RNA was mixed with 14.5  $\mu$ L of a 40% glyoxal solution (Sigma Aldrich) and 50  $\mu$ L DMSO and brought to a final volume of 100  $\mu$ L with nuclease-free water. RNA was caged at 50 °C for 2 h. RNA was then ethanol precipitated and resuspended in nuclease free water at a final concentration of 1  $\mu$ M. 5 pmols of RNA was then hybridized to 5 pmol of complementary DNA (5'- TTCGTCGTCCGATAACAATCTTGTTA -3') in 1X RNase H buffer (New England Biolabs) in a total volume of 50  $\mu$ L for 30 minutes at 37 °C. After hybridization, 5 units of RNase H (New England Biolabs) were added to 10  $\mu$ L of each sample. Reactions were incubated for one hour at 37 °C and halted with addition of 1  $\mu$ L of 125 mM EDTA. Densitometry analysis was performed using ImageJ software. Percent cleavage was calculated by dividing the band intensity of the cleaved product by the sum of all band intensities in that lane. To decage the strand, 10 pmol of caged RNA was incubated in 1X PBS, pH 7.5 at 95 °C for 5 minutes. RNA was then ethanol precipitated and resuspended at a concentrated of 1  $\mu$ M. RNA size shift was analyzed via 20% denaturing PAGE. For full tuning of RNase H activity, we performed the cleavage assay with untreated, caged, and fully decaged RNA. To separate tubes, 5 pmol of the untreated, caged, or decaged RNA were hybridized to 5 pmol of complementary DNA in 1X RNase H1 buffer in a total volume of 50  $\mu$ L at 37 °C for 30 minutes. RNase H1 (5 units) was added to 10  $\mu$ L of each reaction and incubated for one hour at 37 °C. Cleavage was halted with the addition of 1  $\mu$ L of 125 mM EDTA.

#### 4.5.21 *Thermostable RNase*

For one pot decaging of Thermostable RNase H activity, 10 pmol of untreated, caged, or decaged RNA were hybridized with 10 pmol of complementary DNA in 1X RNase H buffer in a total volume of 100  $\mu$ L at 37 °C for 30 minutes. 5 units of Thermostable RNase H (New England Biolabs) was added to 10  $\mu$ L of each duplex (untreated, caged, decaged) and incubated at 90 °C for 0, 0.5, 1, 2, 3, 5, 8, 10 minutes followed by incubation at 37 °C for one hour. Cleavage was halted with the addition of 1  $\mu$ L of 125 mM EDTA. Activity was then measured using 12% denaturing PAGE as described earlier.

#### 4.5.22 RNase A Assay

To test RNase A, we used the same RNA sequence as shown above in RNase H assays. Caging and decaging conditions were also identical as described earlier. RNase A (Sigma Aldrich, ~0.02 units at 0.5  $\mu$ g/mL) was added to 1 pmol of untreated, caged, or decaged RNA diluted to 10  $\mu$ L in 1X PBS, pH 7.5. Reactions were incubated for one hour at 37 °C and halted with the addition of 1  $\mu$ L of 125 mM EDTA. Activity was then measured using 12% denaturing PAGE as described earlier.

#### 4.5.23 Nuclease P1 Assay

To test Nuclease P1, we used the same fluorescein labeled RNA as shown earlier in RNase H assays (5' FAM rArArGrCrArGrCrArGrGrCrUrArUrGrUrUrArGrArArCrArArU 3') and the same fluorescein labeled DNA as used in glyoxal caging kinetics (5' FAM TGCCAAGACTGTT-GAGGAAGATGAGAGAAT 3'). Caging and decaging conditions were also identical as described earlier. Nuclease P1 (New England Biolabs, 1 unit) was added to 1 pmol of untreated, caged, or decaged RNA in a total volume of 10  $\mu$ L in 1X Nuclease P1 buffer (New England Biolabs).

Reactions were incubated for 15 minutes at 37 °C and halted by addition of 1 µL of 125 mM EDTA. All samples were then analyzed on 12% denaturing PAGE.

#### 4.5.24 DNase I Assay

To test DNase I, we used the fluorescein labeled DNA sequence as described in the glyoxal caging kinetics section (5' FAM TGCCAAGACTGTTGAGGAAGATGAGAGAAT 3'). To inhibit DNase activity through caging, 100 pmol of target DNA was mixed with 14.5 µL of a 40% glyoxal solution (Sigma Aldrich) and 50 µL DMSO and brought to a final volume of 100 µL with nuclease-free water. DNA was caged at 50 °C for 1 h. DNA was then ethanol precipitated and resuspended in nuclease free water at a final concentration of 1 µM. To decage the strand, 10 pmol of caged DNA was incubated in 1X PBS, pH 7.5 at 95 °C for 5 minutes. DNA was then ethanol precipitated and resuspended at a concentration of 1 µM. In separate tubes, 10 pmol of untreated, caged, and decaged labeled strand was combined with 10 pmol of a complementary DNA strand (5' ATTCTCTCATCTTCCTCAACAGTCTTGGCA 3') in 100 µL 1X DNase buffer (Thermo Fisher) at 37 °C for 30 minutes. After hybridization, 0.2 units of DNase I (Thermofisher) were added to 10 µL of untreated, caged, or decaged duplexes. Reactions were incubated for one hour at 37 °C and halted with addition of 1 µL of EDTA at 125 mM. All samples were then analyzed with 12% denaturing PAGE.

#### 4.5.25 EcoRI Assay

An DNA oligonucleotide containing a 6-FAM modifier was purchased from IDT as shown below (cut site underlined):

5' FAM TGCCGTACCAGAATTCGCTTAGATGT 3'

To inhibit restriction endonuclease activity through caging, 100 pmol of DNA was mixed with 14.5  $\mu$ L of a 40% glyoxal solution (Sigma Aldrich) and 50  $\mu$ L DMSO and brought to a final volume of 100  $\mu$ L with nuclease-free water. DNA was caged at 50 °C for 2 h. DNA was then ethanol precipitated and resuspended in nuclease free water at a final concentration of 1  $\mu$ M. To decage the strand, 10 pmol of caged DNA was incubated in 1X PBS, pH 7.5 at 95 °C for 5 minutes. DNA was then ethanol precipitated and resuspended at a concentrated of 1  $\mu$ M. In separate tubes, 10 pmol of the untreated, caged, or decaged DNA was hybridized to 10 pmol of complementary DNA (5' ACATCTAAGCGAATTCTGGTACGGCA 3') in 1X CutSmart buffer (New England Biolabs) in a total volume of 100  $\mu$ L for 30 minutes at 37 °C. After hybridization, 20 units of EcoRI-HF (New England Biolabs) was added to 10  $\mu$ L of each sample. Reactions were incubated for one hour at 37 °C and halted with the addition of 1  $\mu$ L of 125 mM EDTA. All samples were then analyzed on 12% denaturing PAGE.

#### 4.5.26 RNase T Assay

To test RNase T, we used the same fluorescein labeled RNA as shown earlier in RNase H assays (5' FAM rArArGrCrArGrCrArGrGrCrUrArUrGrUrUrArGrArArCrArArU 3') and the same fluorescein labeled DNA as used in glyoxal caging kinetics (5' FAM TGCCAAGACTGTTGAG-GAAGATGAGAGAAT 3'). Caging and decaging conditions were also identical as described earlier. RNase T (New England Biolabs, 5 units) was added to 1 pmol of untreated, caged, or decaged RNA and DNA where appropriate in 10  $\mu$ L 1X NEBuffer™ 4 (New England Biolabs). Reactions were incubated for one hour at 25 °C and halted with the addition of 1  $\mu$ L of 125 mM EDTA. All samples were then analyzed on 12% denaturing PAGE.

#### 5.5.27 Phosphodiesterase I Assay

To test phosphodiesterase I, we used the same fluorescein labeled RNA as shown earlier in RNase H assays (5' FAM rArArGrCrArGrCrArGrGrCrUrArUrGrUrUrArGrArArCrArArU 3') and the same fluorescein labeled DNA as used in glyoxal caging kinetics (5' FAM TGCCAA-GACTGTTGAGGAAGATGAGAGAAT 3'). Caging and decaging conditions were also identical as described earlier. Snake venom phosphodiesterase I isolated from *Crotalus adamanteus* (Sigma Aldrich, 0.005 units) was added to 1 pmol of untreated, caged, or decaged RNA and DNA where appropriate in 10  $\mu$ L 1X CutSmart buffer (New England Biolabs). Reactions were incubated for one hour at 37 °C and halted with the addition of 1  $\mu$ L of 125 mM EDTA. All samples were then analyzed on 12% denaturing PAGE.

#### 4.5.28 Cas9 sgRNA Preparation

The following dsDNA gBlock containing a T7 RNA polymerase promoter (underlined) was purchased from IDT as shown below.

5'CCCGGGTTCTAATACGACTCACTATAGGGAGCGCACCATCTTCTTCAGTTTTAGAGCTA-  
GAAATAGCAAGTTAAATAAGGCTAGTCCGTTATCAACTTGAAAAAGTGGCACCGAGTC  
GGTGCTTTT 3'

Template was then amplified with a forward primer (5' CCCGGGTTCTAATACGACTCACTATAG 3') and reverse primer 5' AAAAGCACCGACTCGGTGC 3') using HotStart Taq DNA polymerase (New England Biolabs) according to the manufacturer's instructions, using the following PCR program: 94 °C for 3 min, followed by 30 cycles of (94 °C for 1 m, 56 °C for 45 s, 68 °C for 1 m), 68 °C for 5 m. PCR reactions were then purified using the Monarch PCR & DNA Cleanup Kit (New England Biolabs). DNA was then loaded onto a 1% agarose gel and the desired 126 bp band was excised from the gel and purified using the Monarch DNA Gel Extraction Kit. RNA was then

synthesized and purified using the HiScribe T7 High Yield RNA Synthesis Kit and Monarch RNA Cleanup Kit (New England Biolabs) to yield the full sgRNA sequence shown below:

5'GGAGCGCACCAUCUUCUUCAGUUUUAGAGCUAGAAAUAGCAAGUUAAAAU-  
AAGGCUAGUCCGUUAUCAACUUGAAAAAGUGGCACCGAGUCGGUGCUUUU 3'

#### 4.5.29 dsDNA Target Preparation

A 720 bp region of dsDNA was amplified from a plasmid encoding eGFP (Addgene #60733) sgRNA docking region in bold, cleavage site underlined:

5'ATGGTGAGCAAGGGCGAGGAGCTGTTACCGGGGTGGTGCCCATCCTGGTTCGAGCTGG  
ACGGCGACGTAAACGGCCACAAGTTCAGCGTGTCCGGCGAGGGCGAGGGCGATGCCACC  
TACGGCAAGCTGACCCTGAAGTTCATCTGCACCACCGGCAAGCTGCCCGTGCCCTGGCCC  
ACCCTCGTGACCACCCTGACCTACGGCGTGCAAGTTCAGCCGCTACCCCGACCACATG  
A AGCAGCACGACTTCTTCAAGTCCGCCATGCCCGAAGGCTACGTCC**GGAGCGCACCAT**  
**CTTCTTCA**AAGGACGACGGCAACTACAGACCCGCGCCGAGGTGAAGTTCGAGGGCGACAC  
CCTGGTGAACCGCATC GAGCTGAAGGGCATCGACTTCAAGGAGGACGGCAACATCCTGG  
GGCACAAGCTGGAGTACAACACTACAACAGCCACAACGTCTATATCATGGCCGACAAGCAGA  
AGAACGGCATCAAGGTGAACTTCAAGATCCGCCACAACATCGAGGACGGCAGCGTGCAG  
CTCGCCGACCACTACCAGCAGAACACCCCATCGGGCAGCGGCCCGTGCTGCTGCCCGA  
CAACCACTACCTGAGCACCCAGTCCGCCCTGAGCAAAGACCCCAACGAGAGCGCGATCAC  
ATGGTCCTGCTGGAGTTCGTGACCGCCGCGGGATCACTCTCGGCATGGACGAGCTGTAC  
AAGTAA 3'



Plasmid template (20 ng) was amplified with Hot Start Taq DNA Polymerase according to the instructions with a forward primer (5' ATGGTGAGCAAGGGCGAGGA 3') and a reverse primer (5' TTA CTTGTACAGCTCGTCCATGCCGAGAG 3'). The following PCR steps were used: 94°C for 3 m, followed by 30 cycles of (94°C for 1 m, 60°C for 45 s, 68°C for 1 m), 68°C for 5 m. The PCR product was then purified using the Monarch PCR & DNA cleanup Kit.

#### 4.5.30 Cas9 Cleavage Assays

For all CRISPR Cas9 cleavage reactions, 400 ng (12.44 pmol) of sgRNA was incubated with 500 ng (~3 pmol) of purified recombinant *Streptococcus pyogenes* Cas9 (IDT) in 10 µL 1X PBS, pH 7.5. Samples were incubated for 10 minutes at room temperature to allow for formation of RNP complex. Each RNP complex (10 µL) was then added to 200 ng of dsDNA target in a total volume of 20 µL 1X CRISPR Cas9 buffer (200 mM HEPES, 1 M NaCl, 50 mM MgCl<sub>2</sub>, 1 mM EDTA, pH 6.5). The reactions were incubated at 37 °C for 2 hours and halted with the addition of 1 µL proteinase K (20 mg/mL, Thermo Fisher) and a 10-minute incubation at 56 °C. All samples were diluted with 20 µL nuclease free water and analyzed on 1% agarose gel with 1X SYBR Safe. Densitometry analysis was performed using ImageJ software. Percent cleavage was calculated by dividing the band intensity of the two cleaved product bands by the sum of all band intensities in that lane.

To inhibit Cas9 activity through caging, 2 µg sgRNA was added to separate PCR tubes and mixed with 14.5 µL of a 40% glyoxal solution (Sigma Aldrich) and 50 µL DMSO and brought to a final volume of 100 µL with nuclease-free water. Reactions were incubated at 50 °C for 0 min, 1 min, 5 min, 10 min, 20 min, 30 min, 40 min, 1 h, 2 h, 4 h, 6 h, and 8 h. Immediately after each timepoint, each sample was ethanol precipitated and resuspended in nuclease free water to 100

ng/μL. The size shift from glyoxal addition to sgRNAs was then monitored by 10% denaturing PAGE stained with 1X SYBR Gold solution for 20 minutes.

To decage the sgRNA, 2 μg sgRNA was added to 100 μL 1X PBS, pH 7.5 and incubated at 95 °C for 0, 0.5, 1, 2, 3, 5, 8, and 10 minutes. Samples were ethanol precipitated and resuspended in nuclease free water to 100 ng/μL. Size shift from glyoxal removal was then monitored by 10% denaturing PAGE stained with 1X SYBR Gold solution for 20 minutes. Optimal timepoints for caging (2 h) and decaging (5 min) were then analyzed for size shift with untreated sgRNA on 10% denaturing PAGE with SYBR Gold staining as previously described.

For sgRNA decaging at 37 °C, 1 μg untreated or caged sgRNA was combined in a total of 100 μL 1X PBS and incubated at 37 °C for 0 h, 1 h, 2 h, 4 h, 6 h, 8 h, 1 d, and 2 d. The samples were ethanol precipitated and resuspended in nuclease free water to 100 ng/μL. The size shift from glyoxal removal was then monitored by running the samples on 10% denaturing PAGE stained with SYBR Gold. Each of the timepoints for both untreated and caged sgRNA were tested as described above for Cas9 cleavage activity and analyzed by 1% agarose gel.

#### 4.5.31 ASOs and Plasmids

The following LNA gapmer oligonucleotides were purchased from IDT as shown below. “+” indicates LNA nucleobases and “\*” denotes phosphorothioate modification.

Anti-eGFP: 5' +G\*+A\*+A\*C\*T\*T\*C\*A\*G\*G\*G\*T\*C\*+A\*+G\*+C 3'

Scramble: 5' +A\*+G\*+G\*A\*C\*G\*A\*C\*T\*C\*T\*A\*G\*+G\*+C\*+T 3'

To construct a destabilized eGFP vector, a pCMV plasmid harboring the eGFP coding sequence (<https://www.addgene.org/11153/>) was digested with restriction enzymes bsrGI and NotI (New

England Biolabs) and a dsDNA sequence encoding the CL1 degron tag (ACKNWFSSLSHFVIHL) was cloned into the vector at the eGFP C-terminus. Correct insertion was verified by Sanger sequencing (full plasmid map is included in additional supplemental materials as a SnapGene file).

#### *4.5.32 Transfection and Live-Cell Imaging*

HEK293T cells (ATCC CRL-3216) were cultured in Dulbecco's Modified Eagle's Medium supplemented with 10% fetal bovine serum and maintained at 37 °C, 5% CO<sub>2</sub>. Cells were seeded at 10,000 cells/well in tissue culture-treated clear polystyrene 96-Well Plates (Costar) followed by overnight recovery. For initial tests of GFP expression, 200 ng of constructed eGFP plasmid was introduced into cells with Lipofectamine 3000 (Thermo Fisher Scientific) according to the manufacturer's instructions. After ~12 h incubation at 37 °C, 5% CO<sub>2</sub>, cells were then imaged at 4X magnification using a Biotek FX Lionheart automated live-cell microscope, and images were processed using ImageJ.

To optimize ASO delivery, cells were seeded into 96-well plates and transfected with 200 ng of plasmid using Lipofectamine 3000 as described above. Cells were then exposed to a range of concentrations (0 – 500 nM) of both anti-eGFP and scrambled ASO in 0.2 mL DMEM per well. After ~12 h incubation at 37 °C, 5% CO<sub>2</sub>, cells were then imaged using a Biotek FX Lionheart as described.

Increasingly caged ASO samples were generated by combining 2 µg of anti-eGFP ASO with 14.5 µL of a 40% glyoxal solution (Sigma Aldrich) and 50 µL DMSO. All reactions were brought to a final volume of 100 µL with nuclease-free water and reacted at 50 °C for 0 min, 5 min, 10 min, 20 min, 30 min, 1 hour, 2 hours, 4 hours, 6 hours, and 8 hours. At each time point,

reactions were ethanol precipitated and reconstituted in nuclease free water. To assess caging by gel, 5 pmol of each purified reaction was then mixed with 2X RNA loading dye (New England Biolabs) and then separated with 20% denaturing PAGE. Gels were then stained with 1X SYBR Gold solution (ThermoFisher Scientific) for 20 minutes and visualized with the Typhoon RGB scanner.

To assess cellular uptake, anti-eGFP ASO was first fluorescently labeled with Cyanine 5 (Cy5) using the Label IT® Tracker™ Intracellular Nucleic Acid Localization Kit (Mirus Bio) according to the manufacturer's instructions and purified by ethanol precipitation. A portion of this material was set aside (untreated ASO), and in separate PCR tubes, 2 µg ASO was mixed with 14.5 µL of a 40% glyoxal solution (Sigma Aldrich) and 50 µL DMSO and brought to a final volume of 100 µL with nuclease-free water. Reactions were incubated at 50 °C 8 h, after which it was ethanol precipitated and resuspended in nuclease free water. HEK293T cells were seeded into 96-well plates as described previously, and cells were exposed to untreated or glyoxal caged ASO at a final concentration of 250 nM in 0.2 mL DMEM per well. Cells were incubated overnight at 37 °C, 5% CO<sub>2</sub>, and each well was carefully washed three times with 0.2 mL of prewarmed fresh DMEM, followed by fluorescent microscopy using the Biotek FX lionheart.

To assess GFP expression across different time points, HEK293T cells were seeded into 96-well plates as described previously, and cells were transfected with 200 ng of plasmid using Lipofectamine 3000. Cells were then exposed to 250 nM of increasingly caged anti-eGFP in 0.2 mL DMEM per well. At the indicated time points cells were then imaged using a Biotek FX Lionheart as described. On days 4 and 7 of the experiment, 100 µL of media was carefully removed from the top of each well and replaced with prewarmed fresh complete DMEM. Images were acquired at 4x magnification in the center of each well, and exposure parameters were identical

across cell samples, with GFP exposure times always set at each time point according to “no ASO” sample wells. Raw images were then processed and colorized in ImageJ. To calculate GFP-positive cells per well, fluorescent image thresholds were first normalized using the Huang algorithm, followed by “analyze” particles” ImageJ plugin for cell quantification using a lower area range set at 10 pixels/sq-inch.

#### 4.5.33 Cell Viability Assays

To test viability, plates from the full time-course decaging experiment were tested using WST-1 (Sigma Aldrich) according to the manufacturer’s protocol. In brief, on day 7 after acquiring final images, media was carefully replaced with fresh 100  $\mu$ L DMEM, and 10  $\mu$ L of the WST-1 reagent was added to each well. Plates were incubated at 37  $^{\circ}$ C, 5% CO<sub>2</sub> for four hours, and absorbance of each well at 440 nm was measured. Separately, glyoxal alone was also tested after seeding HEK293T cells at 10,000 cells per well as described previously. Cells were then exposed to a range of glyoxal concentrations (0 – 1 mM) in 0.2 mL DMEM. On days 4 and 7 of the experiment, 100  $\mu$ L of media was carefully removed from the top of each well and replaced with prewarmed fresh complete DMEM supplemented with the appropriate amount of glyoxal. After 7 days, viability was assayed using WST-1. Percent viability was calculated as the net absorbance value compared to untreated HEK293T cells. IC<sub>50</sub> value (mean with 95% confidence interval) was calculated using a dose-response curve fit in Prism.

## Chapter 5: Recruit and Retain a Diverse Workforce<sup>159††</sup>

### 5.1 Abstract

As the world erupts with demands for racial justice, the chemistry community has the obligation, opportunity and momentum to drive for diversity and inclusion in the sciences. Efforts towards that end must begin by allocating opportunities for success on the basis of potential, not privilege, and follow through by soliciting and acting upon feedback from the scholars we have recruited.

### 5.2 Introduction

The heterogeneity of chemists across ethnic, gender and socio-economic spectrums has significance at every echelon, from the young students first discovering the periodic table to the entrepreneurs launching their pharmaceutical startups. Although our scientific community is increasingly engaged in honest dialogue surrounding diversity and inclusion — particularly after the killings of Ahmaud Arbery, Breonna Taylor and George Floyd — efforts to increase diversity through admissions and hiring have historically focused on meeting racial and gender quotas rather than evaluating candidates holistically. That is, academic programs can exhibit tokenism by recruiting a few members from underrepresented groups in order to meet the lowest standard of diversity, rather than to expand the institution's analytical skillset and capacity for community

---

††Material from: Manuel, B.A., Karloff, D.B. Recruit and retain a diverse workforce. *Nat Rev Chem*, 2020. Copyright © 2020, Springer Nature.

engagement. Moreover, compared with the time and resources that we expend to recruit scientists from under-represented groups in science, technology, engineering and mathematics (STEM), far less attention is given to also creating a work environment that respects all individuals and embraces their feedback. As a result, retention of under-represented scientists constitutes a major challenge in academia.

What will it take to make our undergraduate and graduate researchers, our postdoctoral interview candidates, our faculty and our academic leaders reflect local and global populations — and why should we bother? As a melting pot of aspiring innovators, it is both our extraordinary privilege and our duty to answer these questions. We work in a research group whose expertise in enriching functional nucleic acids from a starting pool of trillions of random sequences has, oddly, provided us with a unique perspective on how to select, retain and invest in the potential of would-be members of our own chemistry community. While our experiences are mostly grounded in the American academic system, here we present general insights on how to recruit diverse groups of people, provide them with the resources to flourish and support them in dreaming big.

### **5.3 Assessing Candidates**

Carrying forwards our research analogy, the “first law of directed evolution” coined by Frances Arnold states that “you get what you screen for”.<sup>160</sup> Every application process represents a screening step and, if biases (explicit or implicit) are present at each career stage, these accumulate over time to exponentially skew candidate pools. Admissions and hiring committees must therefore look beyond traditional CV metrics to consider both the context of an applicant’s achievements and the value of the knowledge and perspective that they bring to the community. Additionally, we must challenge the mentality, “Does this person have what it takes to be

successful in our program?” and instead ask, “Does our program have what it takes for this person to be successful?” This approach is a first step in recognizing the inherent structural biases that make success easier for some than others. It also reframes each new student, postdoc or faculty member as someone in whom the institution is deeply invested, as opposed to a diversity statistic. In this section, we discuss approaches for reframing admissions and hiring decisions to focus on the potential of each candidate rather than the diversity needs of the institution.

What exactly is diversity? Kenneth Gibbs Jr, a program director in the Division of Training, Workforce Development and Diversity at the National Institute of General Medical Sciences, defines diversity as, “Difference. Science workforce diversity refers to cultivating talent and promoting the full inclusion of excellence across the social spectrum”.<sup>161</sup> In order to cultivate talent in STEM from diverse groups, we should first recognize that excellent students come from all ethnic, religious, socio-economic and academic backgrounds. Indeed, the ability of co-workers to think in distinct ways fosters creativity and innovation. This concept is exemplified in the acclaimed 2016 film *Hidden Figures*, which is based on the true story of Black NASA mathematicians Katherine Johnson, Mary Jackson and Dorothy Vaughan and honors their essential roles in making John Glenn the first American to orbit the Earth. Multiple examples in the literature also support the role of diversity in positive scientific outcomes<sup>162, 163</sup>, including in industry.

After recognizing the inherent benefits of having varied perspectives, we must next critically evaluate our motivation for soliciting diverse applicants: is it to fulfill social norms? To improve the likelihood of obtaining grant funding? Or is it because we truly believe everyone deserves equal access to educational opportunities? And because we want to invest in people who can provide new insights into our organization’s challenges? Committing to the goal of diversity



for the right reasons ensures that the initiatives we pursue are consistent with the desired end goal: positive personal and professional outcomes for all parties involved.

Another major component of selecting among candidates involves evaluating their experience and past achievements. While a head-to-head comparison of publication output, conference talks, grade point average (GPA) or awards is a tempting basis for evaluating individuals, we must also consider the circumstances under which those achievements were realized. How might socioeconomic or cultural factors have affected access to education and opportunity? It is well known that standardized tests such as the Graduate Record Examination (GRE), which remain widely used in the USA, show poor correlation with research productivity in graduate school while demonstrably disadvantaging non-native English speakers and students of color. Likewise, what does it take to publish at a large, fully equipped and funded university versus a smaller institution with fewer resources? Although privilege often begets early professional success, individuals who face and overcome adversity throughout their careers develop critical skills that uniquely prepare them to face new and bigger challenges at later career stages.<sup>164</sup> Therefore, choosing the candidate who appears more qualified according to conventional metrics may mean losing the one who has become expert in navigating obstacles and persevering through difficulties as an under-represented scientist.

An added benefit to the practices outlined above is that they help to prevent the tokenism that can emerge when seeking to diversify admissions or interview pools. By considering the benefits of recruiting a diverse group of people as well as each individual's merit in the context of their access to resources and opportunities, we recognize that we are recruiting people — not numbers or quotas. Funding agencies may contribute to this process by following up after initial

grant disbursal not only on scientific progress but also on diversity statements. Finally, we define 'potential' as the capacity to choose and then realize ambitious goals. A highly motivated applicant already possesses the fuel — employers simply impart the tools to light the fire.

#### **5.4 Origins of Exclusivity**

Recruiting a diverse group of students, postdocs and faculty is just the first step towards achieving equitable representation in STEM. This work is fruitless without also building an environment that offers resources and mentorship to retain and support these recruits — a particularly pressing issue in STEM, as attrition rates are higher among women<sup>165</sup> and people of color. Below, we describe several factors that exacerbate feelings of exclusion, as well as steps that institutions and departments may take to mitigate these effects.

Not seeing others who look like us engenders feelings of exclusion and negative thoughts such as, "Am I here by mistake? What if I don't succeed?" One way to combat these is by increasing representation at all levels. Toldson reports that historically Black colleges and universities (HBCUs), while representing only 3% of higher education institutions in the USA, graduate more Black science and engineering students than all predominantly white institutions (PWIs) combined. This is due in part to the significantly higher percentage of Black faculty at doctoral-granting HBCUs (67%) than at PWIs (4%).<sup>166</sup> Unsurprisingly, our own success is much easier to envision when we meet and have the opportunity to be mentored by trailblazers who are like us.

Not seeing others who look like us engenders feelings of exclusion and negative thoughts such as, "Am I here by mistake? What if I don't succeed?"

Furthermore, as depicted in the *Hidden Figures* film, a major problem in STEM is the lack of recognition and appreciation for the work done by women and under-represented minorities (URMs). Of the more than 900 Nobel laureates awarded by 2018, only 14 (1.5%) were Black; moreover, only 21 women and no Black researchers have won a Nobel Prize in science. In particular, from 1901 to 1920, only four women won a Nobel Prize. Almost a century later, between 2000 and 2019, only 24 of 244 laureates were women. Likewise, the President's National Medal of Science (National Science Foundation) has been awarded to 482 scientists in STEM from 1962 to 2014 with 8% being women. Meanwhile, from 2017 to 2019, the American Chemical Society awarded over 200 chemists in various subfields. Of these, approximately 27% were women, and only about 5% were URMs. As recent findings indicate, scientific innovations by women and people of color are substantial but also less likely to be valued or pursued further.<sup>167</sup> Meanwhile, career trajectory is heavily influenced by conference talks<sup>168</sup>, citations and the receipt of awards. Therefore, it is critical to recognize how these inequities become compounded across a scientist's career and then to actively promote inclusive practices in literature citation and the selection of speakers and award winners.

Finally, women and URMs in STEM often lack a sense of belonging. When you walk into a room full of people, what do you do? Do you look around? Do you feel like all eyes are on you? Legendary tennis player Arthur Ashe once said, "Like many other Blacks, when I find myself in a new public space situation, I will count. I always count. I count the number of Black and brown faces present".<sup>169</sup> Signs of exclusivity can extend beyond the demographics of students and faculty to also appear in the culture of the department. Oftentimes department-wide activities in STEM fields include trivia, dinners and movie nights. How much might an international student know about local culture, a white student know about Black history, or a man know about women's history?

There can also be a lack of inclusivity in movie choices or even the food served at these events, leaving students feeling as though they need to conform to the exclusive environment in which they find themselves.

### **5.5 Cultivating Inclusion**

Creating spaces for individuals from under-represented groups in STEM to share experiences and build platforms for advocacy helps to kindle a sense of belonging. Within the Emory Department of Chemistry, we have established several graduate student extracurricular groups for female (@AWIS\_Emory on Twitter), international (@IGSSemory) and other under-represented student communities (@NOBCChE\_Emory and @Emory\_SACNAS) to connect and discuss challenges. These organizations regularly host events that foster social networks outside of research, advance professional development and provide opportunities to educate interested members of the majority group and potential allies about the experiences of under-represented populations in chemistry. For example, as board members on the Emory chapter of the National Organization for the Professional Advancement of Black Chemists and Chemical Engineers (NOBCChE), the authors have coordinated events to commemorate Black History Month at Emory, as well as helping to prepare members of the general body for conferences and educational milestones. Overall, these efforts serve to empower our members as departmental leaders while also engaging the greater Atlanta community.

Finally, a crucial component of supporting diversity in the sciences is effective listening. As long as those holding positions of authority come from groups having more privilege than the students and faculty they are recruiting, our employees will have encountered considerable obstacles that our leaders have never conceived. This can be overcome by building robust

infrastructure for anonymous feedback, town halls and private meetings for concerns to be voiced and then heard. For those of us in positions of leadership, when someone is describing an experience foreign to us, that is the time to ask questions, develop a deeper understanding and empathize — not to occupy the silence ourselves — in order to best appreciate and address the issue. Finally, if we cannot immediately remedy the problem, demonstrating to someone that they have been heard and understood is a powerful step towards comprehending the intricacies of exclusion.

## **5.6 Outlook**

Diversifying science for the mere sake of fulfilling societal expectations does a huge disservice to the communities that these efforts are intended to benefit. Further, it squanders the unique perspectives and experiences that each individual can bring to our departments and institutions. Focusing our evaluation criteria on factors beyond GPA, publications and academic pedigree is an important first step towards equitable admissions and hiring. Doing so prepares us to invest in each new student or faculty member's career goals, enabling diversification of science without exhibiting tokenism. Importantly, recruiting diverse applicants is insufficient without simultaneous efforts to foster an inclusive environment for everyone to thrive. This begins with hiring diverse faculty members and establishing support groups such as the Association for Women in Science (AWIS), NOBCChE and the Society for Advancement of Chicanos/Hispanics and Native Americans in Science (SACNAS) in STEM departments. Moreover, while we can increase the diversity of a department by accepting diverse candidates, their efforts and accomplishments must be judged or praised by fair and equal criteria.

As with nucleic acids in our lab, the scientific community begins with a large pool of scientists. Within this large pool are groups of under-represented individuals that possess great skill. If we can enrich these populations of scientists in every round of admissions or hiring, and then provide an environment that allows them to cultivate and utilize their talents, over time we will produce greater diversity in leadership positions. As the cycle repeats, diverse students in later generations will see more and more students, faculty members and academic leaders who look like them. Eventually, instead of constituting a roadblock, diversity and inclusion in STEM will finally become an asset for researchers to fully leverage.

## **Chapter 6: Conclusions and Future Perspectives**

Nucleic acids have emerged as promising biomolecules for applications in biotechnology, biomedicine, and bioremediation. Specifically, aptamers are especially promising due to their tunability, cost, and biocompatibility. In this dissertation, we explored the effects of tuning

molecular recognition of these biomolecules using simple guanosine-to-inosine substitutions. We then explored how this tuned recognition can aid enzyme kinetics and enable modification of the binding portion of an enzymatic reaction. We then explored a reversible modification using glyoxal to reversibly inhibit nucleic acids and enzymes. Lastly, we discuss the importance of promoting a diverse and inclusive environment within chemistry like those of the starting pool of SELEX.

In Chapter 2, we explore the effects of G to I substitutions on aptamer stability, specificity, and selectivity. We also went on to tune the recognition specifically on biosensors. However, more work is still to be done in this area. While we tested G to I on only two of our aptamers, it would be interesting to observe this effect on the remaining six aptamers as biosensors. In addition, we specifically generated structure-switching biosensors with a capture strand. It would be interesting to study this effect on both split aptamers and molecular beacons, considering we noticed a change in thermostability in many cases upon G to I substitutions. In addition, it would be interesting for this to be studied with a panel of aptamers of differing structures. For example, there are aptamers that form 2 stem loops, and those like the cocaine aptamer that forms 3 stem loops. How does G to I affect stability and specificity/selectivity of 2 stem aptamers versus 3 stem?

In Chapter 3, we explore controlling enzyme kinetics by specifically controlling  $K_M$  with the use of aptamers generated in Chapter 2. While we study enzyme kinetics in this chapter, it would be interesting to study our system in a biological system. Bacterial cocaine esterase is the most efficient cocaine-hydrolysing enzyme. In fact, it has been studied for over a decade for its therapeutic potential. However, its stability *in vivo* is subpar, leading many researchers to use directed mutagenesis in an attempt to obtain a more stable enzyme for delivery. However, these enzymes typically result in lower activity ( $k_{cat}/K_M$ ) due to either a perturbed recognition ( $K_M$ ) or slower enzyme ( $k_{cat}$ ). Because encapsulation has been shown to improve enzyme stability, and we have

shown that the use of an affinity reagent improves catalytic activity ( $k_{cat}/K_M$ ) slightly, it would be very interesting to see how our system would function in a living system. Furthermore, because VLPs are known to elicit an immune response, it would be very intriguing to study a panel of differing encapsulants (nanocages, VLPs, liposomes, etc.) with a variety of co-encapsulated affinity reagents (antibodies, aptamers, peptides, etc.) with their respective enzymes. This could provide great insight into what this system overall could be helpful for. In addition, once this panel is characterized, they could be explored in a variety of applications. For example, there are many enzymes that are promising in industrial settings, specifically for bioremediation. Often, pesticides can be harmful to humans and pets. Therefore, treating plants and soil with an enzyme that can degrade the pesticide can create a healthier approach to gardening. The panel can help determine which encapsulant can be best for a garden in Louisiana versus a garden in Colorado based on environment.

In Chapter 4, we investigated the thermoreversible modulation of nucleic acid interactions a variety of targets using glyoxal. To the best of our knowledge, we are the first group of authors to demonstrate thermoreversible control of nucleic acids in such a fashion. While in this dissertation we explore two specific base modifications that we incorporate, glyoxal has also been shown to reversibly cage amino acids. This can specifically be promising in preventing enzyme inhibition. Specifically in the case of organophosphate poisoning. Many agrochemicals and war agents contain organophosphates (OPs). Exposure to these chemicals has been linked to defecation, gastrointestinal distress, emesis, miosis, and in extreme cases, death. OP-containing war agents and pesticides have a diversity of chemical structures, but they share a common mechanism of toxicity, ultimately leading to Acetylcholinesterase (AChE) inhibition. War agents are more potent than pesticides, as they directly inhibit AChE. However, pesticides are degraded prior coming into



contact with AChE, inhibiting other key enzymes in the liver and intestines. AChE is a carboxylesterase consisting of the catalytic triad of a Glu334, Ser203, and His447. The primary function of this enzyme is to hydrolyze the neurotransmitter, acetylcholine (ACh). Glyoxal and its derivatives have been shown to react arginine, lysine, and cysteine. AChE's opening has an arginine residue that is crucial for allowing small molecules in and out. In addition, there are AChE inhibitors that are shown to only partially inhibit the enzyme by reacting with amino acids at the mouth of the gorge. However, this inhibition is very limited, and ACh can still be hydrolyzed at a slower rate. With this in mind, it would be interesting to explore if by incorporating glyoxal and glyoxal derivatives, we can create an OP-resistant AChE enzyme. Overtime, this enzyme would degrade, allowing for OP deactivation, which is necessary, as an overactive AChE is not desirable.

Lastly, in Chapter 5, we discuss ways to promote diversity, equity, and inclusion in chemistry professions, specifically highlighting academia. We highlight that a lack of diversity begins with the selection process, leading to a lack of representation. As a result, we run into the issues of equity and inclusion, because the pool is already not diverse enough to "require" inclusion. While much work has been done in Emory's chemistry department following this discussion, much more remains to be done on a broader scale. To date, one way that I think could help push these efforts forward is by investing in and growing organizations like NOBCCChE. Every year NOBCCChE has a national meeting, and at this meeting is a career expo. Many big companies such as Merck and Pfizer, and big schools such as Duke and LSU go to recruit. Often, these recruiters are Black, as well. Having Black chemists seeing Black employees can be a huge confidence boost and can increase representation at the university and professional levels.

**Appendix A: Omitted Data from Chapter 2<sup>21††</sup>****Figure A1: DNA sequences used in MST and biosensor experiments.** Cy5 = cyanine 5. BHQ3 = blackhole quencher 3

Name	Sequence (5'-3')
MNS-4.1	/Cy5/GGGAGACAAGGATAAATCCTTCAATGAAGTGGGTCGACA
MNS-4.1 Inosine	/Cy5/IIIAGACAAGGATAAATCCTTCAATGAAGTGGGTCGACA

<sup>††</sup> Reproduced from Ref. 1 with permission from Manuel, B. A.; Sterling, S. A.; Sanford, A. A.; Heemstra, J. M., Systematically Modulating Aptamer Affinity and Specificity by Guanosine-to-Inosine Substitution. *Analytical Chemistry* **2022**, 94 (17), 6436-6440. Copyright 2022 American Chemical Society.

38-GT	/Cy5/GGGAGACAAGGAAAATCCTTCAATGAAGTGGGTCTCCC
38-GT Inosine	/Cy5/IIIAGACAAGGAAAATCCTTCAATGAAGTGGGTCTCCC
38-IT	/Cy5/GGGAGACAAGGAAAATCCTTCAATIAAGTGGGTCTCCC
38-GC	/Cy5/GGGAGACAAGGAAAATCCTTCAACGAAGTGGGTCTCCC
38-GC Inosine	/Cy5/IIIAGACAAGGAAAATCCTTCAACGAAGTGGGTCTCCC
38-IC	/Cy5/GGGAGACAAGGAAAATCCTTCAACIAAGTGGGTCTCCC
9-mer	TTGTCTCCC/BHQ3/
12-mer	TCCTTGTCTCCC/BHQ3/
15-mer	TTATCCTTGTCTCCC/BHQ3/

**Figure A2: DNA sequences used in melting temperature experiments.**

Name	Sequence (5'-3')
MNS-4.1	GGGAGACAAGGATAAATCCTTCAATGAAGTGGGTCTGACA
MNS-4.1 Inosine	IIIAGACAAGGATAAATCCTTCAATGAAGTGGGTCTGACA
38-GT	GGGAGACAAGGAAAATCCTTCAATGAAGTGGGTCTCCC
38-GT Inosine	IIIAGACAAGGAAAATCCTTCAATGAAGTGGGTCTCCC
38-IT	GGGAGACAAGGAAAATCCTTCAATIAAGTGGGTCTCCC
38-GC	GGGAGACAAGGAAAATCCTTCAACGAAGTGGGTCTCCC
38-GC Inosine	IIIAGACAAGGAAAATCCTTCAACGAAGTGGGTCTCCC
38-IC	GGGAGACAAGGAAAATCCTTCAACIAAGTGGGTCTCCC

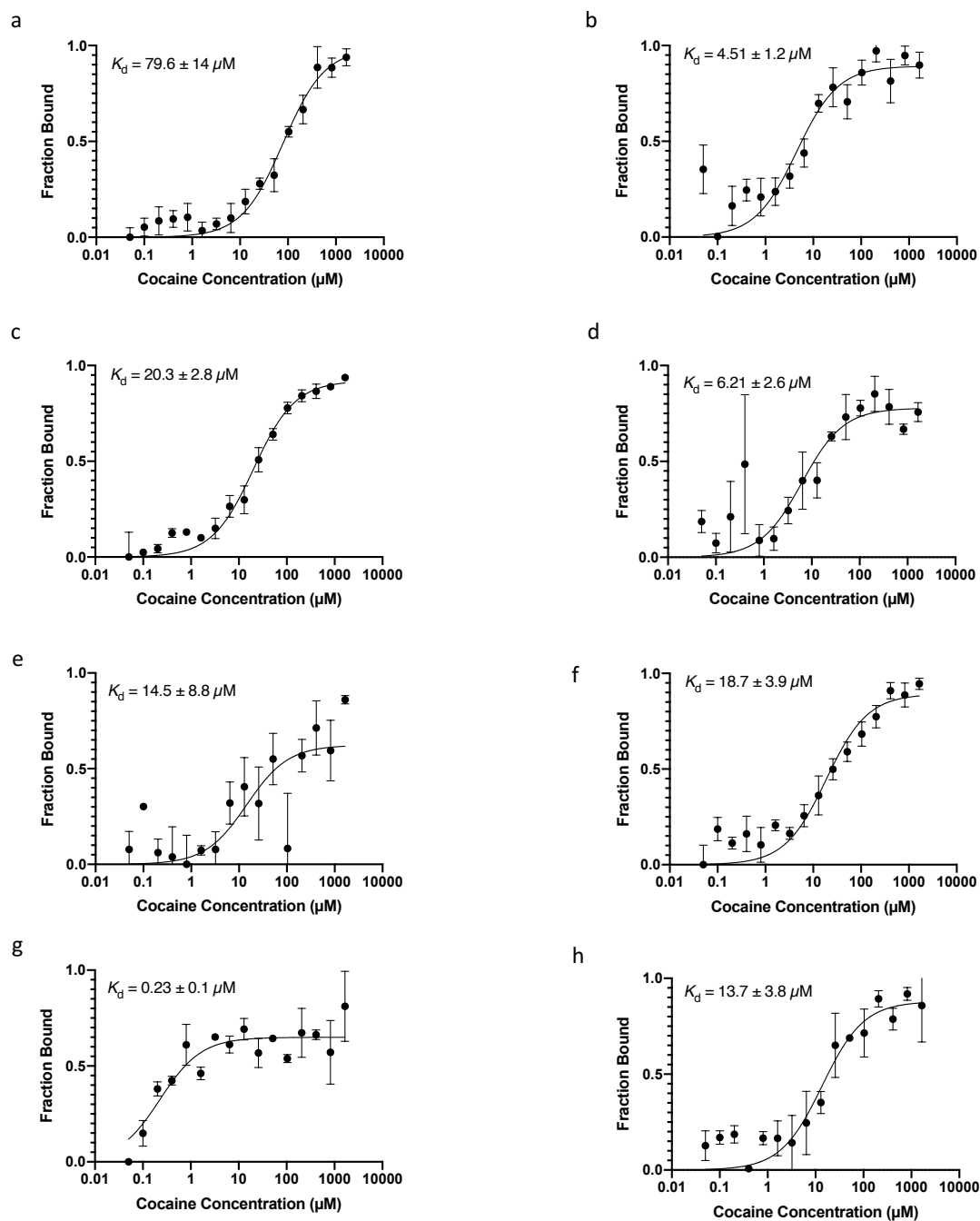


**Figure A3: MST traces of all aptamers with cocaine.** Graphs are displayed as fraction bound versus cocaine concentration. Errors represent the standard error of three independent trials. The data were graphed using GraphPad Prism. (a) MNS-4.1 (b) MNS-4.1 Inosine (c) 38-GT (d) 38-GT Inosine (e) 38-GC (f) 38-GC Inosine (g) 38-IC (h) 38-IT.

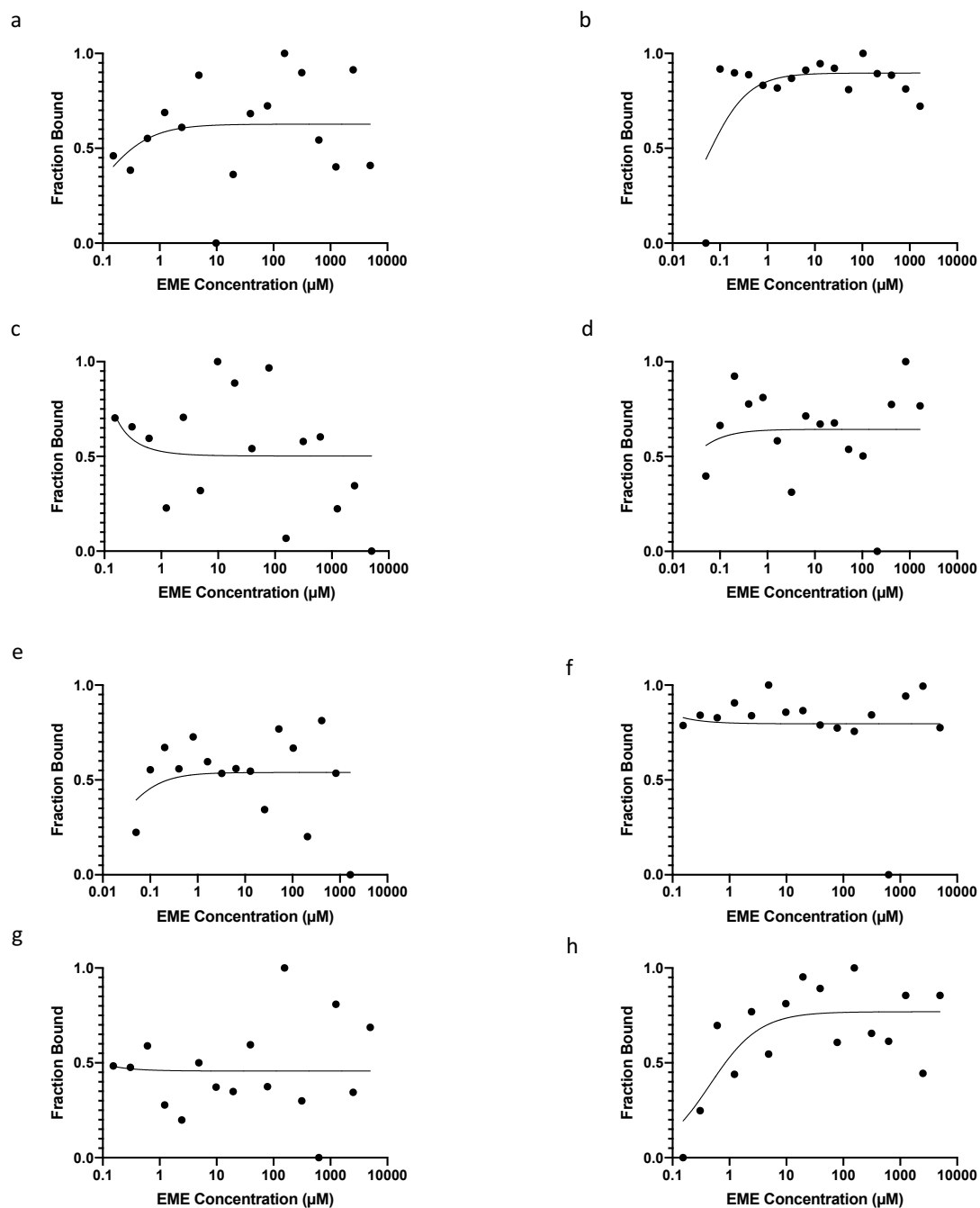


**Figure A4: MST traces of all aptamers with EME.** Graphs are displayed as fraction bound versus EME concentration. The data were graphed using GraphPad Prism. (a) MNS-4.1 (b) MNS-4.1 Inosine (c) 38-GT (d) 38-GT Inosine (e) 38-GC (f) 38-GC Inosine (g) 38-IC (h) 38-IT.

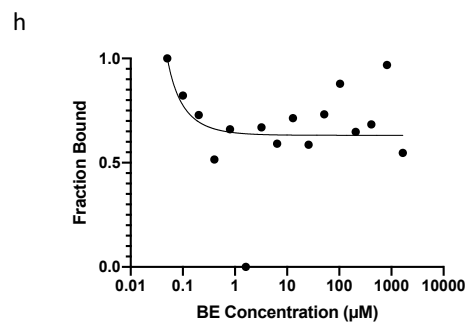
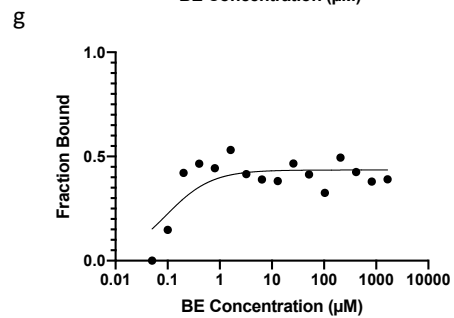
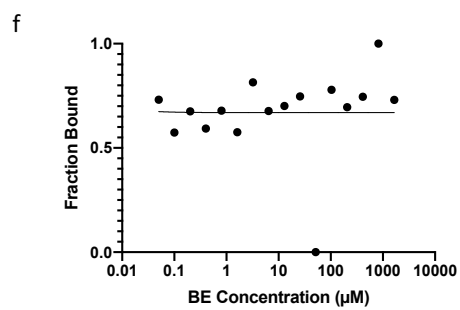
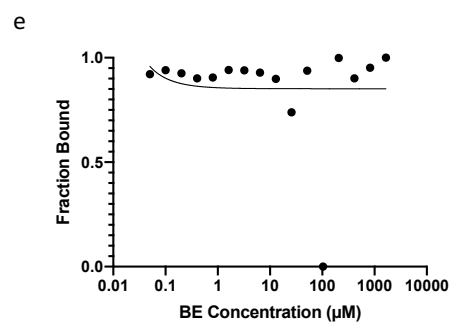
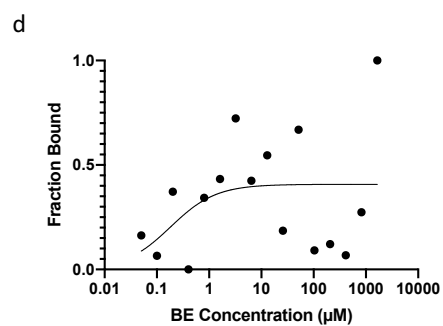
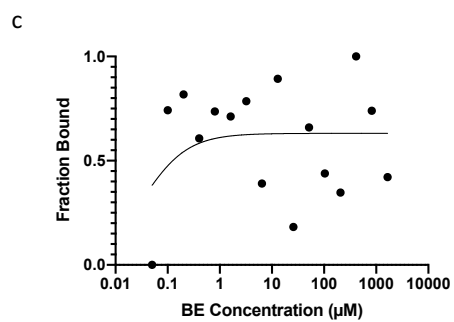
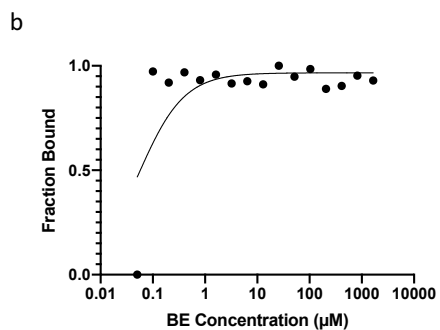
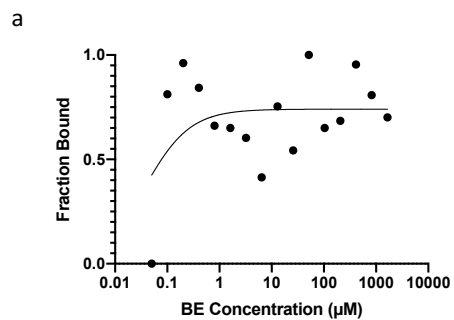


**Figure A5: MST traces of all aptamers with BE.** Graphs are displayed as fraction bound versus BE concentration. The data were graphed using GraphPad Prism. (a) MNS-4.1 (b) MNS-4.1 Inosine (c) 38-GT (d) 38-GT Inosine (e) 38-GC (f) 38-GC Inosine (g) 38-IC (h) 38-IT.

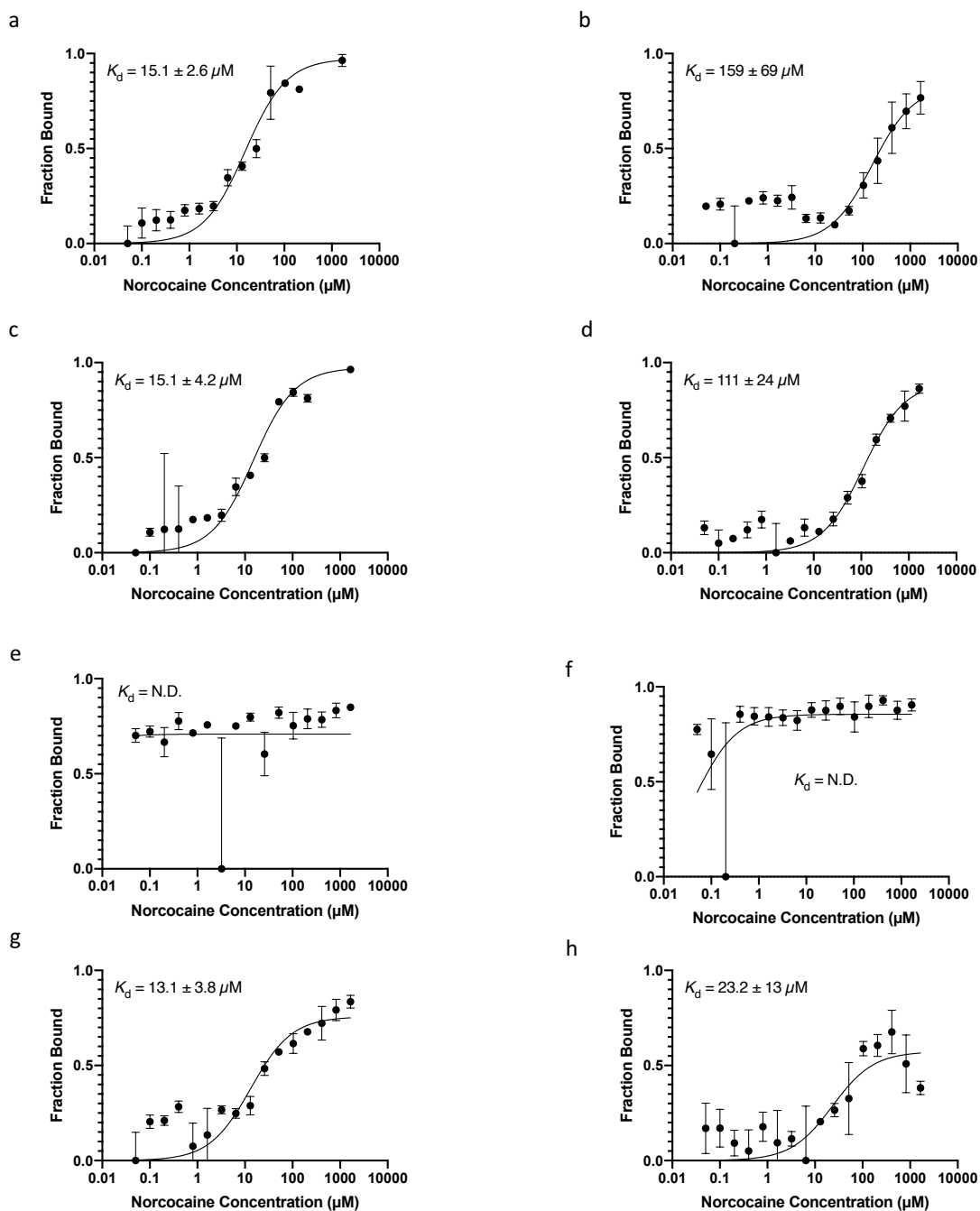


**Figure A6: MST traces of all aptamers with norcocaine.** Graphs are displayed as fraction bound versus norcocaine concentration. Errors represent the standard error of three independent trials. The data were graphed using GraphPad Prism. (a) MNS-4.1 (b) MNS-4.1 Inosine (c) 38-GT (d) 38-GT Inosine (e) 38-GC (f) 38-GC Inosine (g) 38-IC (h) 38-IT.



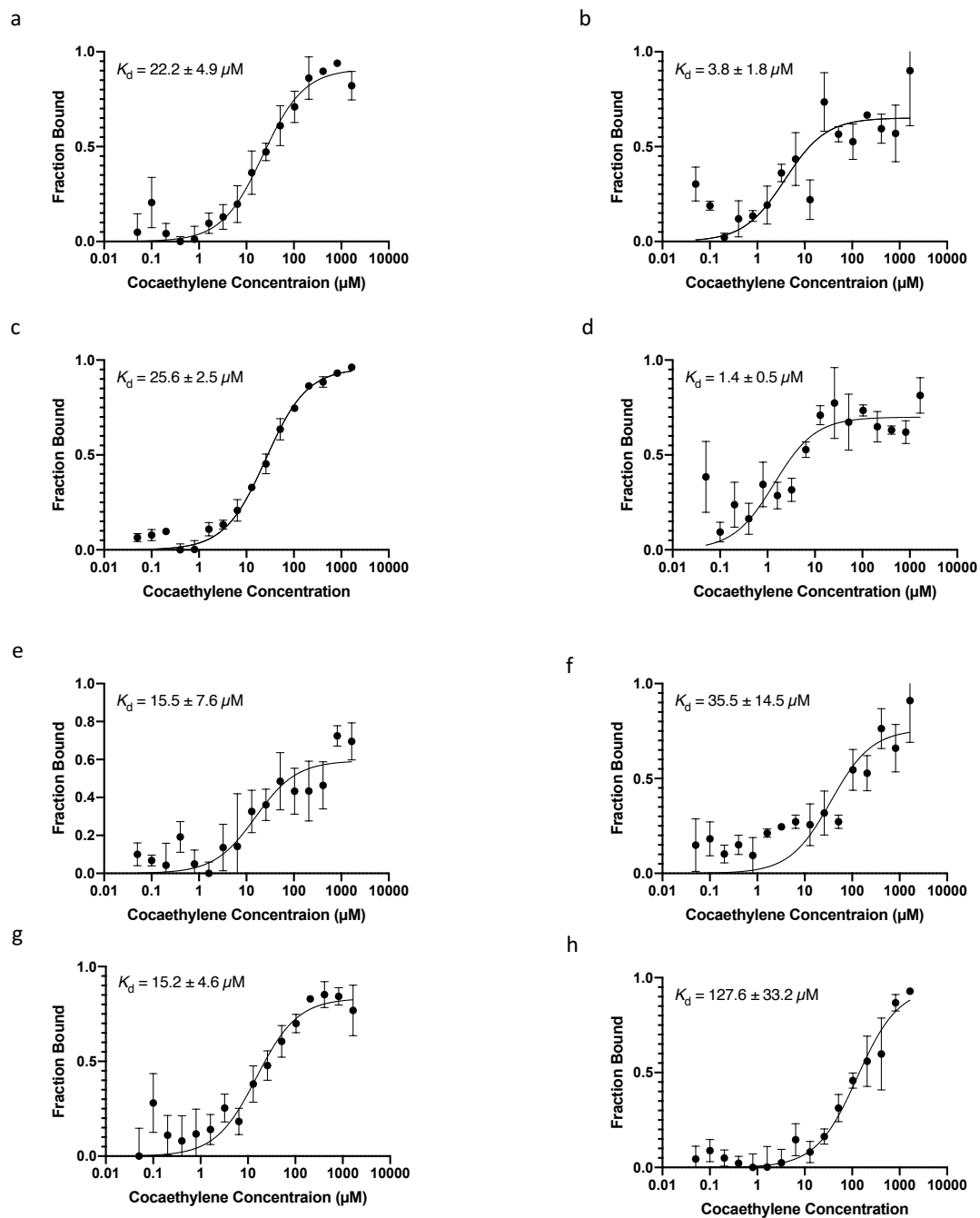


**Figure A7. MST traces of all aptamers with cocaethylene.** Graphs are displayed as fraction bound versus norcocaine concentration. Errors represent the standard error of three independent

trials. The data were graphed using GraphPad Prism. (a) MNS-4.1 (b) MNS-4.1 Inosine (c) 38-GT (d) 38-GT Inosine (e) 38-GC (f) 38-GC Inosine (g) 38-IC (h) 38-IT.

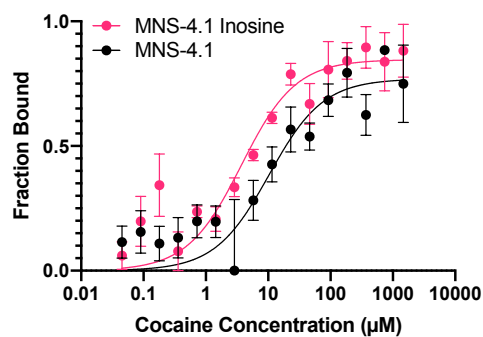


**Figure A8. MST traces for MNS-4.1 and MNS-4.1 Inosine in saliva.** Cocaine binding of parent MNS-4.1 aptamer in comparison to MNS-4.1 Inosine in 2.5% saliva measured using MST. All MST experiments were performed in triplicate.

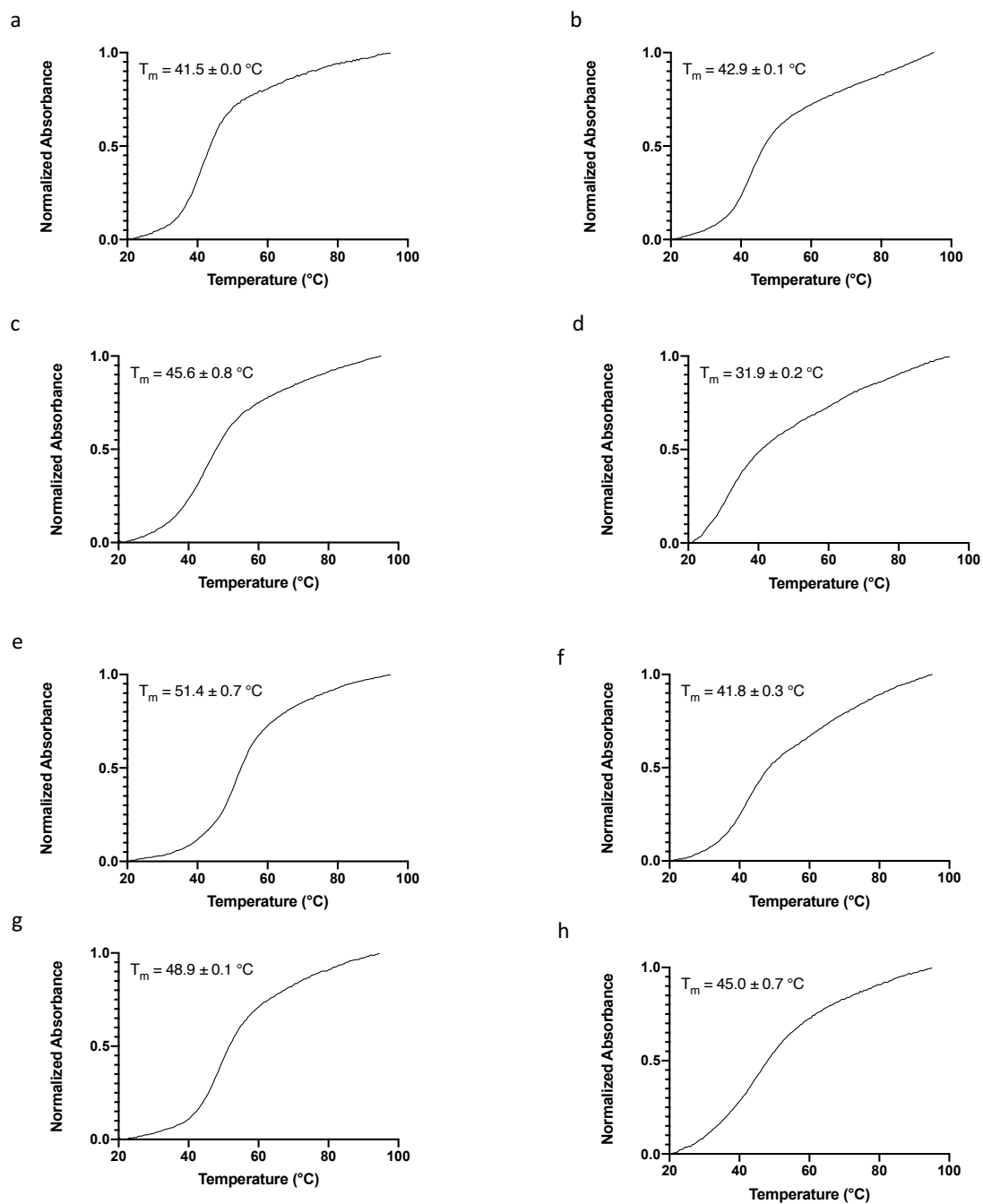


**Figure A9: Melting temperature curves of all aptamers.** Errors represent the standard error of three independent trials. The data were graphed using GraphPad Prism and  $T_m$  was determined by the first derivative method.

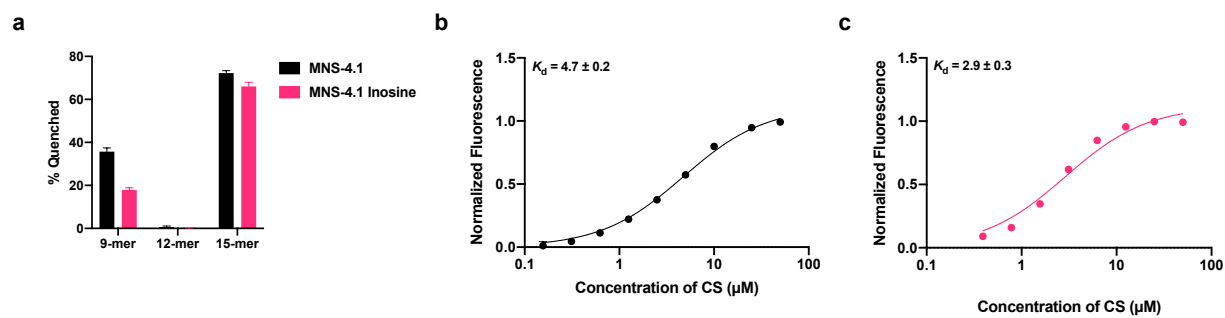


**Figure A10. Biosensor characterizations.** Errors represent the standard error of three independent trials. The data were graphed using GraphPad Prism. (a) % Quenched for MNS-4.1 and MNS-4.1 Inosine for each capture strand. (b) MST Data for MNS-4.1 and (c) MNS-4.1 Inosine with increasing concentrations of the 15-mer CS.

### Appendix B: Omitted Data from Chapter 3

**Figure B1. DNA sequences used in MST and kinetic.** Cy5 = cyanine 5. FAM = fluorescein

Name	Sequence (5'-3')
MNS-4.1	/Cy5/GGGAGACAAGGATAAATCCTTCAATGAAGTGGGTCGACA
38-GC	/Cy5/GGGAGACAAGGAAAATCCTTCAACGAAGTGGGTCTCCC
38-IC	/Cy5/GGGAGACAAGGAAAATCCTTCAACIAAGTGGGTCTCCC
MNS-4.1	/FAM/GGGAGACAAGGATAAATCCTTCAATGAAGTGGGTCGACA
38-GC	/FAM/GGGAGACAAGGAAAATCCTTCAACGAAGTGGGTCTCCC
38-IC	/FAM/GGGAGACAAGGAAAATCCTTCAACIAAGTGGGTCTCCC
Scrambled	/FAM/ GGCGATTGTTGGAGAGCCAGCAGCGATTGCAAATGTCAG

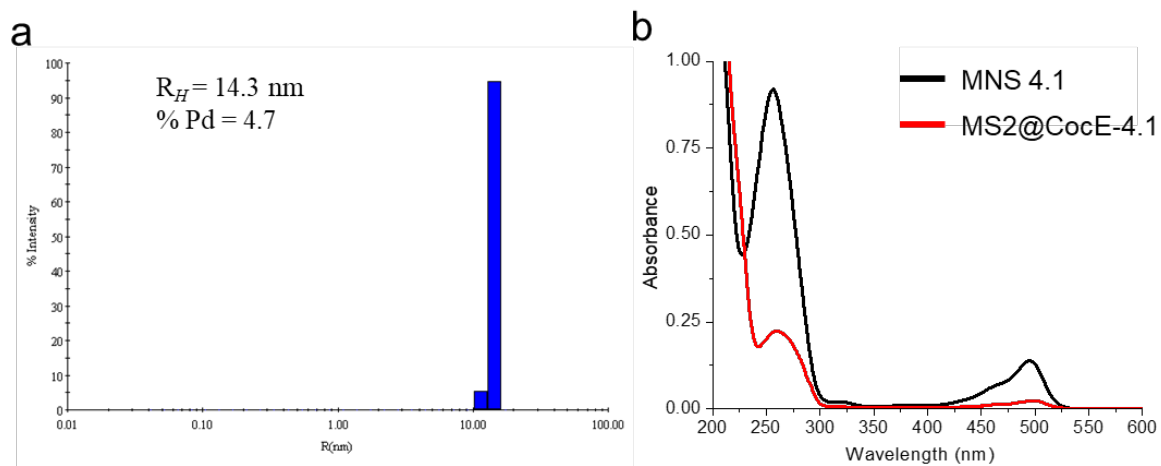
**Figure B2. Incubation concentrations and average numbers of packaged cocaine aptamers per VLP.**

Ratio for Incubation		After Purification		
Entry	MS2 CP per aptamer	Encapsulation efficiency	Aptamers/VLP	Yield
1	25	100%	18	65%
2	10	80%	45	60%
3	5	66%	74	62%
4	2.5	17%	25	35%

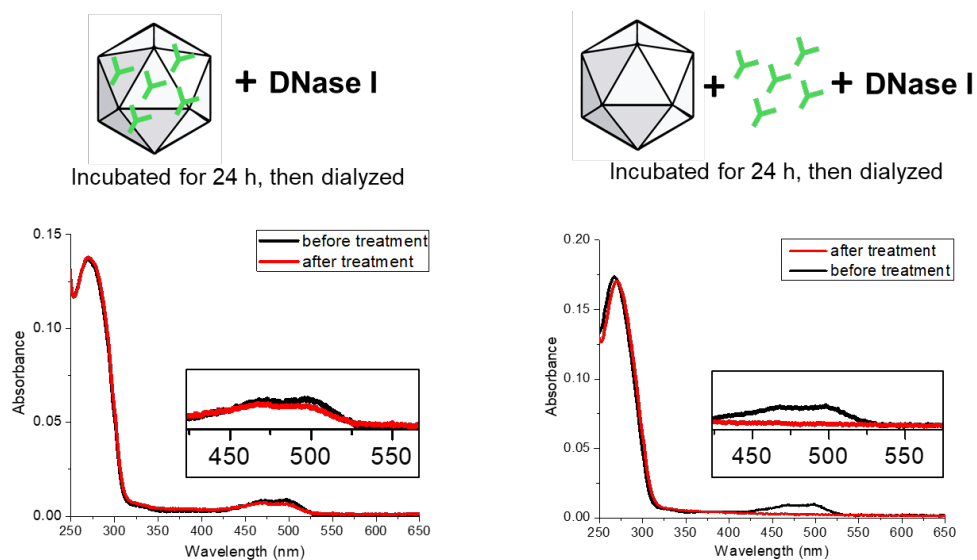
**Figure B3. Kinetic parameters of packaged enzyme with free aptamer and co-packaged enzyme with scrambled DNA.**

Catalyst	Aptamer	Aptamer $K_D$ ( $\mu\text{M}$ )	Aptamer conc. ( $\mu\text{M}$ )	$K_M$ ( $\mu\text{M}$ )	$k_{cat}$ ( $\text{min}^{-1}$ )	$k_{cat}/K_M$ ( $\mu\text{M}^{-1} \text{min}^{-1}$ )
CocE-wt	-	-	-	$10.3 \pm 1.0$	$281 \pm 4$	$27.4 \pm 1.9$
MS2@CocE	-	-	-	$19.9 \pm 1.0$	$403 \pm 8$	$20.3 \pm 1.0$
MS2@CocE	MNS-4.1	98.3	4	$15.4 \pm 2.9$	$365 \pm 15$	$23.8 \pm 3.9$
	38-GC	8.5		$30.1 \pm 6.4$	$413 \pm 22$	$13.7 \pm 0.8$
	38-IC	0.3		$20.8 \pm 2.8$	$405 \pm 12$	$19.6 \pm 3.0$
	MNS-4.1	98.3	8	$18.8 \pm 4.5$	$377 \pm 19$	$20.2 \pm 2.8$

	38-GC	8.5		$27.2 \pm 3.7$	$405 \pm 13$	$14.9 \pm 1.2$
	38-IC	0.3		$17.1 \pm 2.7$	$400 \pm 14$	$23.3 \pm 1.6$

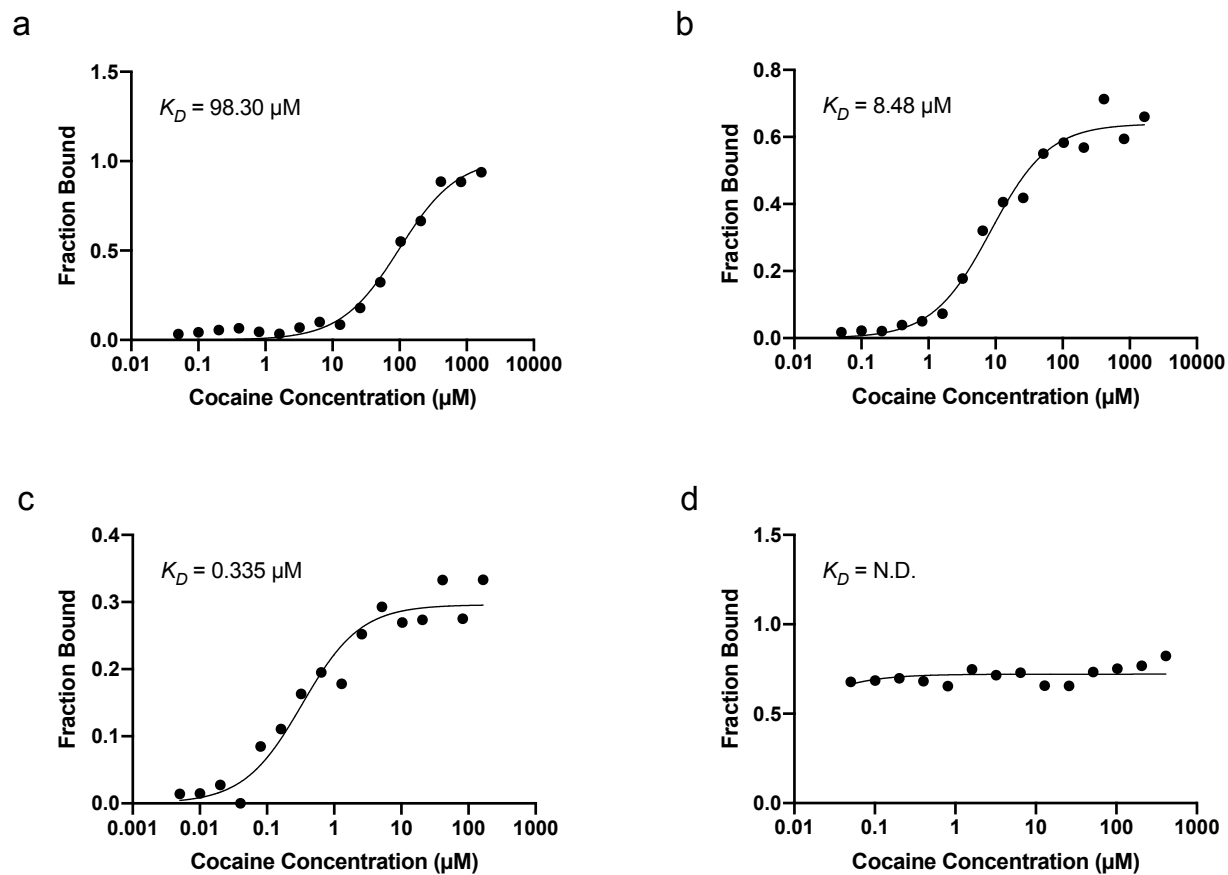


**Figure B4. Characterization of MS2@CocE-4.122 particles:** (a) dynamic light scattering, (b) UV-vis spectra.

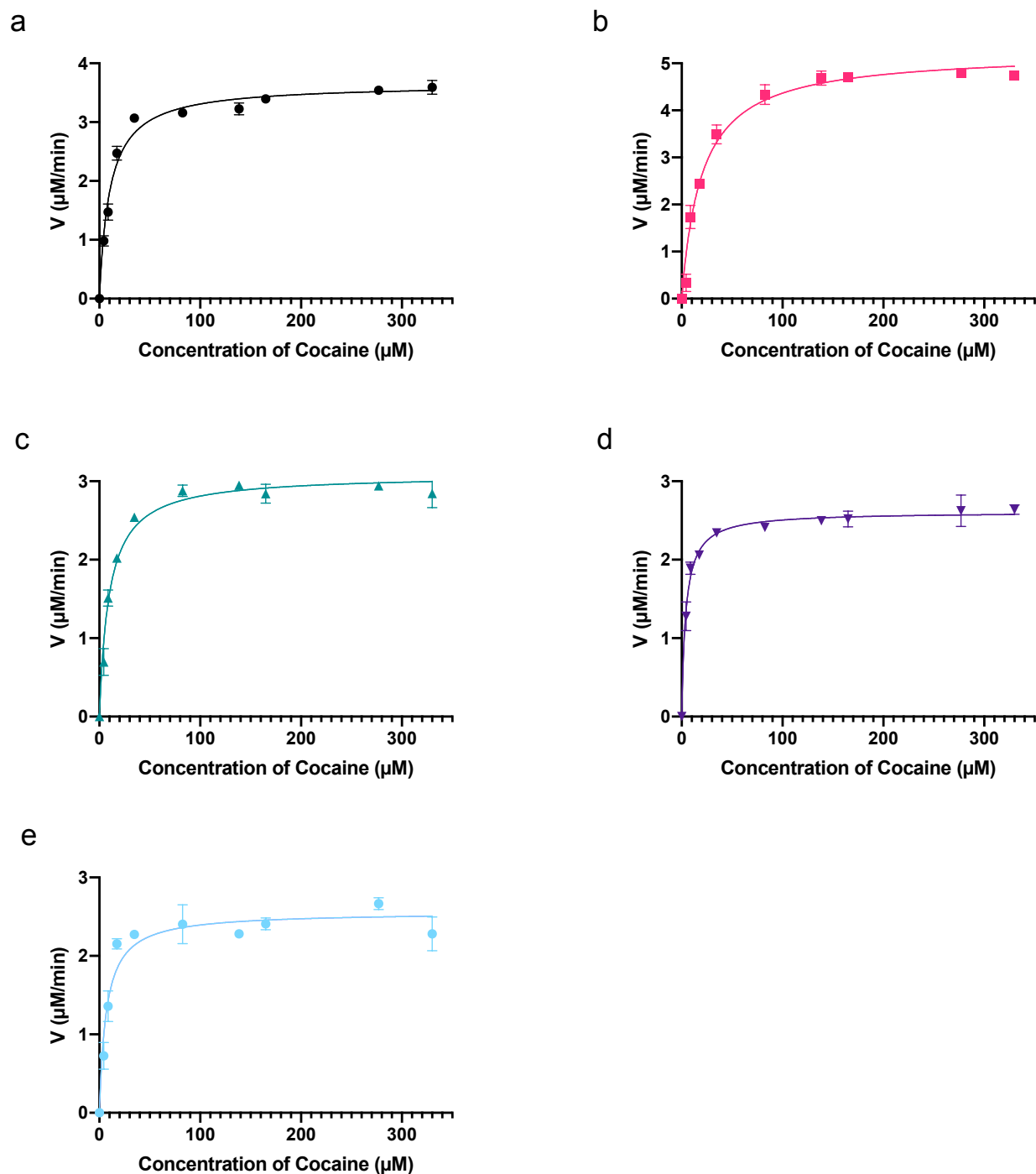


**Figure B5. Packaging of cocaine-binding aptamers in MS2 VLP confirmed by treatment with DNase-I:** respective samples were treated with DNase-I at 37 °C for 24 h. Each reaction mixture was then transferred into a dialysis bag (m.w. cut off 3 kDa) and dialyzed against water for 24 h. The absorbance of the sample present inside of the dialysis bag was measured to determine the concentration of cocaine-binding aptamer. A control experiment using only aptamer confirmed that DNA cannot cross the dialysis membrane unless it is degraded by DNase-I.

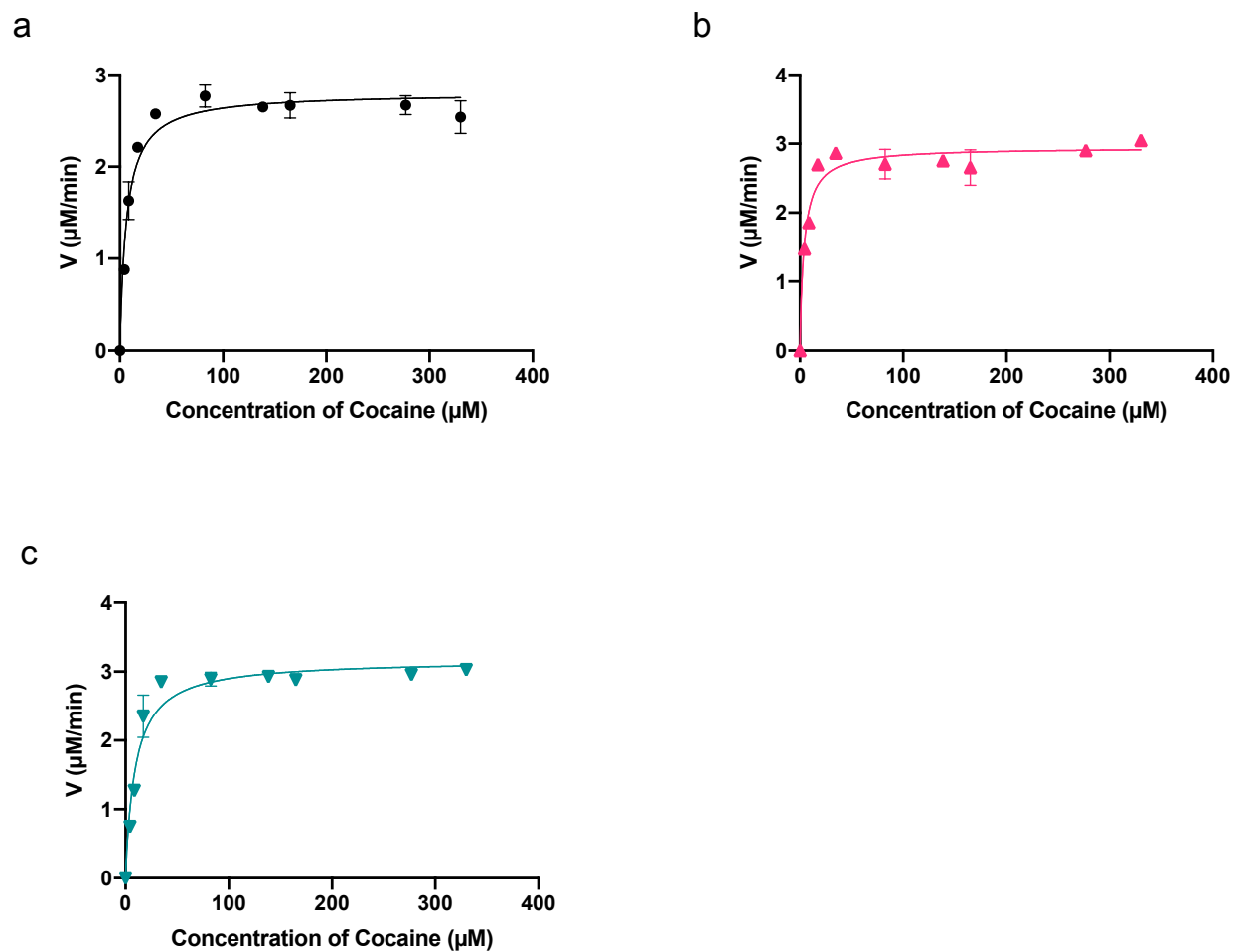




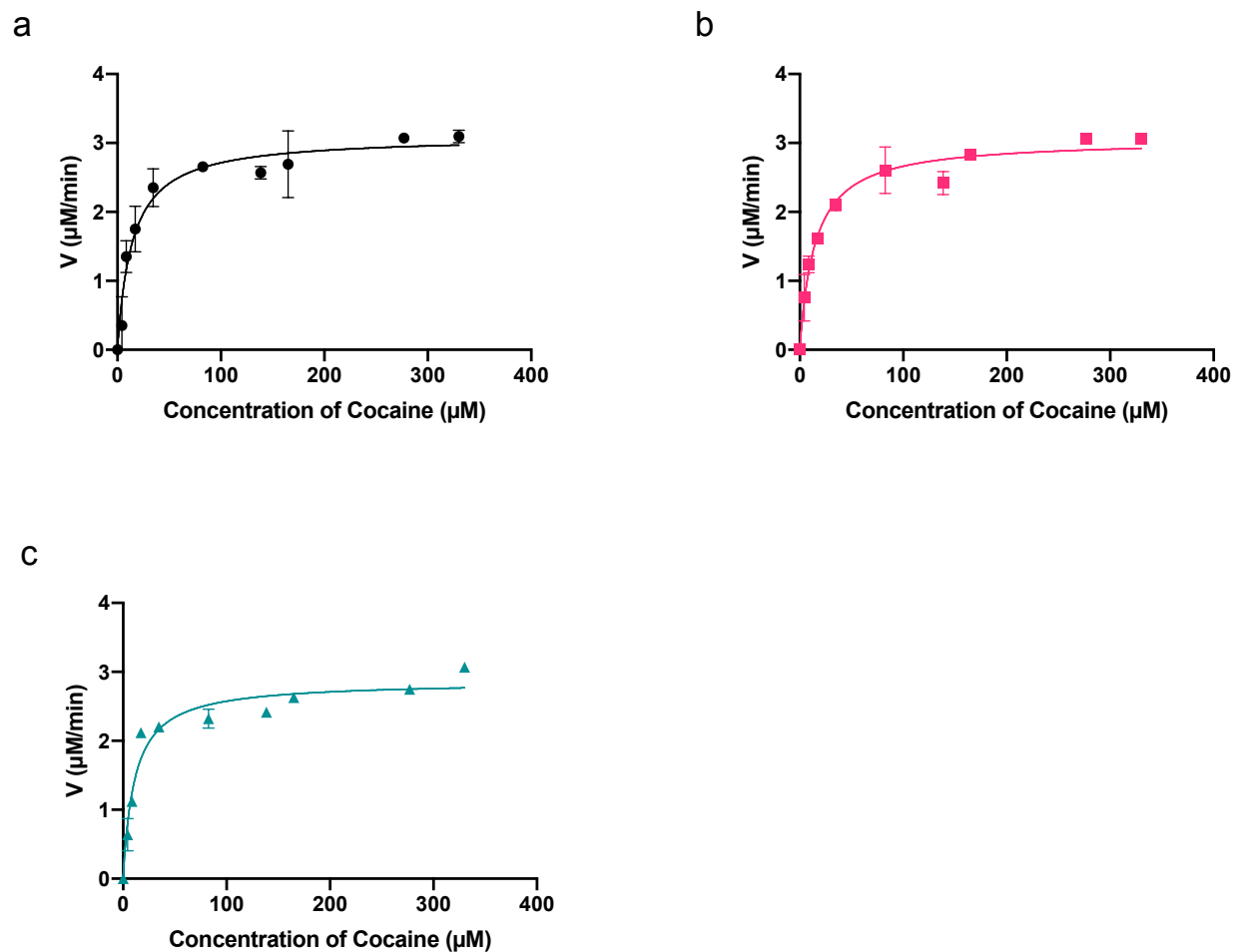
**Figure B6. Determination of cocaine binding by aptamers by MST, plotted using GraphPad Prism.** (a) MNS-4.1, (b) 38-GC, (c) 38-IC, (d) scrambled DNA.



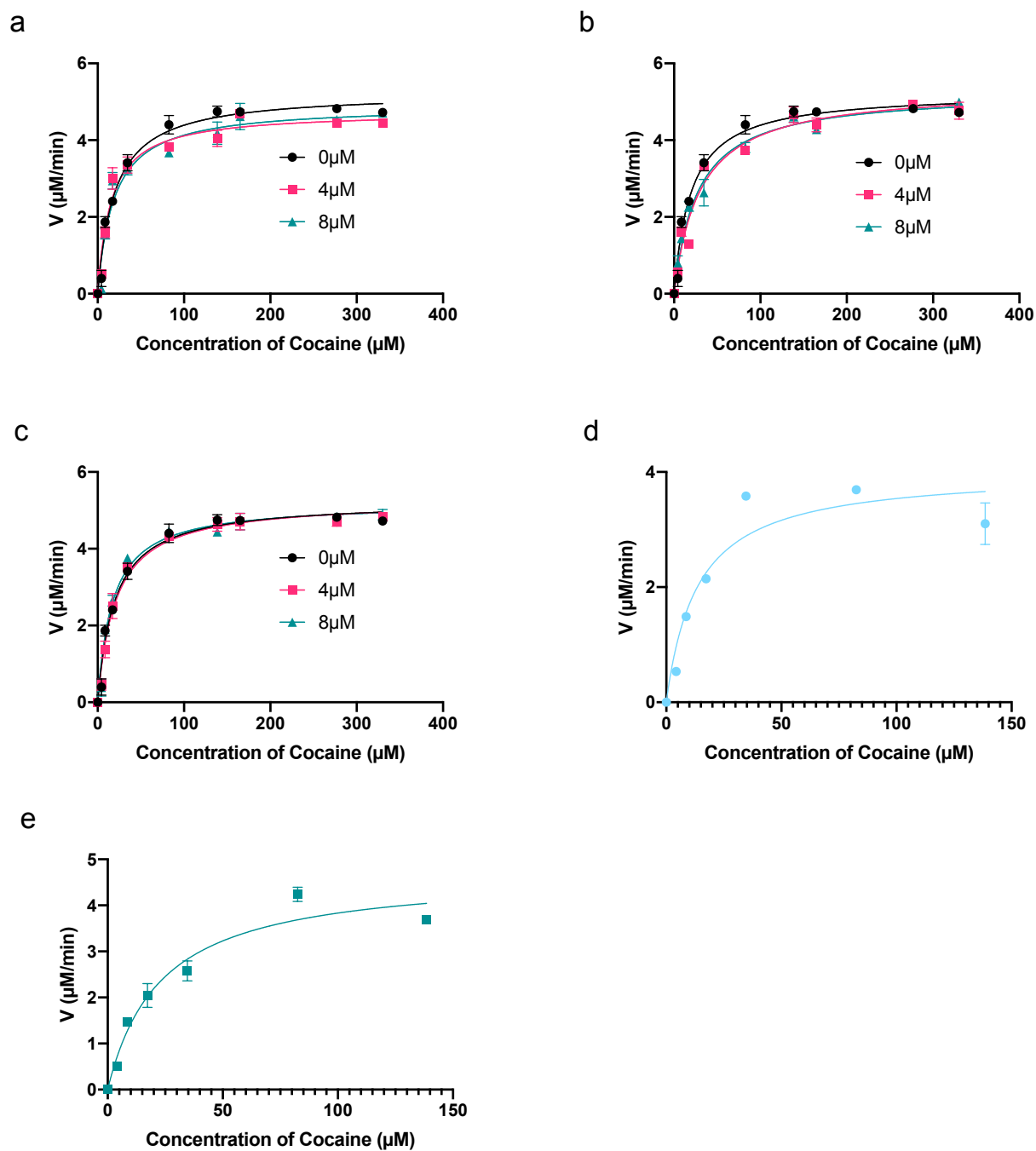
**Figure B7. Michaelis-Menten plots for (a) CocE-wt (b) MS2@CocE (c) MS2@CocE-4.13 (d) MS2@CocE-4.19 and (e) MS2@CocE-4.122.** Error bars represent the standard deviation of three independent trials. The data were graphed using GraphPad Prism.



**Figure B8. Michaelis-Menten traces for (a) MS2@CocE-GC5 (b) MS2@CocE-GC11 (c) MS2@CocE-GC21.** Error bars represent the standard deviation of three independent trials. The data were graphed using GraphPad Prism.



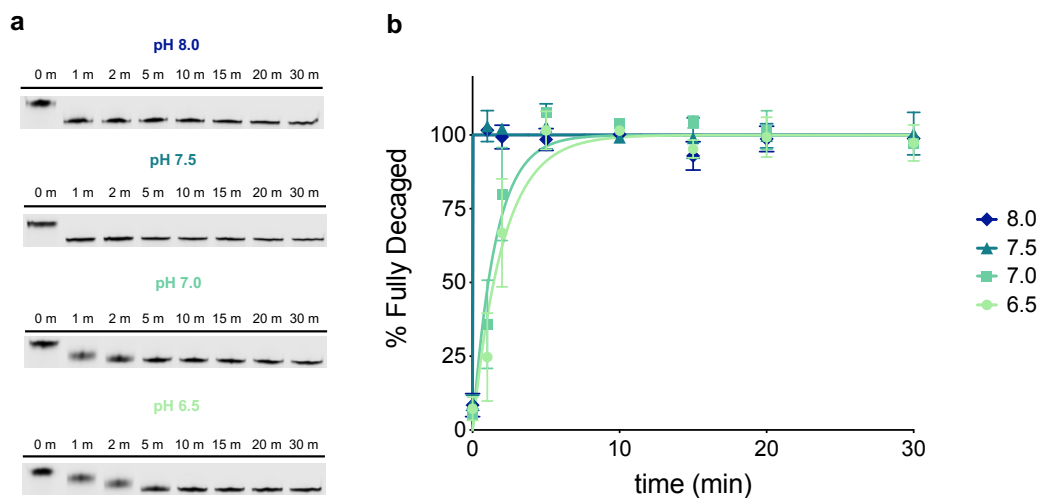
**Figure B9. Michaelis-Menten traces for (a) MS2@CocE-IC4 (b) MS2@CocE-IC10 (c) MS2@CocE-IC20.** Error bars represent the standard deviation of three independent trials. The data were graphed using GraphPad Prism.



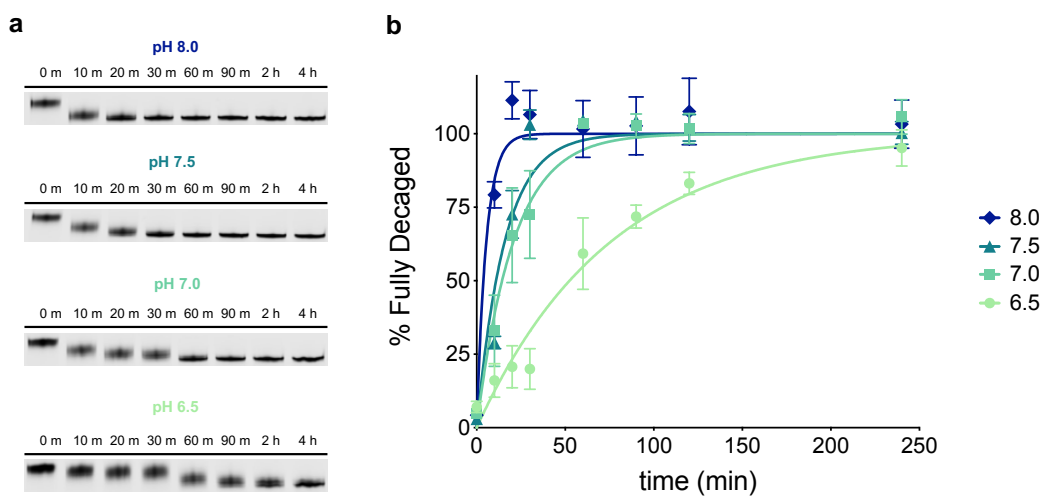
**Figure B10.** (a-c) Michaelis-Menten plots for MS2@CocE in the presence of aptamer added to the reaction solution (not co-packaged), compared to the absence of aptamer. (a) aptamer MNS-4.1, (b) aptamer 38-GC, (c) aptamer 38-IC. Error bars for represent the standard deviation of two independent trials. (d-e) Michaelis-Menten plots for co-packaged scrambled aptamers: (d)

MS2@CocE•Scr<sub>10</sub> and (e) MS2@Coc•EScr<sub>20</sub>. Error bars for represent the standard deviation of three independent trials. The data were graphed using GraphPad Prism.

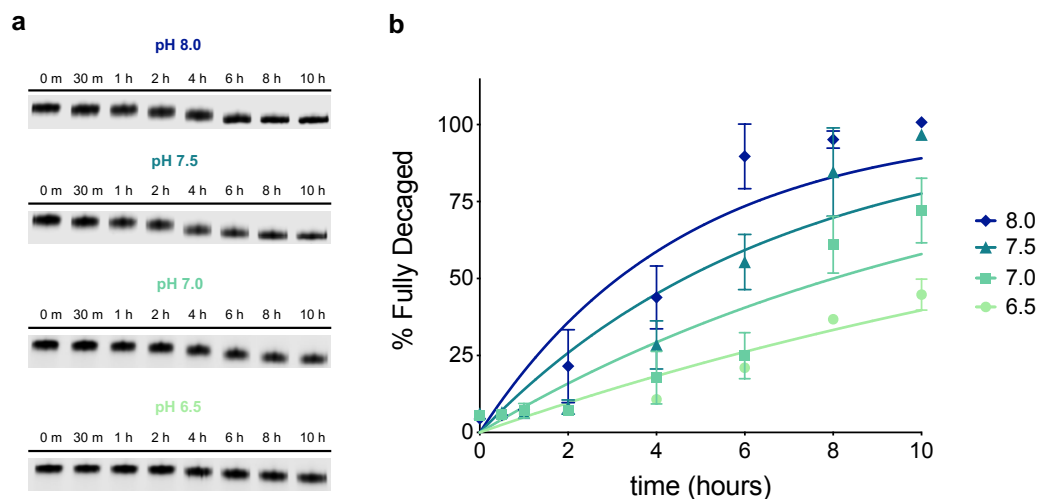
### Appendix C: Omitted Data from Chapter 4



**Figure C1: Decaging kinetics of a fully glyoxalated DNA strand at 95 °C with increasing pH.** a) Representative images of decaging with 20% PAGE analysis. 20 pmol of a fully caged DNA strand was incubated at 95 °C for the indicated times and immediately loaded onto a 20% polyacrylamide gel. b) Densitometric quantification of caging as a function of time. Values represent mean ( $n = 2$ ) normalized percentages versus band intensity of an untreated DNA control. Error bars denote standard deviation.



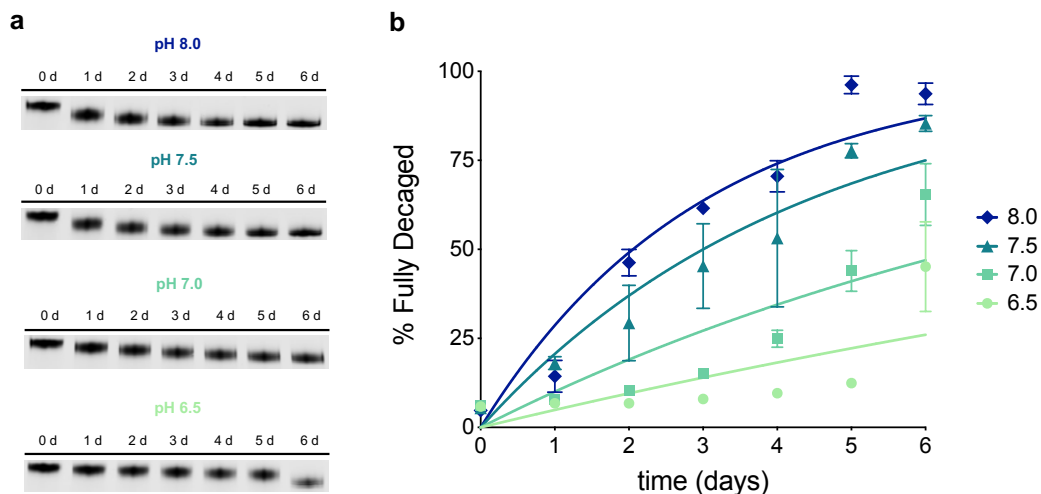
**Figure C2: Decaging kinetics of a fully glyoxalated DNA strand at 70 °C with increasing pH.** a) Representative images of decaging with 20% PAGE analysis. 20 pmol of a fully caged DNA strand was incubated at 70 °C for the indicated times and immediately loaded onto a 20% polyacrylamide gel. b) Densitometric quantification of caging as a function of time. Values represent mean ( $n = 2$ ) normalized percentages versus band intensity of an untreated DNA control. Error bars denote standard deviation.



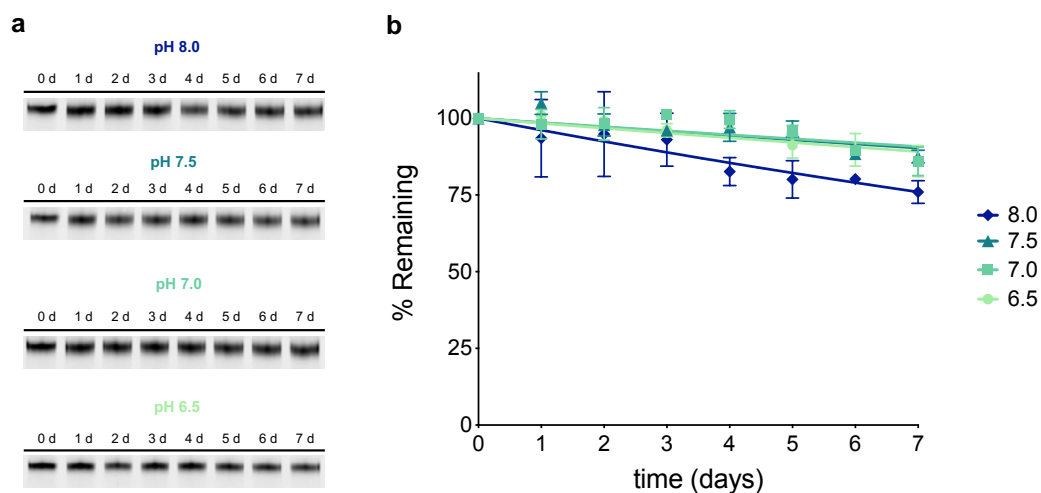
**Figure C3: Decaging kinetics of a fully glyoxalated DNA strand at 50 °C with increasing pH.** a) Representative images of decaging with 20% PAGE analysis. 20 pmol of a fully caged DNA strand was incubated at 50 °C for the indicated times and immediately loaded onto a 20% polyacrylamide gel. b) Densitometric quantification of caging as a function of time. Values represent



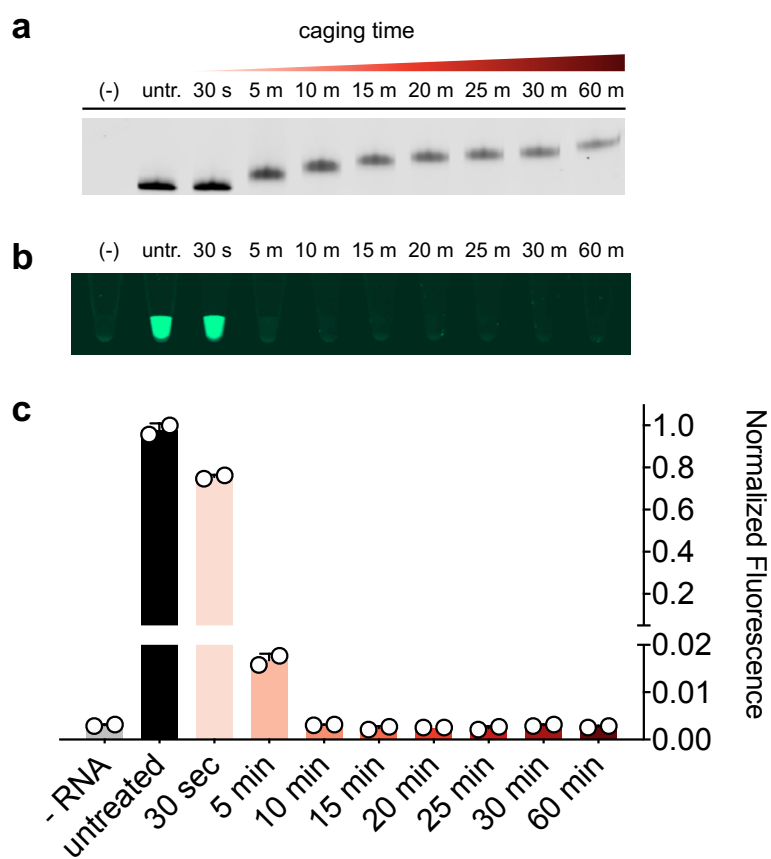
mean ( $n = 2$ ) normalized percentages versus band intensity of an untreated DNA control. Error bars denote standard deviation.



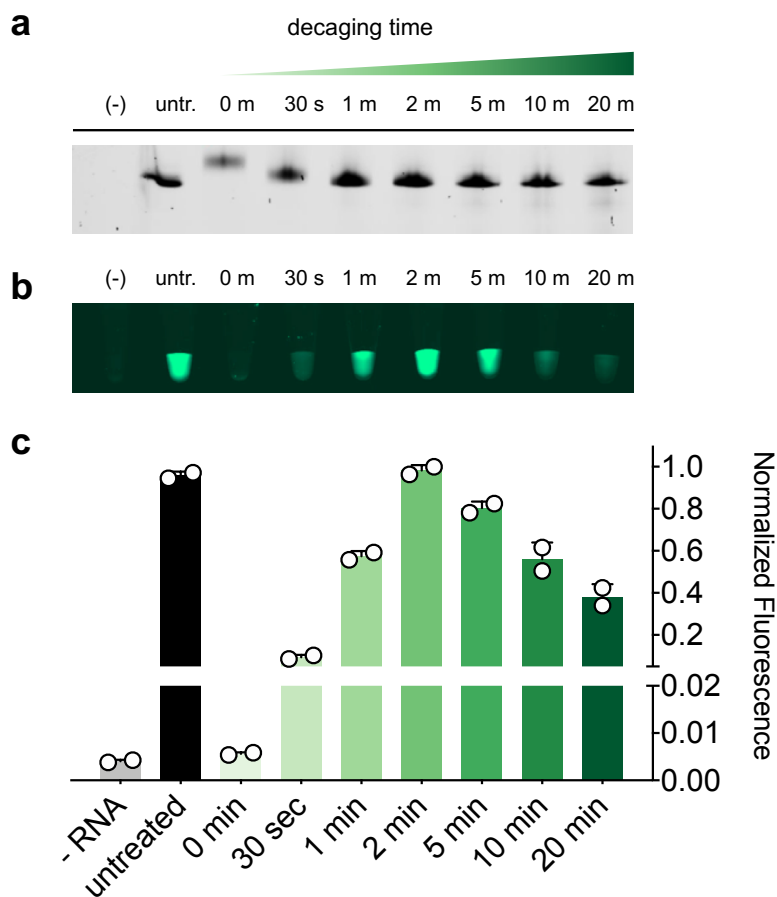
**Figure C4: Decaging kinetics of a fully glyoxalated DNA strand at 37 °C with increasing pH.** a) Representative images of decaging with 20% PAGE analysis. 20 pmol of a fully caged DNA strand was incubated at 37 °C for the indicated times and immediately loaded onto a 20% polyacrylamide gel. b) Densitometric quantification of caging as a function of time. Values represent mean ( $n = 2$ ) normalized percentages versus band intensity of an untreated DNA control. Error bars denote standard deviation.



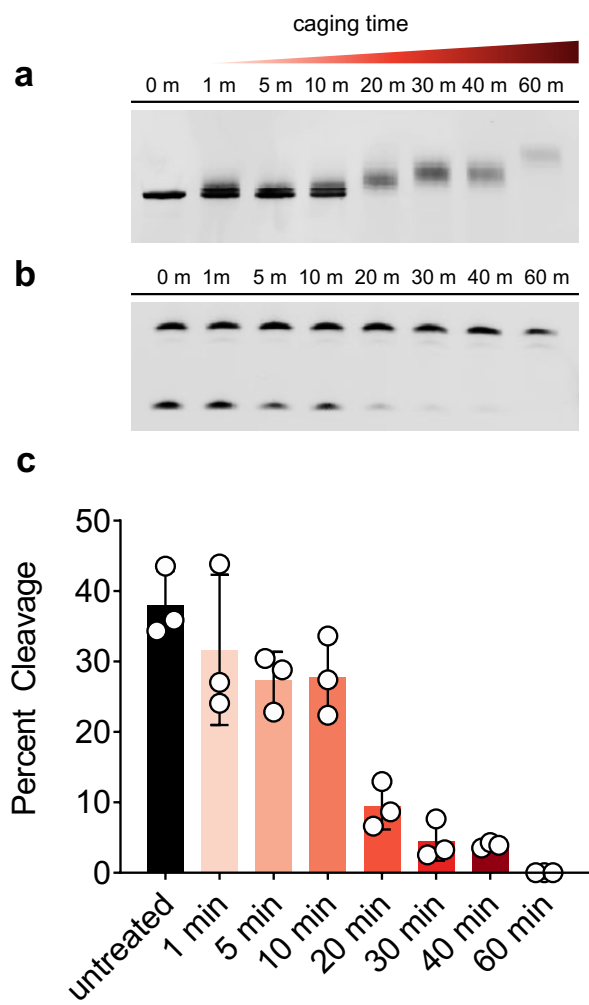
**Figure C5: Room temperature stability of a glyoxalated DNA strand with increasing pH.** a) Representative images of decaging with 20% PAGE analysis. 20 pmol of a fully caged DNA strand was incubated at room temperature for the indicated times and immediately loaded onto a 20% polyacrylamide gel. b) Densitometric quantification of caging as a function of time. Values represent mean ( $n = 2$ ) normalized percentages versus band intensity of the fully caged DNA strand at  $T = 0$  hours. Error bars denote standard deviation.



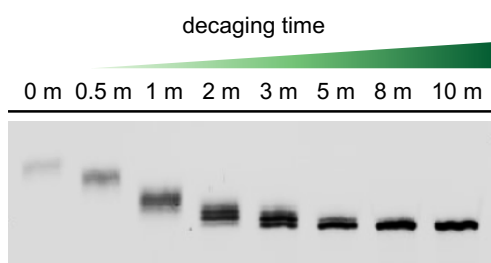
**Figure C6: Fluorogenic performance of the broccoli RNA aptamer with increasing caging times.** a) 20% PAGE analysis of broccoli RNA aptamer (104nt) after various amounts of glyoxal caging, illustrating an increase in apparent molecular weight. b,c) Functional performance of broccoli aptamers with increasing degrees of caging, demonstrating that only partial glyoxalation (5–10 minutes) is necessary to ablate fluorogenic activity.



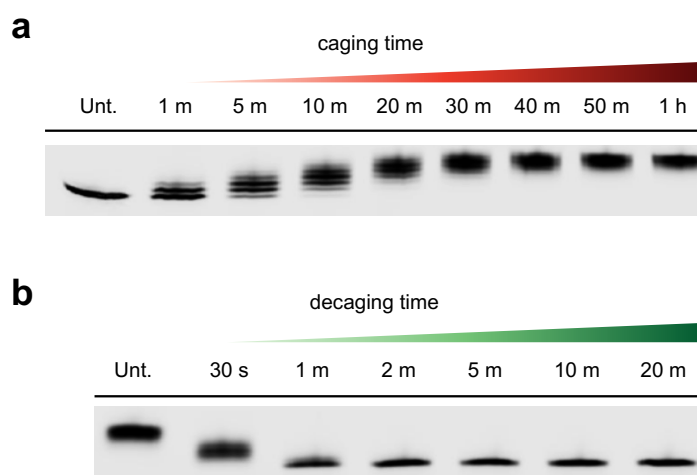
**Figure C7: Restoration of fluorogenic activity in a caged broccoli RNA aptamer as a function of increasing decaging times.** a) 20% PAGE analysis of caged broccoli RNA aptamer (104 nt) after increasing decaging times at 95 °C pH 7.5 illustrating a decrease in apparent molecular weight. b,c) Fluorescent activity of caged broccoli aptamers as a function of decaging times, demonstrating that ~2 minutes is optimal for full restoration of fluorogenic activity.



**Figure C8: Glyoxalation disrupts 10-23 DNAzyme structure and target cleavage.** a) 20% PAGE analysis of the 10-23 DNAzyme with increasing amounts of glyoxal caging, illustrating an increase in apparent molecular weight. b) 12% PAGE analysis monitoring target cleavage by increasingly caged 10-23 DNAzyme. c) Densitometric quantification of caged DNAzyme activity. Band intensity was used to quantify activity as percent target cleavage (n = 3). Error bars denote standard deviation.

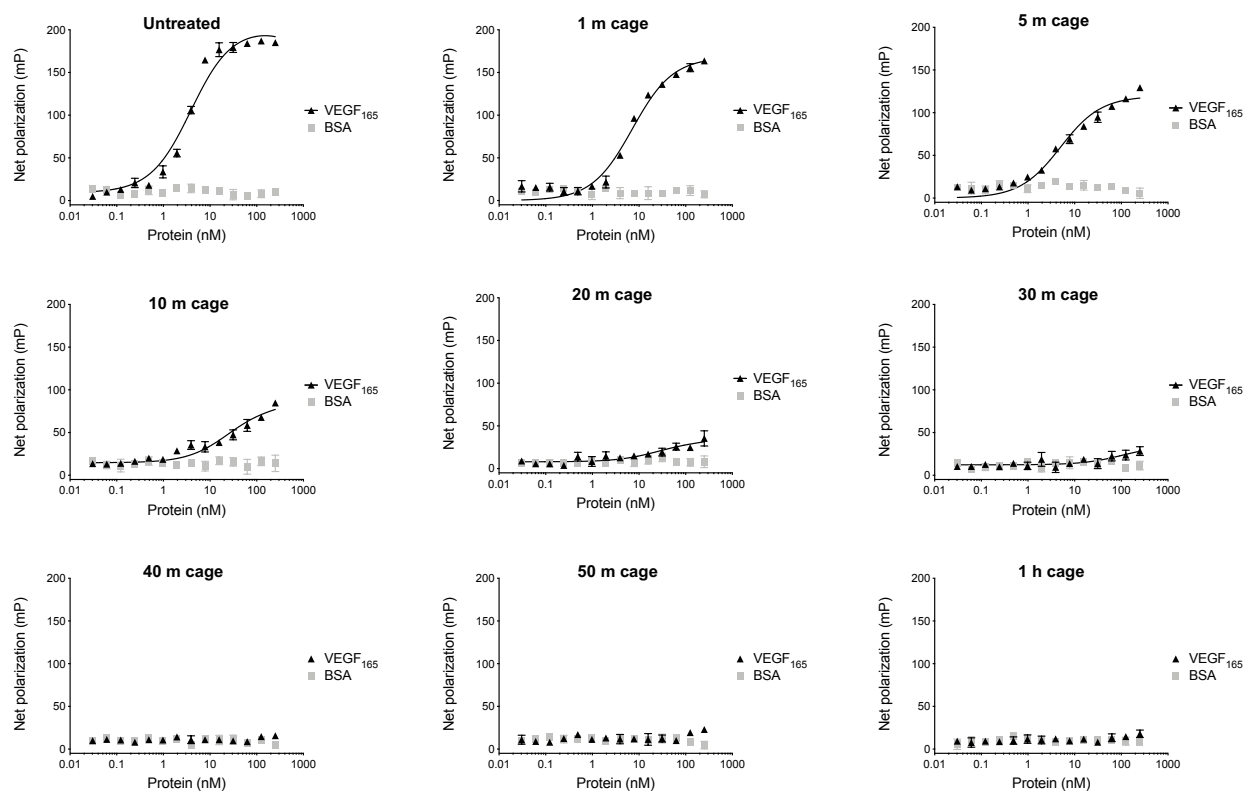


**Figure C9: DNAzyme decaging kinetics.** 20% PAGE analysis of caged 10-23 DNAzyme after increasing decaging times at 95 °C pH 7.5 illustrating a decrease in apparent molecular weight.



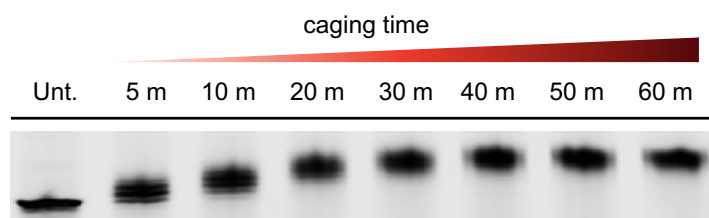
**Figure C10. Glyoxal caging and decaging of a fully 2'-O-methylated RNA aptamer.** a) 20% PAGE analysis of caged ARC259 (23nt) after increasing caging times, illustrating an increase in

apparent molecular weight. b) 20% PAGE analysis of caged ARC259 after increasing decaging times at 95 °C, pH 7.5 illustrating a decrease in apparent molecular weight.

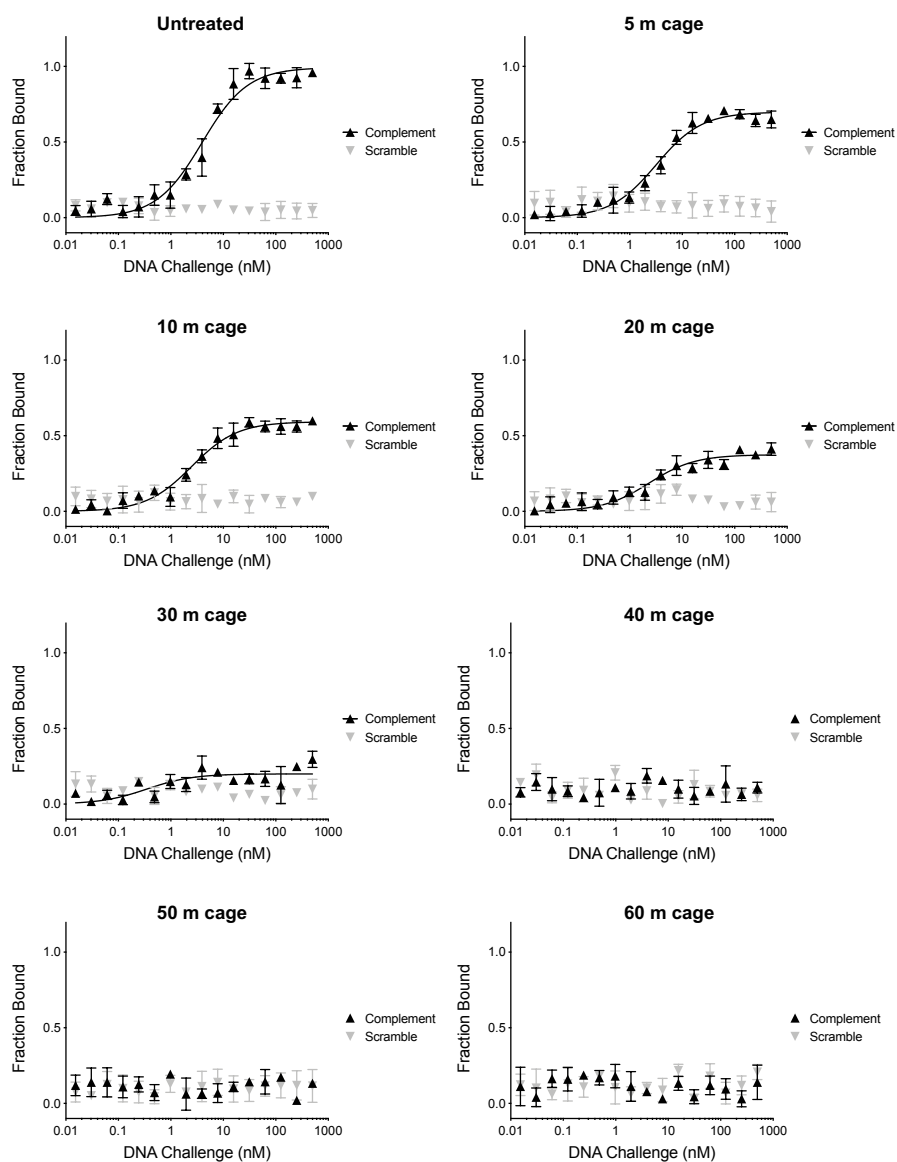


**Figure C11: Functional binding activity of increasingly caged ARC259.** Fluorescence polarization (FP) curves of aptamer binding towards VEGF<sub>165</sub> or bovine serum albumin (BSA). All values were normalized to a buffer blank and represent mean (n = 3) of independent replicates.

3' CATGACATGAGCTAACCGACAG 2'

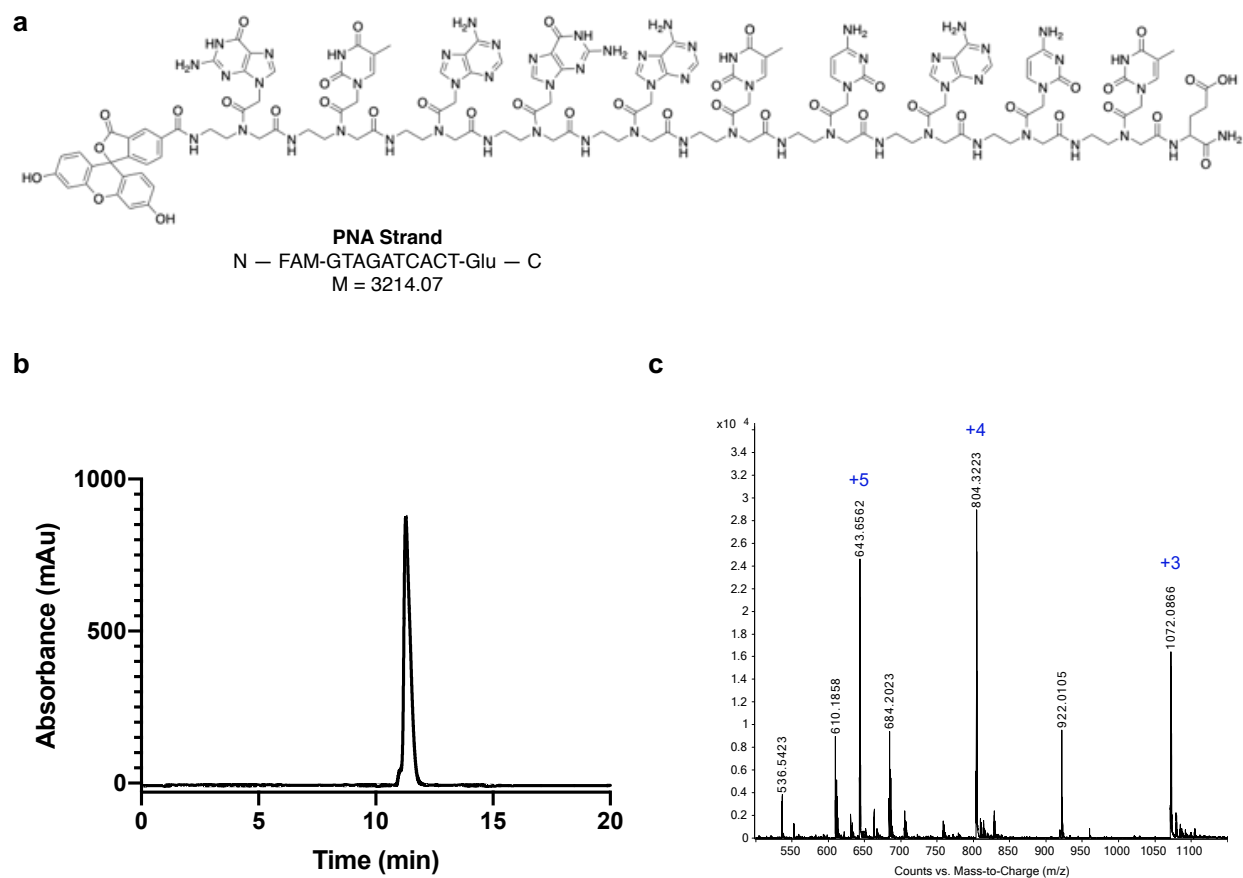


**Figure C12: Glyoxal caging of a TNA oligonucleotide.** Sequence of model TNA strand (23 nt) and 20% PAGE analysis after increasing caging times, illustrating an increase in apparent molecular weight

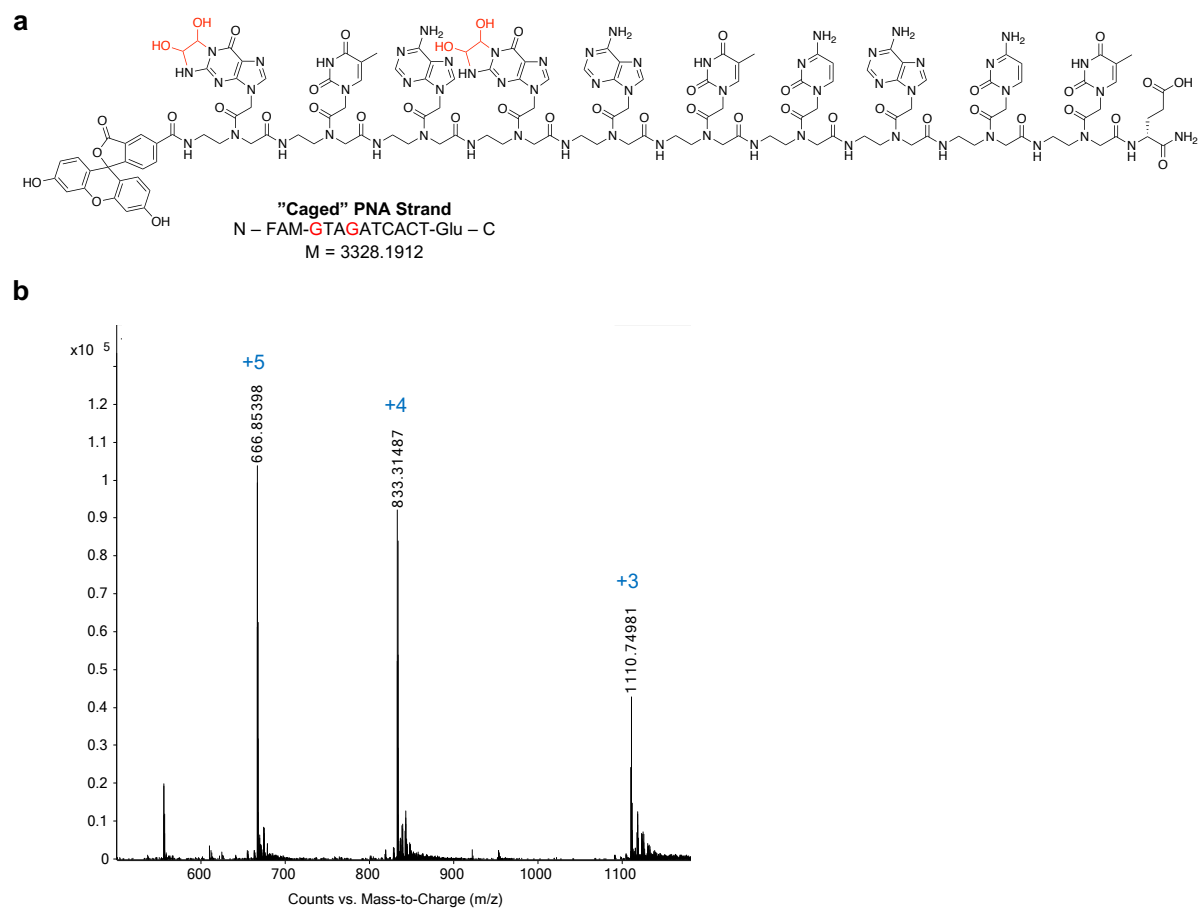




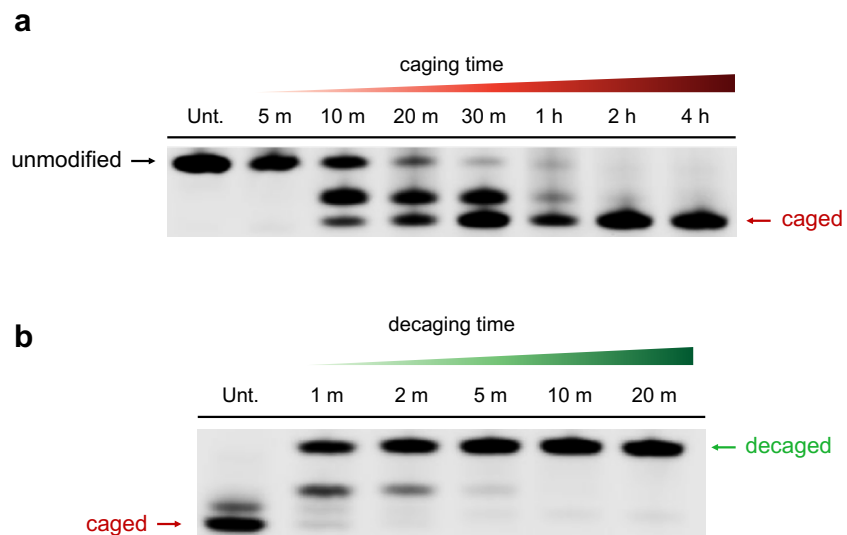
**Figure C13: Glyoxal caging of TNA disrupts hybridization to DNA.** Microscale thermophoresis (MST) of TNA binding towards a complementary (black) or scrambled DNA sequence (grey) with increasing caging times. Values represent mean (n = 3) of independent replicates.



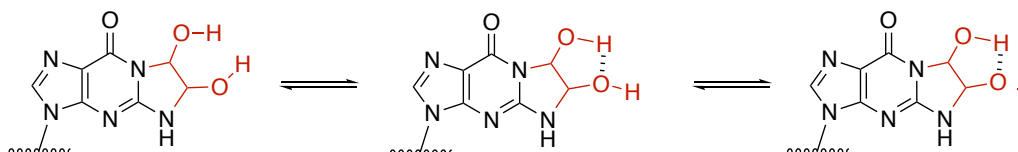
**Figure C14: Analytical characterization of synthesized model PNA strand.** a) Chemical structure and sequence of model PNA strand used in the study. Glu = glutamic acid. b) HPLC (A260 nm) and c) TOF ESI-MS analysis of purified PNA.



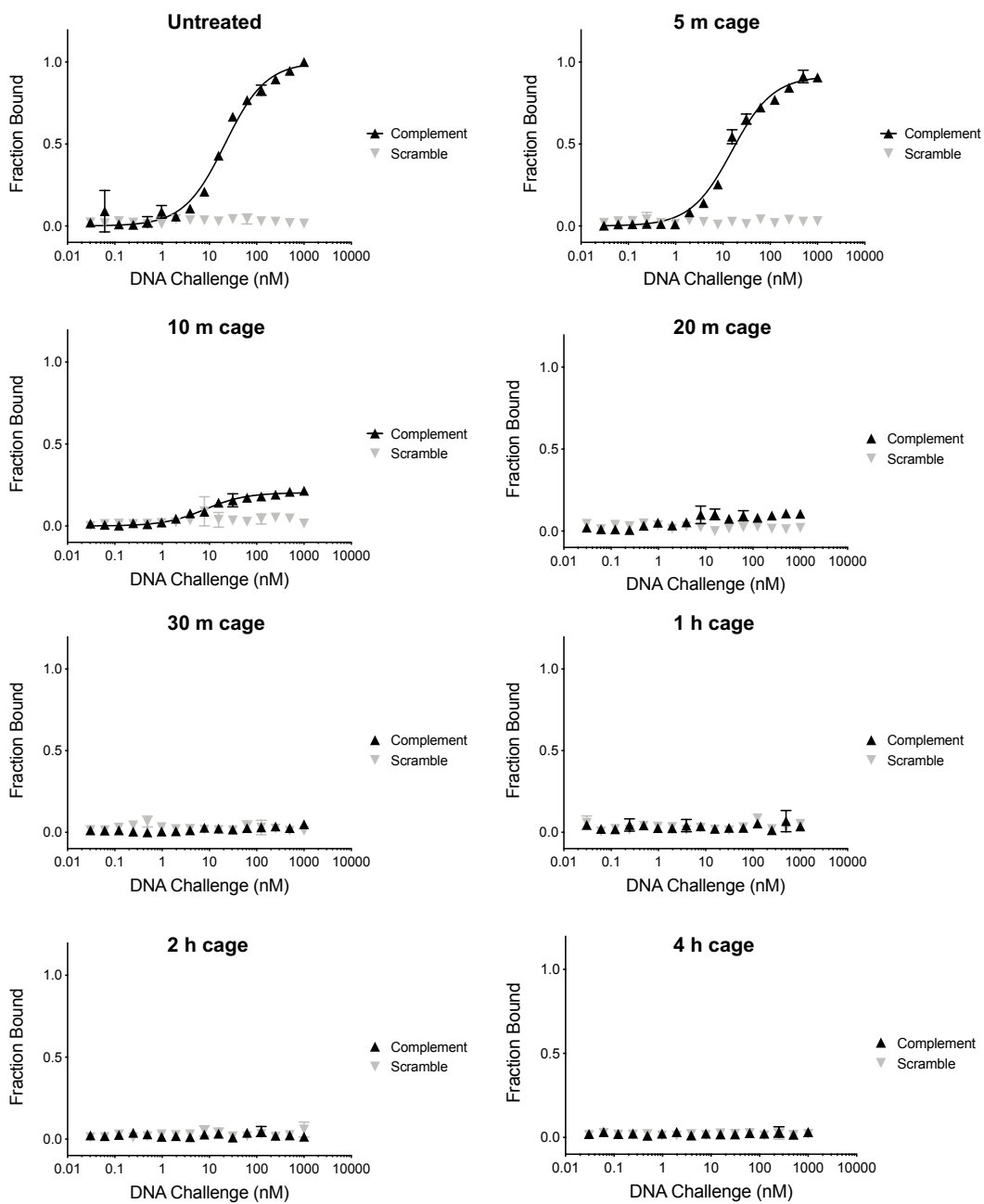
**Figure C15: Analytical characterization of glyoxal-treated PNA.** a) Chemical structure and sequence of PNA strand with putative glyoxal adducts (red). Glu = glutamic acid. b) TOF ESI-MS analysis of purified PNA treated with glyoxal.



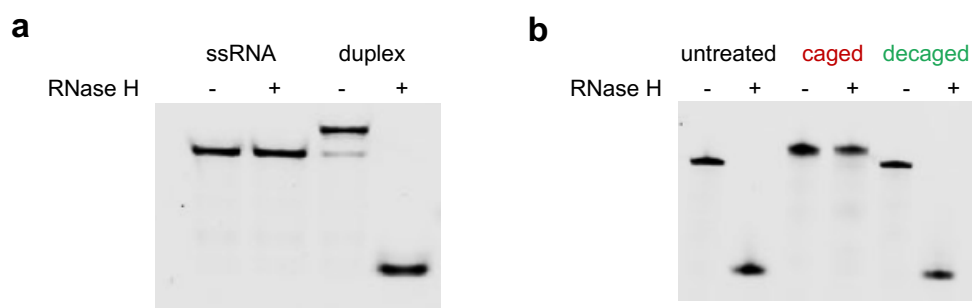
**Figure C16: PAGE analysis of PNA caging and decaging.** a) 20% PAGE analysis after increasing caging times, illustrating observed downward shift in electrophoretic mobility. b) 20% PAGE analysis of caged PNA after increasing decaging times at 95 °C pH 7.5, illustrating restoration in electrophoretic mobility.



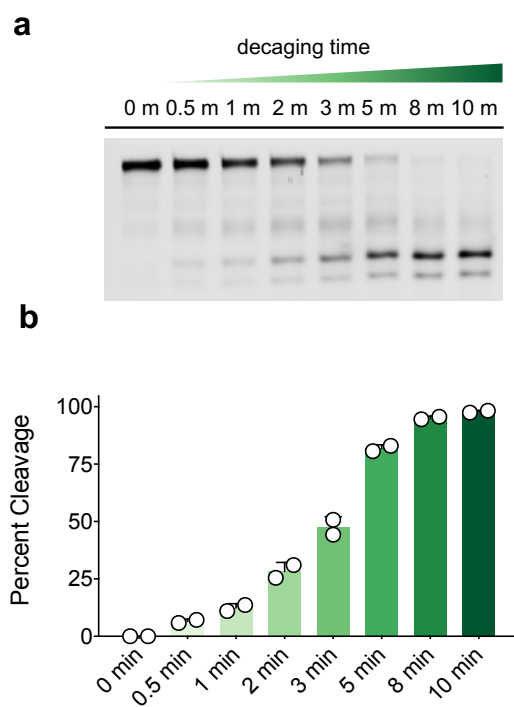
**Figure C17: Proposed molecular mechanism of PNA mobility shifts.** Bis-hemiaminal adducts introduced by glyoxal may result in an ionizable proton and overall gain in negative charge through hydrogen bond sharing between hydroxyl moieties.



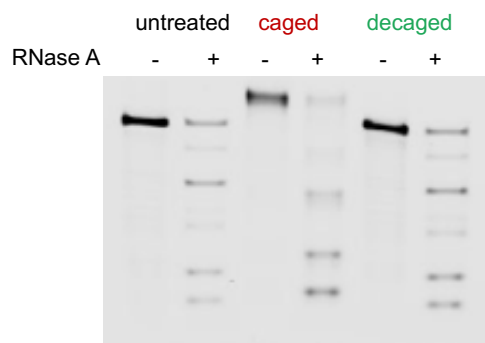
**Figure C18: Glyoxal caging of PNA caging inhibits hybridization to DNA.** a) Microscale thermophoresis (MST) of PNA binding towards a complementary (black) or scrambled DNA sequence (grey) with increasing caging times. Values represent mean (n = 3) of independent replicates.



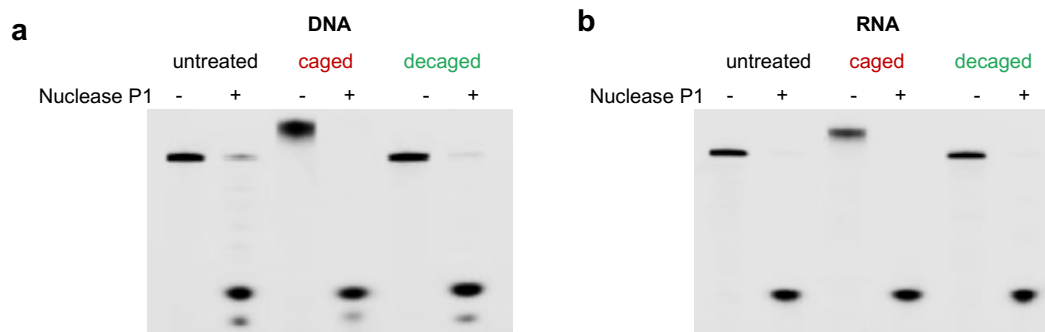
**Figure C19: Reversible control of RNase H with glyoxal caging.** a) 12% native PAGE gel showing requirement of RNA :DNA duplexes for RNase H cleavage activity. b) 12% denaturing PAGE gel of RNase H mediated target cleavage of untreated, caged, and decaged RNA.



**Figure C20: One-pot activation of thermostable RNase H.** a) 12% PAGE analysis and b) quantified percent target cleavage (n = 2) by thermostable RNase H with increased decaging time at 95 °C.

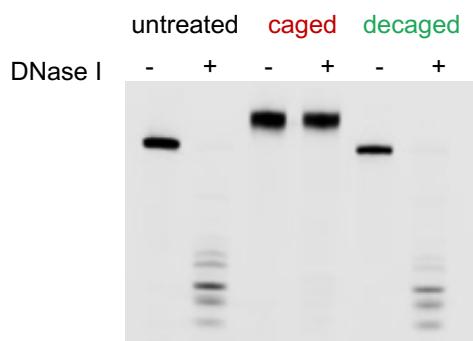


**Figure C21: Glyoxal does not inhibit RNase A.** 12% PAGE analysis of RNase A activity towards untreated, caged, and decaged RNA, illustrating cleavage of all substrates.

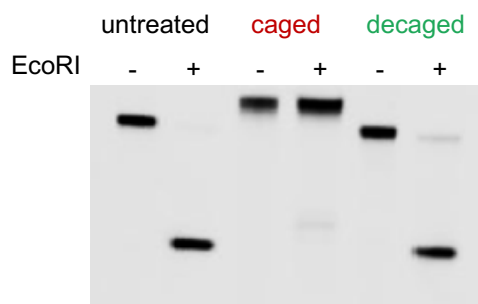


**Figure C22: Glyoxal does not inhibit Nuclease P1.** 12% PAGE gel of nuclease P1 cleavage of untreated, caged, and decaged a) DNA and b) RNA.

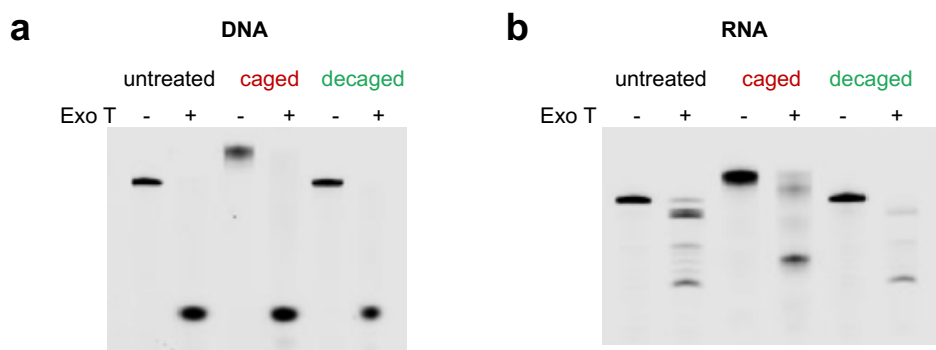




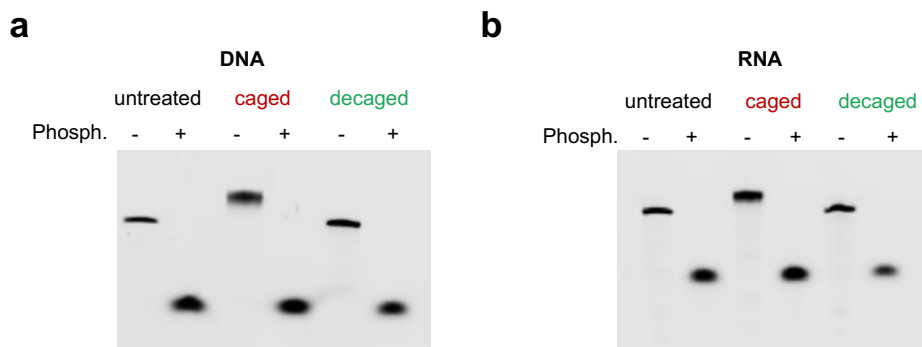
**Figure C23: Reversible control of DNase I recognition and cleavage.** 12% PAGE gel of DNase I cleavage of untreated, caged, and decaged DNA.



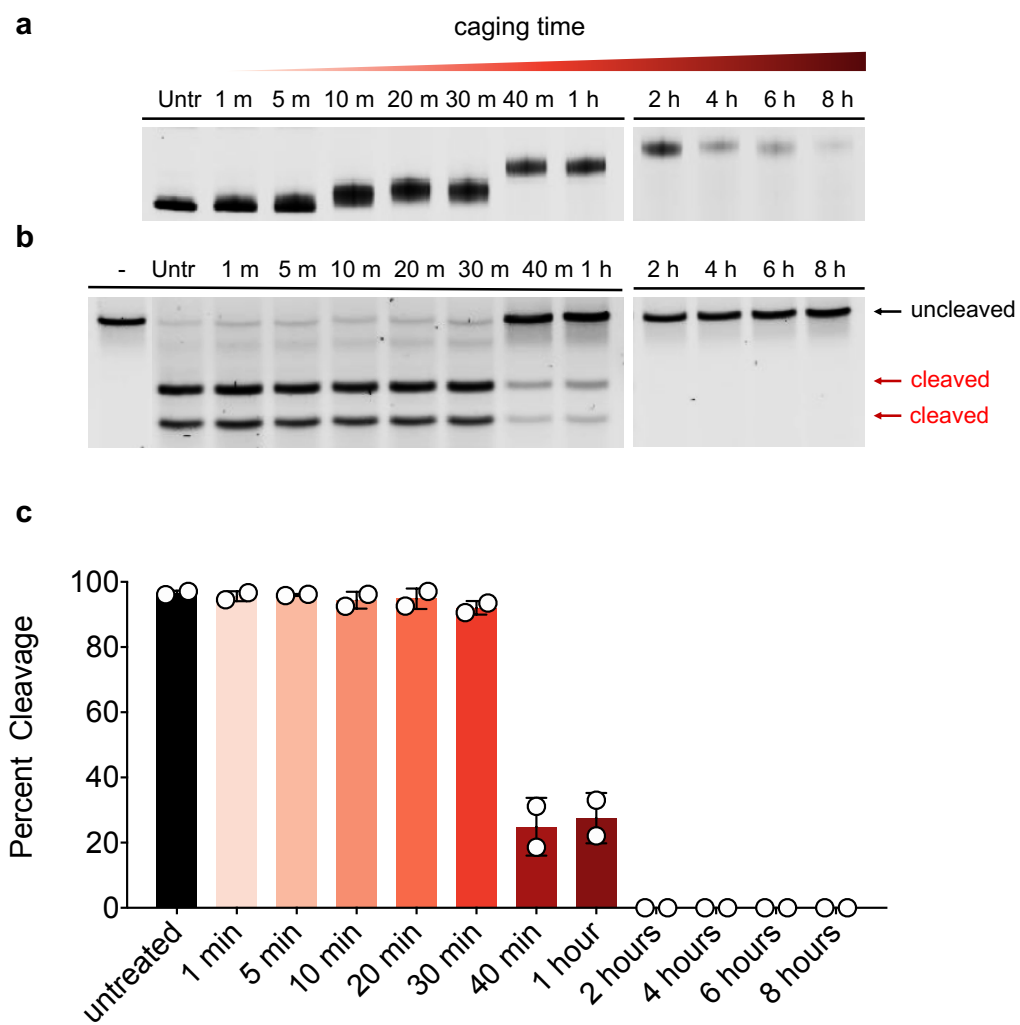
**Figure C24: Reversible control of EcoRI.** 12% PAGE gel of EcoRI mediated target cleavage by untreated, caged, and decaged DNA.



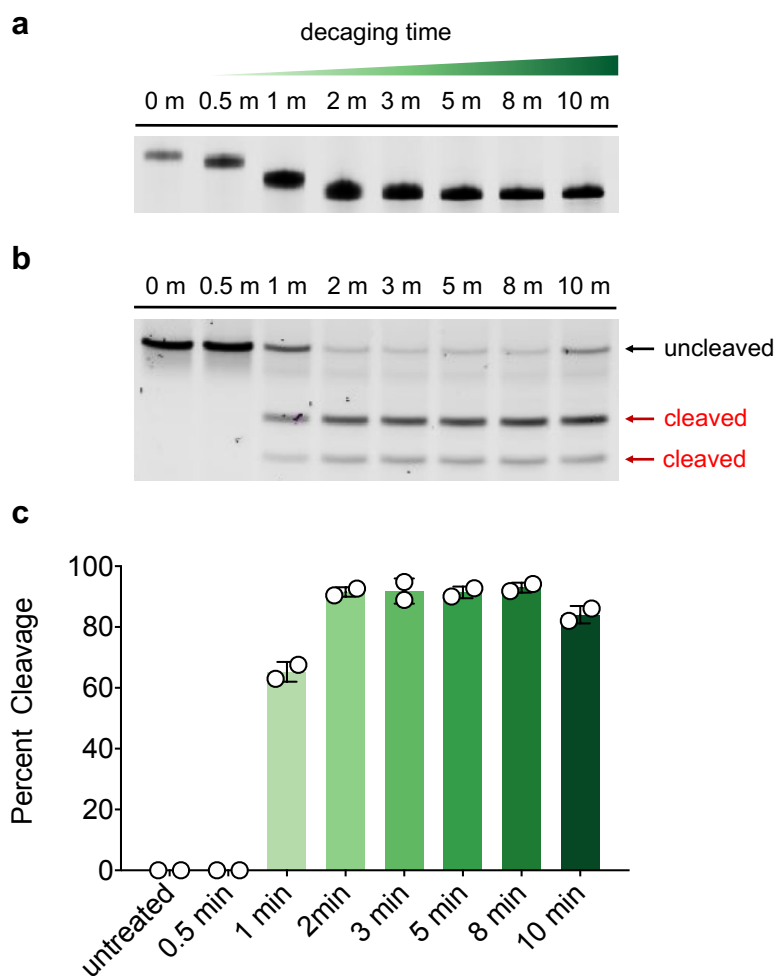
**Figure C25: Glyoxal does not inhibit RNase T.** 12% PAGE gel of RNase T cleavage of untreated, caged, and decaged a) DNA and b) RNA.



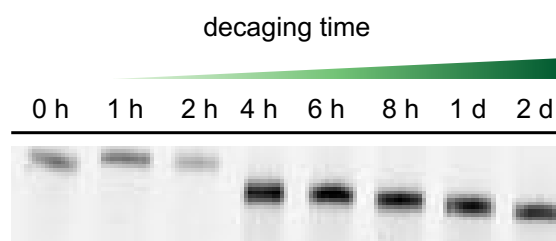
**Figure C26: Glyoxal does not inhibit snake venom phosphodiesterase I.** 12% PAGE gel of phosphodiesterase cleavage of untreated, caged, and decaged a) DNA and b) RNA.



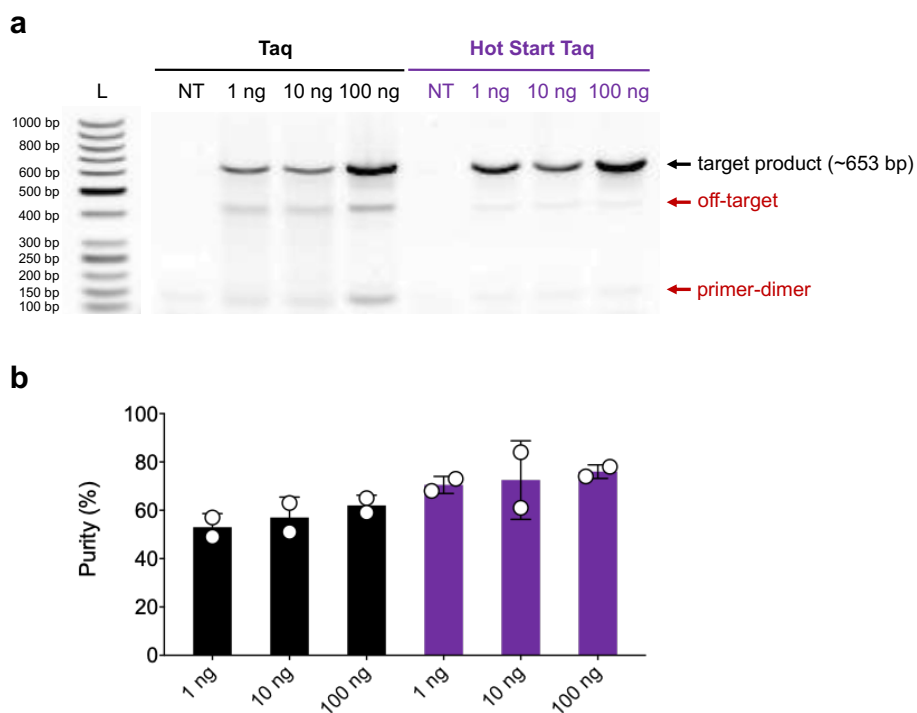
**Figure C27: Glyoxalation disrupts sgRNA and Cas9 mediated target cleavage.** a) Caging kinetics of sgRNA were monitored by 10% PAGE gel illustrating an increase in apparent molecular weight. b) 1% agarose gel analysis monitoring dsDNA target cleavage by increasingly caged sgRNA. “-“ indicates no sgRNA or RNP included in reaction. c) Densitometric quantification of Cas9 activity with increasingly caged sgRNA. Band intensity was used to quantify activity as percent target cleavage (n = 2). Error bars denote standard deviation.



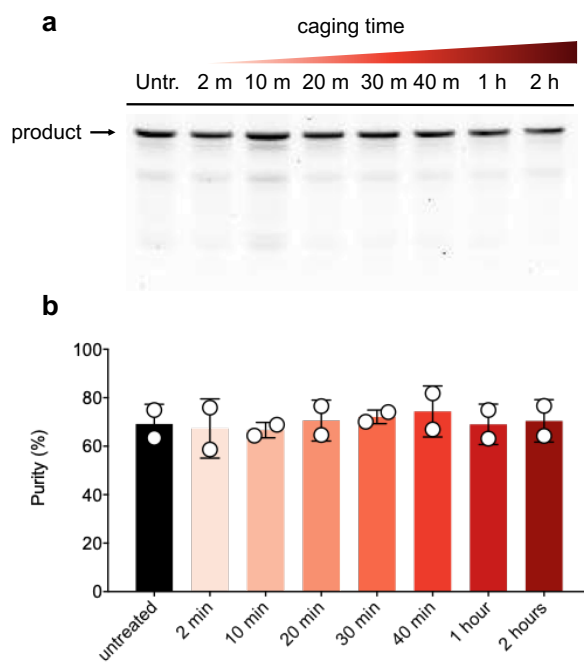
**Figure C28: Glyoxalation of sgRNA is reversible with rapid decaging.** a) Decaging kinetics of sgRNA at 95 °C were monitored by 10% PAGE gel illustrating decrease in apparent molecular weight. b) 1% agarose gel analysis monitoring target cleavage by increasingly decaged sgRNA. c) Densitometric quantification of caged sgRNA- Cas9 activity. Band intensity was used to quantify activity as percent target cleavage (n = 2). Error bars denote standard deviation.



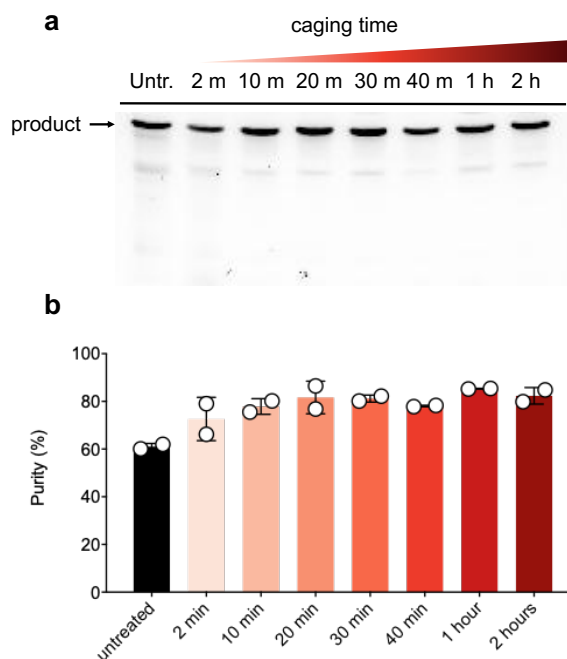
**Figure C29: Glyoxalation of sgRNA is reversible with slow decaging.** Decaging kinetics of sgRNA at 37 °C were monitored by 10% PAGE gel illustrating decrease in apparent molecular weight.



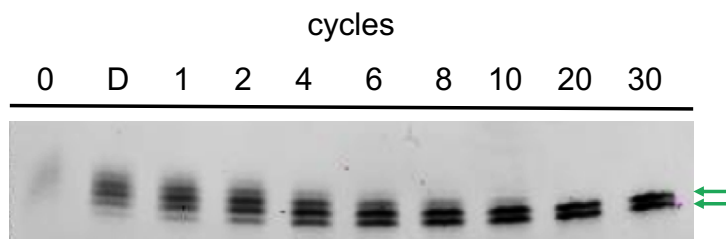
**Figure C30: Amplification of  $\beta$ -actin from human genomic DNA using Taq and Hot Start Taq polymerases.** a) PCR amplification with increasing genomic DNA template visualized by 1% agarose gel stained with SYBR Safe (NT = no template). Expected target band (~653 bp) is indicated by black arrows, while off-target and putative primer-dimer bands are labeled with red arrows. b) Densitometric quantification of amplicon purity. Bars represent mean and S.D. from 2 independent trials.



**Figure C31: Forward primer glyoxal treatment and PCR specificity.** a) PCR reactions using increasingly caged forward primer as visualized by 1% agarose gel and b) quantified using densitometry. Bars represent mean and S.D. from 2 independent trials.

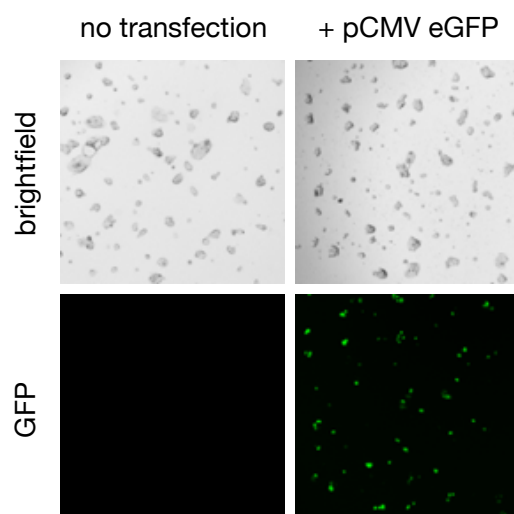


**Figure C32: Reverse primer glyoxal treatment and PCR specificity.** a) PCR reactions with increasingly caged reverse primer as visualized by 1% agarose gel and b) quantified using densitometry. Bars represent mean and S.D. from 2 independent trials.

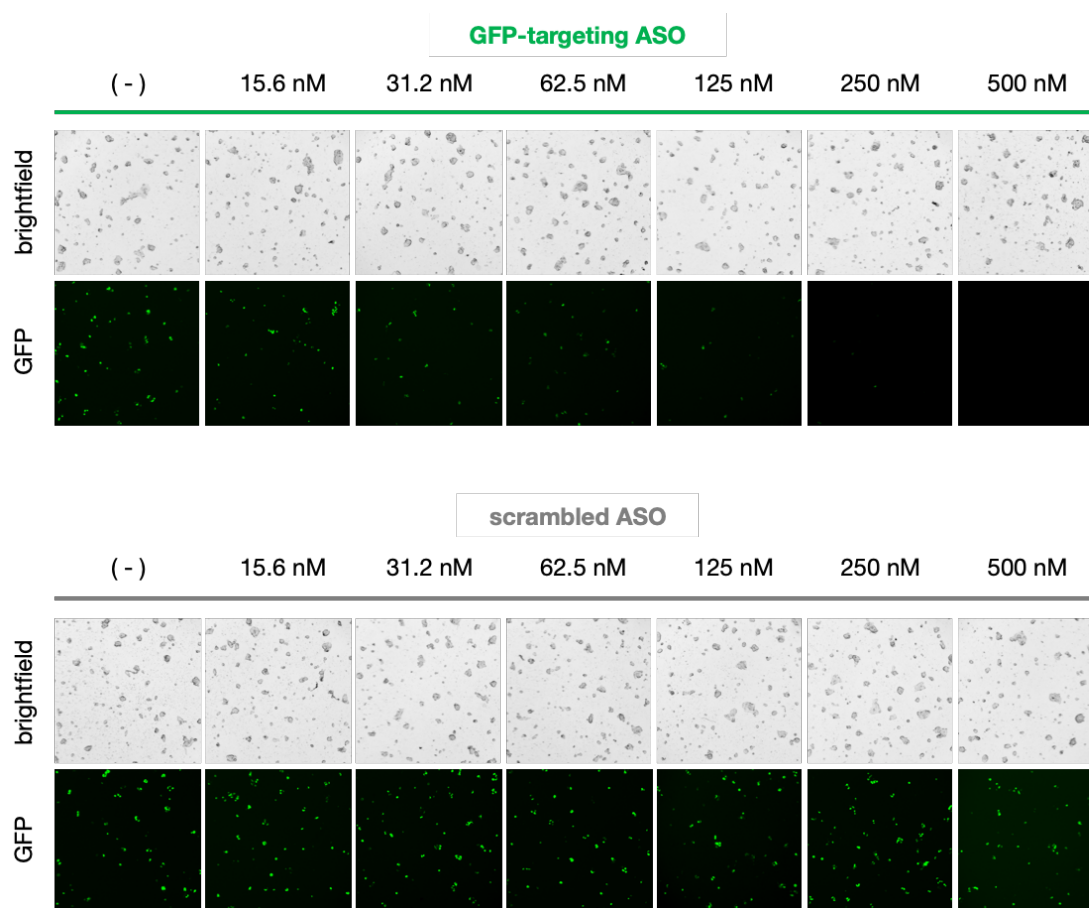


**Figure C33: Primer decaging during PCR.** 20% PAGE analysis of caged forward/primer mix after increasing PCR cycles in 1X PCR buffer, illustrating a decrease in apparent molecular weight. D = initial denaturation step (94 °C for 2 min). Reactions contain a mix of two primers, resulting in two distinct bands in each lane. Green arrows denote fully decaged forward and reverse primer.

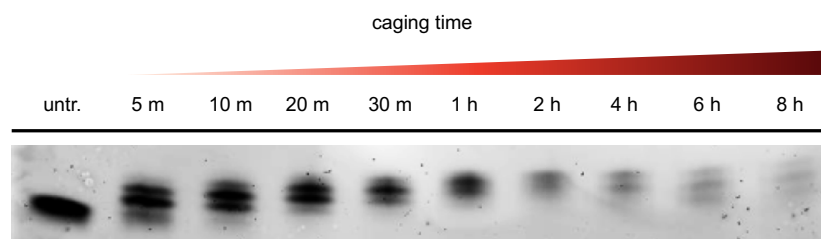




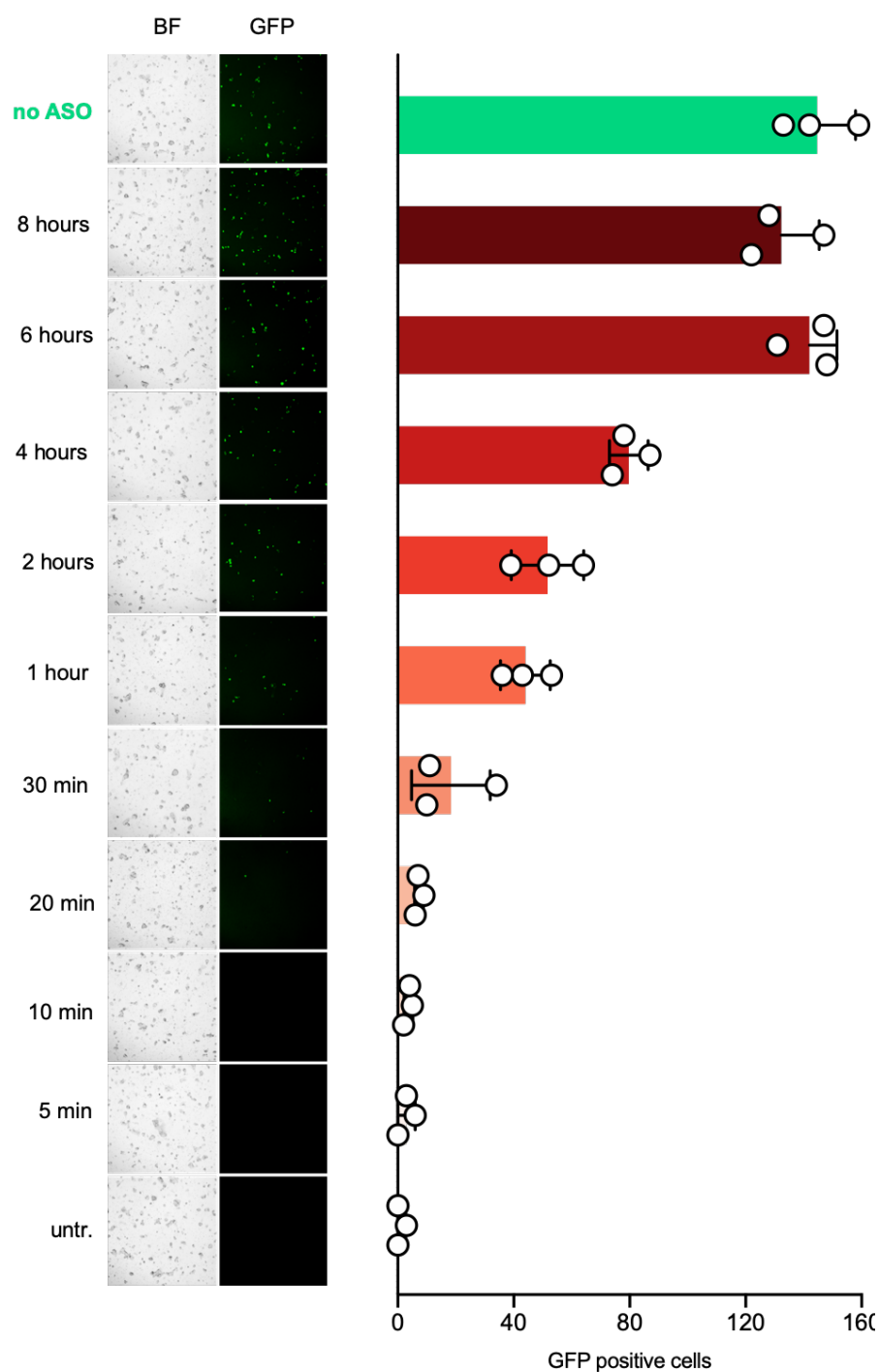
**Figure C34: Confirming transfection efficiency and specificity.** HEK293T cells were transfected with 200 ng of a pCMV vector encoding eGFP. Control cells received PBS. After 12 hours, GFP expression was detected by live-cell imaging using a BioTek Lionheart FX automated microscope.



**Figure C35: Optimizing ASO concentration and confirming sequence specificity.** HEK293T cells were co-transfected with both a pCMV vector encoding eGFP (200 ng) as well as increasing amounts of either an eGFP-targeting or scrambled ASO (“-“ denotes no ASO). After 24 hours, GFP expression was detected by live-cell imaging using a BioTek Lionheart FX automated microscope (4X magnification).

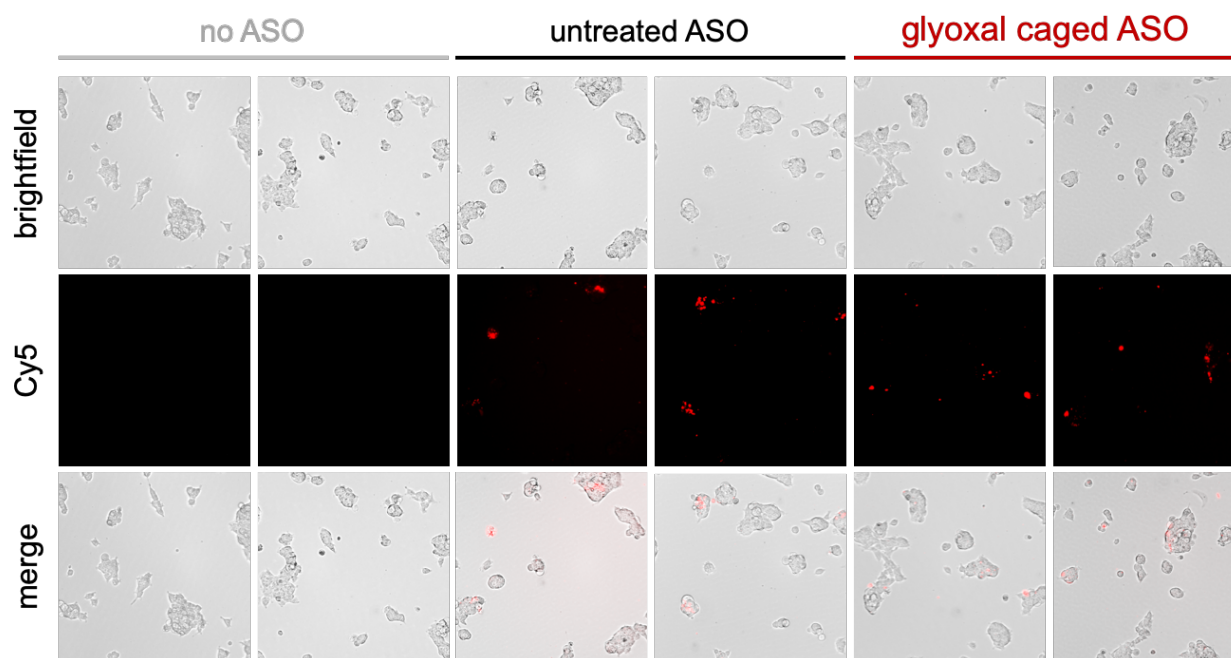


**Figure C36: Caging kinetics of an eGFP-targeting ASO as monitored by 20% PAGE gel illustrating an increase in apparent molecular weight.**

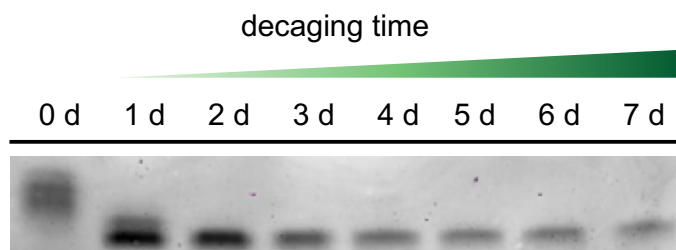


**Figure C37: Optimizing ASO glyoxal treatment time for inhibiting gene silencing.** HEK293T cells were co-transfected with both a pCMV-eGFP vector (200 ng) as well as 250 nM increasingly caged eGFP-targeting ASO. After 12 hours, expression was detected by live-cell imaging using

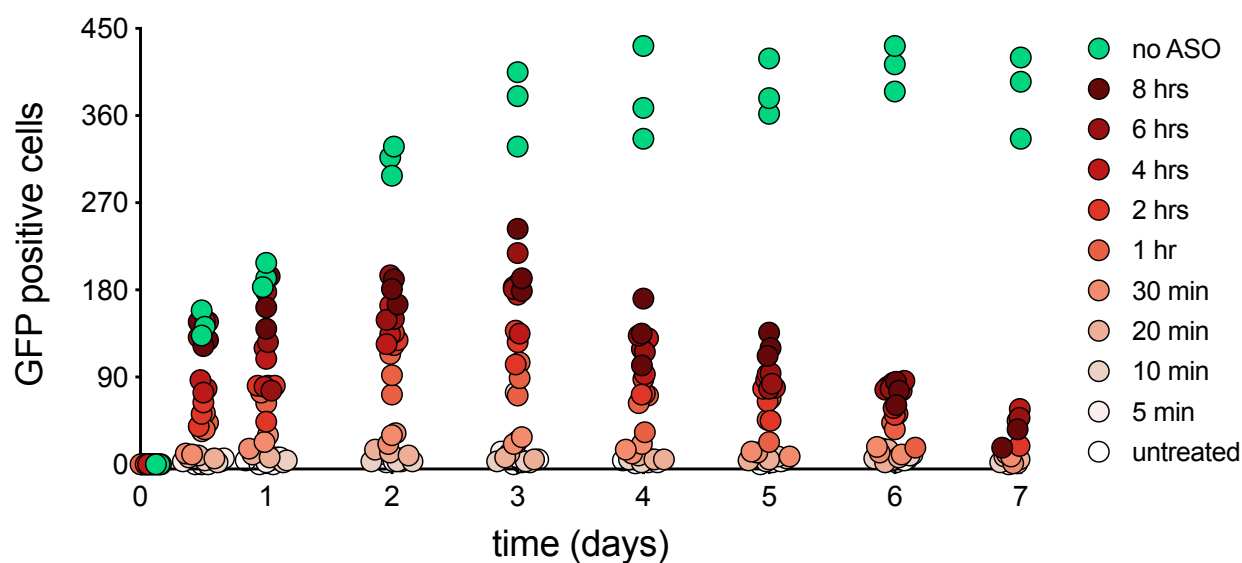
a BioTek Lionheart FX automated microscope (4X magnification). GFP positive cells per field were counted using ImageJ, and values represent mean with S.D (n = 3 wells). BF = brightfield.



**Figure C38: Untreated and glyoxal caged ASOs are cell permeable.** LNA ASOs were first Cy5-labeled, followed by either no treatment or glyoxal caging for 8 h. HEK293T cells were incubated with 250 nM respective ASO for 18 hours. Media was then removed, and cells were washed 3x with fresh media. Cells were then imaged using a BioTek Lionheart FX automated microscope (10X magnification).

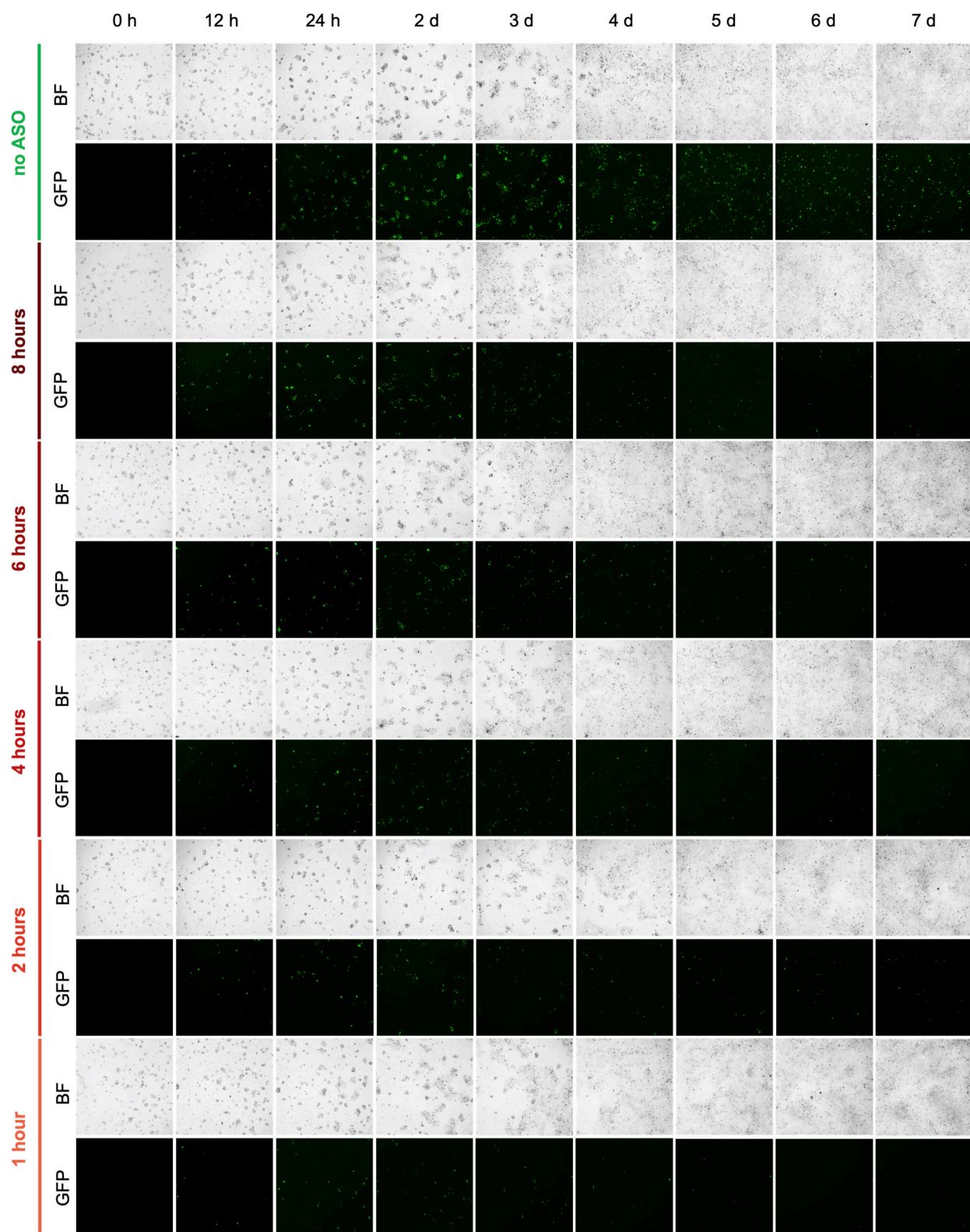


**Figure C39: ASO glyoxalation is reversible with slow decaging.** Decaging kinetics of fully caged (8 hour treatment time) ASO at 37 °C in complete DMEM were monitored by 20% PAGE gel illustrating decrease in apparent molecular weight.



**Figure C40: Increasingly caged ASO proportionally tunes the amount of GFP positive cells.** At  $t = 0$ , HEK293T cells were transfected with a pCMV-GFP plasmid as well as 250 nM of untreated or increasingly glyoxal caged ASO. Graph shows quantification of GFP-positive cells in each field across treatment groups during the experimental time course. Circles represent individual wells ( $n = 3$ ) from a 96-well plate.







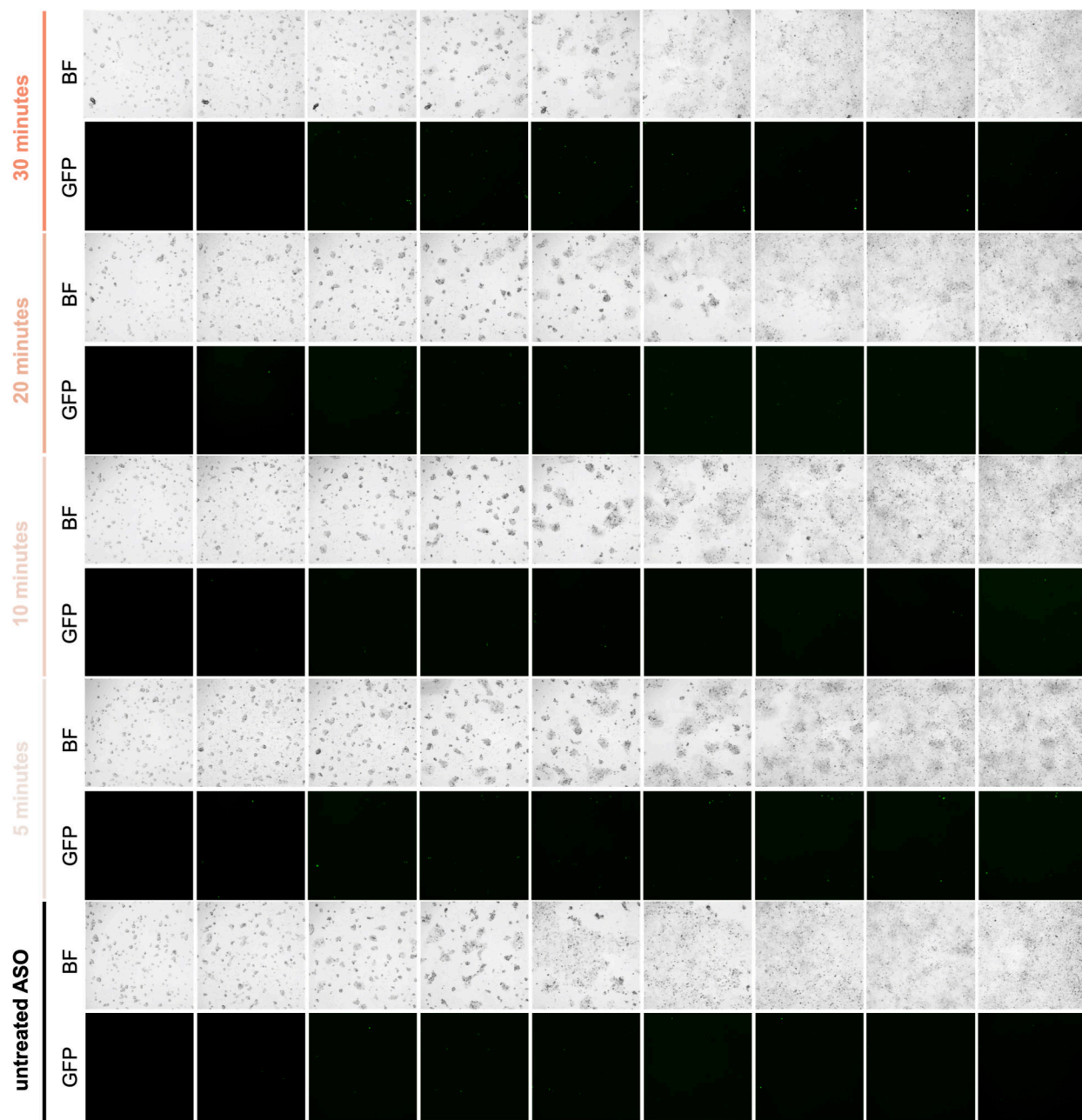


**Figure C41: Representative live-cell fluorescence microscopy images during in cellulo ASO decaging.** HEK293T cells were co-transfected with both a pCMV-eGFP vector (200 ng) as well as 250 nM increasingly caged eGFP-targeting ASO. At the indicated time points, expression was detected by live-cell imaging using a BioTek Lionheart FX automated microscope (4X magnification). BF = brightfield. Media was replaced on days 4 and 7.

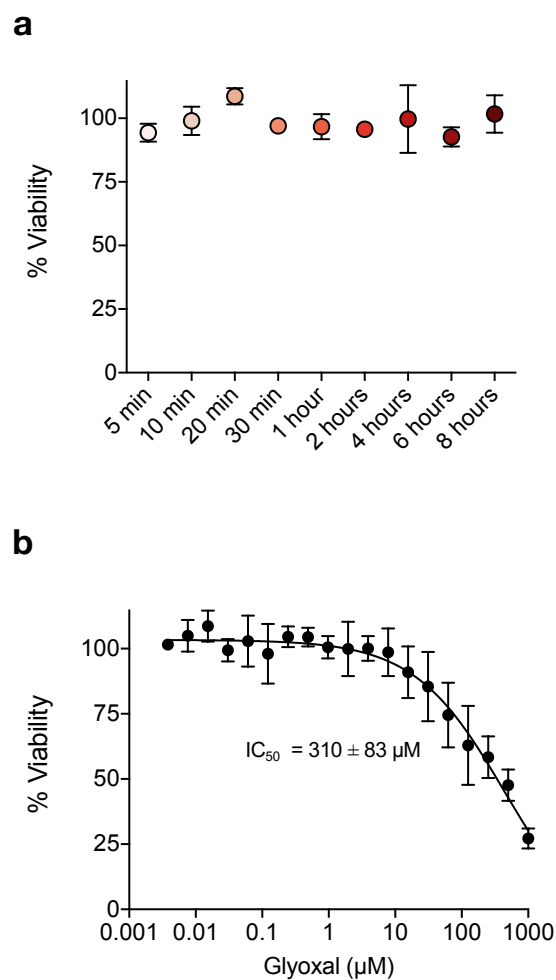


**Figure C42: Caged ASOs do not affect cell viability.** a) On day 7, plates from the time course decaging experiment were tested using a WST-1 assay to measure cell viability. Values represent mean and S.D. of 3 wells calculated as a percentage of untreated control cells. b) In parallel, HEK293T cells were seeded in a 96-well plate at 10,000 cells/well and incubated with a range of glyoxal concentrations for 7 days. Media was replaced on days 4 and 7, and viability was then measured using a WST-1 assay. Values represent mean and S.D. of 3 wells calculated as a percentage of untreated control cells. IC<sub>50</sub> value (mean with 95% confidence interval) was calculate using a dose-response curve fit in Prism.

## References

- (1) Roncancio, D.; Yu, H.; Xu, X.; Wu, S.; Liu, R.; Debord, J.; Lou, X.; Xiao, Y. A label-free aptamer-fluorophore assembly for rapid and specific detection of cocaine in biofluids. *Anal Chem* **2014**, *86* (22), 11100-11106. DOI: 10.1021/ac503360n From NLM.
- (2) Sanford, A. A.; Manuel, B. A.; Romero-Reyes, M. A.; Heemstra, J. M. Combating small molecule environmental contaminants: detection and sequestration using functional nucleic acids. *Chemical Science* **2022**, *13* (26), 7670-7684, 10.1039/D2SC00117A. DOI: 10.1039/D2SC00117A.
- (3) Ellington, A. D.; Szostak, J. W. In vitro selection of RNA molecules that bind specific ligands. *Nature* **1990**, *346* (6287), 818-822. DOI: 10.1038/346818a0.
- (4) Höbartner, C.; Silverman, S. K. Recent advances in DNA catalysis. *Biopolymers* **2007**, *87* (5-6), 279-292. DOI: <https://doi.org/10.1002/bip.20813>.
- (5) Silverman, S. K. Catalytic DNA: Scope, Applications, and Biochemistry of Deoxyribozymes. *Trends in Biochemical Sciences* **2016**, *41* (7), 595-609. DOI: 10.1016/j.tibs.2016.04.010 (accessed 2022/08/16).
- (6) Silverman, S. K. Nucleic Acid Enzymes (Ribozymes and Deoxyribozymes): In Vitro Selection and Application. In *Wiley Encyclopedia of Chemical Biology*, pp 1-17.
- (7) Breaker, R. R.; Joyce, G. F. A DNA enzyme that cleaves RNA. *Chemistry & Biology* **1994**, *1* (4), 223-229. DOI: 10.1016/1074-5521(94)90014-0 (accessed 2022/08/16).
- (8) Chandra, M.; Sachdeva, A.; Silverman, S. K. DNA-catalyzed sequence-specific hydrolysis of DNA. *Nature Chemical Biology* **2009**, *5* (10), 718-720. DOI: 10.1038/nchembio.201.
- (9) Purtha, W. E.; Coppins, R. L.; Smalley, M. K.; Silverman, S. K. General Deoxyribozyme-Catalyzed Synthesis of Native 3'-5' RNA Linkages. *Journal of the American Chemical Society* **2005**, *127* (38), 13124-13125. DOI: 10.1021/ja0533702.
- (10) Wang, Y.; Silverman, S. K. Directing the Outcome of Deoxyribozyme Selections To Favor Native 3'-5' RNA Ligation. *Biochemistry* **2005**, *44* (8), 3017-3023. DOI: 10.1021/bi0478291.
- (11) Silverman, S. K. Deoxyribozymes: DNA catalysts for bioorganic chemistry. *Organic & Biomolecular Chemistry* **2004**, *2* (19), 2701-2706, 10.1039/B411910J. DOI: 10.1039/B411910J.
- (12) Silverman, S. K. Catalytic DNA (deoxyribozymes) for synthetic applications—current abilities and future prospects. *Chemical Communications* **2008**, (30), 3467-3485, 10.1039/B807292M. DOI: 10.1039/B807292M.

- (13) Kim, D.; Hwang, H.-Y.; Ji, E. S.; Kim, J. Y.; Yoo, J. S.; Kwon, H. J. Activation of mitochondrial TUFM ameliorates metabolic dysregulation through coordinating autophagy induction. *Communications Biology* **2021**, *4* (1), 1. DOI: 10.1038/s42003-020-01566-0.
- (14) Huang, P.-J. J.; Liu, J. An Ultrasensitive Light-up Cu<sup>2+</sup> Biosensor Using a New DNAzyme Cleaving a Phosphorothioate-Modified Substrate. *Analytical Chemistry* **2016**, *88* (6), 3341-3347. DOI: 10.1021/acs.analchem.5b04904.
- (15) Si, H.; Sheng, R.; Li, Q.; Feng, J.; Li, L.; Tang, B. Highly Sensitive Fluorescence Imaging of Zn<sup>2+</sup> and Cu<sup>2+</sup> in Living Cells with Signal Amplification Based on Functional DNA Self-Assembly. *Analytical Chemistry* **2018**, *90* (15), 8785-8792. DOI: 10.1021/acs.analchem.7b05268.
- (16) Wang, Y.; Liu, E.; Lam, C. H.; Perrin, D. M. A densely modified M<sup>2+</sup>-independent DNAzyme that cleaves RNA efficiently with multiple catalytic turnover. *Chemical Science* **2018**, *9* (7), 1813-1821, 10.1039/C7SC04491G. DOI: 10.1039/C7SC04491G.
- (17) Zhou, W.; Zhang, Y.; Ding, J.; Liu, J. In Vitro Selection in Serum: RNA-Cleaving DNAzymes for Measuring Ca<sup>2+</sup> and Mg<sup>2+</sup>. *ACS Sensors* **2016**, *1* (5), 600-606. DOI: 10.1021/acssensors.5b00306.
- (18) Romero-Reyes, M. A.; Heemstra, J. M. Small-Molecule Sequestration Using Aptamer-Functionalized Membranes. *ACS Materials Letters* **2019**, *1* (5), 568-572. DOI: 10.1021/acsmaterialslett.9b00288.
- (19) Romero-Reyes, M. A.; Heemstra, J. M. Sequestration and Removal of Multiple Small-Molecule Contaminants Using an Optimized Aptamer-Based Ultrafiltration System. *Bioconjugate Chemistry* **2021**, *32* (9), 2043-2051. DOI: 10.1021/acs.bioconjchem.1c00344.
- (20) Ruscito, A.; DeRosa, M. C. Small-Molecule Binding Aptamers: Selection Strategies, Characterization, and Applications. *Front Chem* **2016**, *4*, 14. DOI: 10.3389/fchem.2016.00014 From NLM.
- (21) Manuel, B. A.; Sterling, S. A.; Sanford, A. A.; Heemstra, J. M. Systematically Modulating Aptamer Affinity and Specificity by Guanosine-to-Inosine Substitution. *Analytical Chemistry* **2022**, *94* (17), 6436-6440. DOI: 10.1021/acs.analchem.2c00422.
- (22) Neves, M. A. D.; Slavkovic, S.; Churcher, Z. R.; Johnson, P. E. Salt-mediated two-site ligand binding by the cocaine-binding aptamer. *Nucleic acids research* **2017**, *45* (3), 1041-1048. DOI: 10.1093/nar/gkw1294 PubMed.
- (23) Neves, M. A. D.; Shoara, A. A.; Reinstein, O.; Abbasi Borhani, O.; Martin, T. R.; Johnson, P. E. Optimizing Stem Length To Improve Ligand Selectivity in a Structure-Switching Cocaine-Binding Aptamer. *ACS Sensors* **2017**, *2* (10), 1539-1545. DOI: 10.1021/acssensors.7b00619.
- (24) Knutson, S. D.; Sanford, A. A.; Swenson, C. S.; Korn, M. M.; Manuel, B. A.; Heemstra, J. M. Thermoreversible Control of Nucleic Acid Structure and Function with Glyoxal Caging. *Journal of the American Chemical Society* **2020**, *142* (41), 17766-17781. DOI: 10.1021/jacs.0c08996.
- (25) Fiedler, J. D.; Brown, S. D.; Lau, J. L.; Finn, M. G. RNA-directed packaging of enzymes within virus-like particles. *Angew Chem Int Ed Engl* **2010**, *49* (50), 9648-9651. DOI: 10.1002/anie.201005243 From NLM.
- (26) Fiedler, J. D.; Fishman, M. R.; Brown, S. D.; Lau, J.; Finn, M. G. Multifunctional Enzyme Packaging and Catalysis in the Q $\beta$  Protein Nanoparticle. *Biomacromolecules* **2018**, *19* (10), 3945-3957. DOI: 10.1021/acs.biomac.8b00885.
- (27) Das, S.; Zhao, L.; Eloffson, K.; Finn, M. G. Enzyme Stabilization by Virus-Like Particles. *Biochemistry* **2020**, *59* (31), 2870-2881. DOI: 10.1021/acs.biochem.0c00435.

- (28) Das, S.; Zhao, L.; Crooke, S. N.; Tran, L.; Bhattacharya, S.; Gaucher, E. A.; Finn, M. G. Stabilization of Near-Infrared Fluorescent Proteins by Packaging in Virus-like Particles. *Biomacromolecules* **2020**, *21* (6), 2432-2439. DOI: 10.1021/acs.biomac.0c00362.
- (29) Das, S.; Yau, M.-K.; Noble, J.; De Pascalis, L.; Finn, M. G. Transport of Molecular Cargo by Interaction with Virus-Like Particle RNA. *Angewandte Chemie International Edition* **2022**, *61* (2), e202111687. DOI: <https://doi.org/10.1002/anie.202111687>.
- (30) Schöning, K.; Scholz, P.; Guntha, S.; Wu, X.; Krishnamurthy, R.; Eschenmoser, A. Chemical etiology of nucleic acid structure: the alpha-threofuranosyl-(3'-->2') oligonucleotide system. *Science* **2000**, *290* (5495), 1347-1351. DOI: 10.1126/science.290.5495.1347 From NLM.
- (31) Egholm, M.; Buchardt, O.; Nielsen, P. E.; Berg, R. H. Peptide nucleic acids (PNA). Oligonucleotide analogs with an achiral peptide backbone. *Journal of the American Chemical Society* **1992**, *114* (5), 1895-1897. DOI: 10.1021/ja00031a062.
- (32) Wittung, P.; Nielsen, P. E.; Buchardt, O.; Egholm, M.; Nordén, B. DNA-like double helix formed by peptide nucleic acid. *Nature* **1994**, *368* (6471), 561-563. DOI: 10.1038/368561a0.
- (33) Stojanovic, M. N.; de Prada, P.; Landry, D. W. Aptamer-Based Folding Fluorescent Sensor for Cocaine. *Journal of the American Chemical Society* **2001**, *123* (21), 4928-4931. DOI: 10.1021/ja0038171.
- (34) Sachan, A.; Ilgu, M.; Kempema, A.; Kraus, G. A.; Nilsen-Hamilton, M. Specificity and Ligand Affinities of the Cocaine Aptamer: Impact of Structural Features and Physiological NaCl. *Analytical Chemistry* **2016**, *88* (15), 7715-7723. DOI: 10.1021/acs.analchem.6b01633.
- (35) Roncancio, D.; Yu, H.; Xu, X.; Wu, S.; Liu, R.; Debord, J.; Lou, X.; Xiao, Y. A Label-Free Aptamer-Fluorophore Assembly for Rapid and Specific Detection of Cocaine in Biofluids. *Analytical Chemistry* **2014**, *86* (22), 11100-11106. DOI: 10.1021/ac503360n.
- (36) Guo, W.; Zhang, C.; Ma, T.; Liu, X.; Chen, Z.; Li, S.; Deng, Y. Advances in aptamer screening and aptasensors' detection of heavy metal ions. *J Nanobiotechnology* **2021**, *19* (1), 166. DOI: 10.1186/s12951-021-00914-4 From NLM.
- (37) Kaur, H.; Yung, L.-Y. L. Probing High Affinity Sequences of DNA Aptamer against VEGF165. *PLOS ONE* **2012**, *7* (2), e31196. DOI: 10.1371/journal.pone.0031196.
- (38) Li, Q.; Liu, L.; Mao, D.; Yu, Y.; Li, W.; Zhao, X.; Mao, C. ATP-Triggered, Allosteric Self-Assembly of DNA Nanostructures. *Journal of the American Chemical Society* **2020**, *142* (2), 665-668. DOI: 10.1021/jacs.9b10272.
- (39) Qi, C.; Bing, T.; Mei, H.; Yang, X.; Liu, X.; Shanguan, D. G-quadruplex DNA aptamers for zeatin recognizing. *Biosens Bioelectron* **2013**, *41*, 157-162. DOI: 10.1016/j.bios.2012.08.004 From NLM.
- (40) Ferris, Z. E.; Li, Q.; Germann, M. W. Substituting Inosine for Guanosine in DNA: Structural and Dynamic Consequences. *Natural Product Communications* **2019**, *14* (5), 1934578X19850032. DOI: 10.1177/1934578x19850032.
- (41) Liu, L. S.; Wang, F.; Ge, Y.; Lo, P. K. Recent Developments in Aptasensors for Diagnostic Applications. *ACS Applied Materials & Interfaces* **2021**, *13* (8), 9329-9358. DOI: 10.1021/acsami.0c14788.
- (42) Song, H.; You, J.-A.; Chen, C.; Zhang, H.; Ji, X. Z.; Li, C.; Yang, Y.; Xu, N.; Huang, J. Manganese functionalized mesoporous molecular sieves Ti-HMS as a Fenton-like catalyst for dyes wastewater purification by advanced oxidation processes. *Journal of Environmental Chemical Engineering* **2016**, *4* (4, Part A), 4653-4660. DOI: <https://doi.org/10.1016/j.jece.2016.09.039>.



- (43) Wang, J.; Shen, H.; Hu, X.; Li, Y.; Li, Z.; Xu, J.; Song, X.; Zeng, H.; Yuan, Q. A Targeted "Capture" and "Removal" Scavenger toward Multiple Pollutants for Water Remediation based on Molecular Recognition. *Advanced Science* **2016**, *3* (3), 1500289. DOI: <https://doi.org/10.1002/advs.201500289>.
- (44) Kim, Y. S.; Niazi, J. H.; Chae, Y. J.; Ko, U.-R.; Gu, M. B. Aptamers-in-Liposomes for Selective and Multiplexed Capture of Small Organic Compounds. *Macromolecular Rapid Communications* **2011**, *32* (15), 1169-1173. DOI: <https://doi.org/10.1002/marc.201100177>.
- (45) Li, W.; Szoka, F. C., Jr. Lipid-based nanoparticles for nucleic acid delivery. *Pharm Res* **2007**, *24* (3), 438-449. DOI: 10.1007/s11095-006-9180-5 From NLM.
- (46) Raval, N.; Jogi, H.; Gondaliya, P.; Kalia, K.; Tekade, R. K. Method and its Composition for encapsulation, stabilization, and delivery of siRNA in Anionic polymeric nanoplex: An In vitro- In vivo Assessment. *Scientific Reports* **2019**, *9* (1), 16047. DOI: 10.1038/s41598-019-52390-4.
- (47) Aydindogan, E.; Balaban, S.; Evran, S.; Coskunol, H.; Timur, S. A Bottom-Up Approach for Developing Aptasensors for Abused Drugs: Biosensors in Forensics. *Biosensors* **2019**, *9* (4), 118.
- (48) Liu, J.; Cao, Z.; Lu, Y. Functional Nucleic Acid Sensors. *Chemical Reviews* **2009**, *109* (5), 1948-1998. DOI: 10.1021/cr030183i.
- (49) Pfeiffer, F.; Mayer, G. Selection and Biosensor Application of Aptamers for Small Molecules. *Front Chem* **2016**, *4*, 25. DOI: 10.3389/fchem.2016.00025.
- (50) Wu, Y.; Belmonte, I.; Sykes, K. S.; Xiao, Y.; White, R. J. Perspective on the Future Role of Aptamers in Analytical Chemistry. *Analytical Chemistry* **2019**, *91* (24), 15335-15344. DOI: 10.1021/acs.analchem.9b03853.
- (51) Yoo, H.; Jo, H.; Oh, S. S. Detection and beyond: challenges and advances in aptamer-based biosensors. *Materials Advances* **2020**, *1* (8), 2663-2687. DOI: 10.1039/d0ma00639d.
- (52) Yu, H.; Alkhamis, O.; Canoura, J.; Liu, Y.; Xiao, Y. Advances and Challenges in Small-Molecule DNA Aptamer Isolation, Characterization, and Sensor Development. *Angewandte Chemie International Edition* **2021**, *60* (31), 16800-16823. DOI: <https://doi.org/10.1002/anie.202008663>.
- (53) McConnell, E. M.; Nguyen, J.; Li, Y. Aptamer-Based Biosensors for Environmental Monitoring. *Frontiers in Chemistry* **2020**, *8* (434), Review. DOI: 10.3389/fchem.2020.00434.
- (54) Krepl, M.; Otyepka, M.; Banáš, P.; Šponer, J. Effect of Guanine to Inosine Substitution on Stability of Canonical DNA and RNA Duplexes: Molecular Dynamics Thermodynamics Integration Study. *The Journal of Physical Chemistry B* **2013**, *117* (6), 1872-1879. DOI: 10.1021/jp311180u.
- (55) Xu, G.; Zhao, J.; Liu, N.; Yang, M.; Zhao, Q.; Li, C.; Liu, M. Structure-guided post-SELEX optimization of an ochratoxin A aptamer. *Nucleic Acids Res* **2019**, *47* (11), 5963-5972. DOI: 10.1093/nar/gkz336 PubMed.
- (56) Karsisiotis, A. I.; O'Kane, C.; Webba da Silva, M. DNA quadruplex folding formalism--a tutorial on quadruplex topologies. *Methods* **2013**, *64* (1), 28-35. DOI: 10.1016/j.ymeth.2013.06.004 From NLM.
- (57) Riccardi, C.; Napolitano, E.; Musumeci, D.; Montesarchio, D. Dimeric and Multimeric DNA Aptamers for Highly Effective Protein Recognition. *Molecules* **2020**, *25* (22), 5227.
- (58) Tucker, W. O.; Shum, K. T.; Tanner, J. A. G-quadruplex DNA aptamers and their ligands: structure, function and application. *Curr Pharm Des* **2012**, *18* (14), 2014-2026. DOI: 10.2174/138161212799958477 From NLM.

- (59) Stojanovic, M. N.; de Prada, P.; Landry, D. W. Aptamer-based folding fluorescent sensor for cocaine. *J Am Chem Soc* **2001**, *123* (21), 4928-4931. DOI: 10.1021/ja0038171 From NLM.
- (60) Shoara, A. A.; Churcher, Z. R.; Steele, T. W. J.; Johnson, P. E. Analysis of the role played by ligand-induced folding of the cocaine-binding aptamer in the photochrome aptamer switch assay. *Talanta* **2020**, *217*, 121022. DOI: 10.1016/j.talanta.2020.121022 From NLM.
- (61) Neves, M. A. D.; Reinstein, O.; Johnson, P. E. Defining a Stem Length-Dependent Binding Mechanism for the Cocaine-Binding Aptamer. A Combined NMR and Calorimetry Study. *Biochemistry* **2010**, *49* (39), 8478-8487. DOI: 10.1021/bi100952k.
- (62) Jerabek-Willemsen, M.; Wienken, C. J.; Braun, D.; Baaske, P.; Duhr, S. Molecular interaction studies using microscale thermophoresis. *Assay Drug Dev Technol* **2011**, *9* (4), 342-353. DOI: 10.1089/adt.2011.0380 PubMed.
- (63) Mrázková, J.; Malinová, L.; Wimmerová, M. Microscopy examination of red blood and yeast cell agglutination induced by bacterial lectins. *PLOS ONE* **2019**, *14* (7), e0220318. DOI: 10.1371/journal.pone.0220318.
- (64) Corfield, P. W.; Hunter, W. N.; Brown, T.; Robinson, P.; Kennard, O. Inosine.adenine base pairs in a B-DNA duplex. *Nucleic Acids Res* **1987**, *15* (19), 7935-7949. DOI: 10.1093/nar/15.19.7935 From NLM.
- (65) Nakano, S.-i.; Sugimoto, N. Roles of the Amino Group of Purine Bases in the Thermodynamic Stability of DNA Base Pairing. *Molecules* **2014**, *19* (8), 11613-11627.
- (66) Gorelick, D. Enhancing cocaine metabolism with butyrylcholinesterase as a treatment strategy. *Drug and Alcohol Dependence* **1998**, *48*, 159-165. DOI: 10.1016/S0376-8716(97)00119-1.
- (67) Kamendulis, L. M.; Brzezinski, M. R.; Pindel, E. V.; Bosron, W. F.; Dean, R. A. Metabolism of cocaine and heroin is catalyzed by the same human liver carboxylesterases. *J Pharmacol Exp Ther* **1996**, *279* (2), 713-717. From NLM.
- (68) Zhan, C.-G.; Zheng, F.; Landry, D. W. Fundamental Reaction Mechanism for Cocaine Hydrolysis in Human Butyrylcholinesterase. *Journal of the American Chemical Society* **2003**, *125* (9), 2462-2474. DOI: 10.1021/ja020850+.
- (69) Jindal, S. P.; Lutz, T.; Vestergaard, P. Mass spectrometric determination of cocaine and its biologically active metabolite, norcocaine, in human urine. *Biomed Mass Spectrom* **1978**, *5* (12), 658-663. DOI: 10.1002/bms.1200051205 From NLM.
- (70) Lackey, H. H.; Peterson, E. M.; Harris, J. M.; Heemstra, J. M. Probing the Mechanism of Structure-Switching Aptamer Assembly by Super-Resolution Localization of Individual DNA Molecules. *Analytical Chemistry* **2020**, *92* (10), 6909-6917. DOI: 10.1021/acs.analchem.9b05563.
- (71) Sanford, A. A.; Rangel, A. E.; Feagin, T. A.; Lowery, R. G.; Argueta-Gonzalez, H. S.; Heemstra, J. M. RE-SELEX: restriction enzyme-based evolution of structure-switching aptamer biosensors. *Chemical Science* **2021**, *12* (35), 11692-11702, 10.1039/D1SC02715H. DOI: 10.1039/D1SC02715H.
- (72) Hu, J.; Easley, C. J. A simple and rapid approach for measurement of dissociation constants of DNA aptamers against proteins and small molecules via automated microchip electrophoresis. *Analyst* **2011**, *136* (17), 3461-3468, 10.1039/C0AN00842G. DOI: 10.1039/C0AN00842G.
- (73) Bhatia, S. *Introduction to Pharmaceutical Biotechnology, Volume 2*; IOP Publishing, 2018. DOI: 10.1088/978-0-7503-1302-5.

- (74) de la Fuente, M.; Lombardero, L.; Gómez-González, A.; Solari, C.; Angulo-Barturen, I.; Acera, A.; Vecino, E.; Astigarraga, E.; Barreda-Gómez, G. Enzyme Therapy: Current Challenges and Future Perspectives. *Int J Mol Sci* **2021**, *22* (17). DOI: 10.3390/ijms22179181 From NLM.
- (75) Kunamneni, A.; Ogaugwu, C.; Goli, D. Chapter 15 - Enzymes as therapeutic agents. In *Enzymes in Human and Animal Nutrition*, Nunes, C. S., Kumar, V. Eds.; Academic Press, 2018; pp 301-312.
- (76) Otten, L. G.; Hollmann, F.; Arends, I. W. C. E. Enzyme engineering for enantioselectivity: from trial-and-error to rational design? *Trends in Biotechnology* **2010**, *28* (1), 46-54. DOI: <https://doi.org/10.1016/j.tibtech.2009.10.001>.
- (77) Narasimhan, D.; Nance, M. R.; Gao, D.; Ko, M. C.; Macdonald, J.; Tamburi, P.; Yoon, D.; Landry, D. M.; Woods, J. H.; Zhan, C. G.; et al. Structural analysis of thermostabilizing mutations of cocaine esterase. *Protein Eng Des Sel* **2010**, *23* (7), 537-547. DOI: 10.1093/protein/gzq025 From NLM.
- (78) Turner, N. J. Directed evolution drives the next generation of biocatalysts. *Nature Chemical Biology* **2009**, *5* (8), 567-573. DOI: 10.1038/nchembio.203.
- (79) Kaul, P.; Asano, Y. Strategies for discovery and improvement of enzyme function: state of the art and opportunities. *Microb Biotechnol* **2012**, *5* (1), 18-33. DOI: 10.1111/j.1751-7915.2011.00280.x From NLM.
- (80) Fallah-Araghi, A.; Baret, J.-C.; Ryckelynck, M.; Griffiths, A. D. A completely in vitro ultrahigh-throughput droplet-based microfluidic screening system for protein engineering and directed evolution. *Lab on a Chip* **2012**, *12* (5), 882-891, 10.1039/C2LC21035E. DOI: 10.1039/C2LC21035E.
- (81) Friedrich, B.; Daniela, R.; Christian, F. W. B. Biomimetic and biopolymer-based enzyme encapsulation. *Enzyme and Microbial Technology* **2021**, *150*, 109864. DOI: <https://doi.org/10.1016/j.enzmictec.2021.109864>.
- (82) Hwang, E. T.; Lee, S. Multienzymatic Cascade Reactions via Enzyme Complex by Immobilization. *ACS Catalysis* **2019**, *9* (5), 4402-4425. DOI: 10.1021/acscatal.8b04921.
- (83) Berne, C.; Betancor, L.; Luckarift, H. R.; Spain, J. C. Application of a Microfluidic Reactor for Screening Cancer Prodrug Activation Using Silica-Immobilized Nitrobenzene Nitroreductase. *Biomacromolecules* **2006**, *7* (9), 2631-2636. DOI: 10.1021/bm060166d.
- (84) Betancor, L.; Berne, C.; Luckarift, H. R.; Spain, J. C. Coimmobilization of a redox enzyme and a cofactor regeneration system. *Chemical Communications* **2006**, (34), 3640-3642, 10.1039/B604689D. DOI: 10.1039/B604689D.
- (85) Cui, J.; Sun, B.; Lin, T.; Feng, Y.; Jia, S. Enzyme shielding by mesoporous organosilica shell on Fe(3)O(4)@silica yolk-shell nanospheres. *Int J Biol Macromol* **2018**, *117*, 673-682. DOI: 10.1016/j.ijbiomac.2018.05.227 From NLM.
- (86) Cui, J.; Zhao, Y.; Feng, Y.; Lin, T.; Zhong, C.; Tan, Z.; Jia, S. Encapsulation of Spherical Cross-Linked Phenylalanine Ammonia Lyase Aggregates in Mesoporous Biosilica. *Journal of Agricultural and Food Chemistry* **2017**, *65* (3), 618-625. DOI: 10.1021/acs.jafc.6b05003.
- (87) Gülay, S.; Şanlı-Mohamed, G. Immobilization of thermoalkalophilic recombinant esterase enzyme by entrapment in silicate coated Ca-alginate beads and its hydrolytic properties. *International Journal of Biological Macromolecules* **2012**, *50* (3), 545-551. DOI: <https://doi.org/10.1016/j.ijbiomac.2012.01.017>.
- (88) Hong, S.-G.; Kim, B. C.; Na, H. B.; Lee, J.; Youn, J.; Chung, S.-W.; Lee, C.-W.; Lee, B.; Kim, H. S.; Hsiao, E.; et al. Single enzyme nanoparticles armored by a thin silicate network:



- Single enzyme caged nanoparticles. *Chemical Engineering Journal* **2017**, 322, 510-515. DOI: <https://doi.org/10.1016/j.cej.2017.04.022>.
- (89) Huang, R.; Wu, M.; Goldman, M. J.; Li, Z. Encapsulation of enzyme via one-step template-free formation of stable organic–inorganic capsules: A simple and efficient method for immobilizing enzyme with high activity and recyclability. *Biotechnology and Bioengineering* **2015**, 112 (6), 1092-1101. DOI: <https://doi.org/10.1002/bit.25536>.
- (90) Hwang, E. T.; Seo, B.-K.; Gu, M. B.; Zeng, A.-P. Successful bi-enzyme stabilization for the biomimetic cascade transformation of carbon dioxide. *Catalysis Science & Technology* **2016**, 6 (19), 7267-7272, 10.1039/C6CY00783J. DOI: 10.1039/C6CY00783J.
- (91) Kadir, O.; Pavel, S. P.; Marina, E. T.; Vladimir, S.; Antonio. Polysaccharides based microspheres for multiple encapsulations and simultaneous release of proteases. *International Journal of Biological Macromolecules* **2019**, 132, 24-31. DOI: <https://doi.org/10.1016/j.ijbiomac.2019.03.189>.
- (92) Kumar, R. S. S.; Vishwanath, K. S.; Sridevi Annapurna, S.; Rao, A. G. A. Entrapment of  $\alpha$ -amylase in alginate beads: Single step protocol for purification and thermal stabilization. *Process Biochemistry* **2006**, 41 (11), 2282-2288. DOI: <https://doi.org/10.1016/j.procbio.2006.05.028>.
- (93) Le Truc, N.; Yun Song, L.; Kun-Lin, Y. Entrapment of cross-linked cellulase colloids in alginate beads for hydrolysis of cellulose. *Colloids and Surfaces B: Biointerfaces* **2016**, 145, 862-869. DOI: <https://doi.org/10.1016/j.colsurfb.2016.06.008>.
- (94) Luckarift, H. R.; Dickerson, M. B.; Sandhage, K. H.; Spain, J. C. Rapid, Room-Temperature Synthesis of Antibacterial Bionanocomposites of Lysozyme with Amorphous Silica or Titania. *Small* **2006**, 2 (5), 640-643. DOI: <https://doi.org/10.1002/sml.200500376>.
- (95) Luckarift, H. R.; Ku, B. S.; Dordick, J. S.; Spain, J. C. Silica-immobilized enzymes for multi-step synthesis in microfluidic devices. *Biotechnology and Bioengineering* **2007**, 98 (3), 701-705. DOI: <https://doi.org/10.1002/bit.21447>.
- (96) Luckarift, H. R.; Spain, J. C.; Naik, R. R.; Stone, M. O. Enzyme immobilization in a biomimetic silica support. *Nature Biotechnology* **2004**, 22 (2), 211-213. DOI: 10.1038/nbt931.
- (97) Martelli, T.; Ravera, E.; Louka, A.; Cerofolini, L.; Hafner, M.; Fragai, M.; Becker, C. F. W.; Luchinat, C. Atomic-Level Quality Assessment of Enzymes Encapsulated in Bioinspired Silica. *Chemistry – A European Journal* **2016**, 22 (1), 425-432. DOI: <https://doi.org/10.1002/chem.201503613>.
- (98) Miller, S. A.; Hong, E. D.; Wright, D. Rapid and Efficient Enzyme Encapsulation in a Dendrimer Silica Nanocomposite. *Macromolecular Bioscience* **2006**, 6 (10), 839-845. DOI: <https://doi.org/10.1002/mabi.200600140>.
- (99) Min, K.-H.; Son, R. G.; Ki, M.-R.; Choi, Y. S.; Pack, S. P. High expression and biosilica encapsulation of alkaline-active carbonic anhydrase for CO<sub>2</sub> sequestration system development. *Chemosphere* **2016**, 143, 128-134. DOI: <https://doi.org/10.1016/j.chemosphere.2015.07.020>.
- (100) Naik, R. R.; Tomczak, M. M.; Luckarift, H. R.; Spain, J. C.; Stone, M. O. Entrapment of enzymes and nanoparticles using biomimetically synthesized silica. *Chemical Communications* **2004**, (15), 1684-1685, 10.1039/B404586F. DOI: 10.1039/B404586F.
- (101) Neville, F.; Broderick, M. J. F.; Gibson, T.; Millner, P. A. Fabrication and Activity of Silicate Nanoparticles and Nanosilicate-Entrapped Enzymes Using Polyethyleneimine As a Biomimetic Polymer. *Langmuir* **2011**, 27 (1), 279-285. DOI: 10.1021/la1033492.

- (102) Patterson, D. P.; Prevelige, P. E.; Douglas, T. Nanoreactors by Programmed Enzyme Encapsulation Inside the Capsid of the Bacteriophage P22. *ACS Nano* **2012**, *6* (6), 5000-5009. DOI: 10.1021/nn300545z.
- (103) Roth, K. M.; Zhou, Y.; Yang, W.; Morse, D. E. Bifunctional Small Molecules Are Biomimetic Catalysts for Silica Synthesis at Neutral pH. *Journal of the American Chemical Society* **2005**, *127* (1), 325-330. DOI: 10.1021/ja045308v.
- (104) Traffano-Schiffo, M. V.; Aguirre Calvo, T. R.; Castro-Giraldez, M.; Fito, P. J.; Santagapita, P. R. Alginate Beads Containing Lactase: Stability and Microstructure. *Biomacromolecules* **2017**, *18* (6), 1785-1792. DOI: 10.1021/acs.biomac.7b00202.
- (105) Wan, L.; Chen, Q.; Liu, J.; Yang, X.; Huang, J.; Li, L.; Guo, X.; Zhang, J.; Wang, K. Programmable Self-Assembly of DNA-Protein Hybrid Hydrogel for Enzyme Encapsulation with Enhanced Biological Stability. *Biomacromolecules* **2016**, *17* (4), 1543-1550. DOI: 10.1021/acs.biomac.6b00233.
- (106) Wu, F.; Wang, W.; Liu, L.; Ju, X.-J.; Xie, R.; Liu, Z.; Chu, L.-Y. Monodisperse hybrid microcapsules with an ultrathin shell of submicron thickness for rapid enzyme reactions. *Journal of Materials Chemistry B* **2015**, *3* (5), 796-803, 10.1039/C4TB01803F. DOI: 10.1039/C4TB01803F.
- (107) Zhang, C.; Yan, K.; Hu, C.; Zhao, Y.; Chen, Z.; Zhu, X.; Möller, M. Encapsulation of enzymes in silica nanocapsules formed by an amphiphilic precursor polymer in water. *Journal of Materials Chemistry B* **2015**, *3* (7), 1261-1267, 10.1039/C4TB01701C. DOI: 10.1039/C4TB01701C.
- (108) Zhe, X.; Ji-Wei, H.; Chao-Jie, X.; Shu-Ping, Z.; Ya-Ping, X.; Yu-Guo, Z. Enhanced catalytic stability and reusability of nitrilase encapsulated in ethyleneamine-mediated biosilica for regioselective hydrolysis of 1-cyanocycloalkaneacetonitrile. *International Journal of Biological Macromolecules* **2019**, *130*, 117-124. DOI: <https://doi.org/10.1016/j.ijbiomac.2019.02.131>.
- (109) Zhao, Z.; Fu, J.; Dhakal, S.; Johnson-Buck, A.; Liu, M.; Zhang, T.; Woodbury, N. W.; Liu, Y.; Walter, N. G.; Yan, H. Nanocaged enzymes with enhanced catalytic activity and increased stability against protease digestion. *Nature Communications* **2016**, *7* (1), 10619. DOI: 10.1038/ncomms10619.
- (110) Zhang, Y.; Wu, H.; Li, J.; Li, L.; Jiang, Y.; Jiang, Y.; Jiang, Z. Protamine-Templated Biomimetic Hybrid Capsules: Efficient and Stable Carrier for Enzyme Encapsulation. *Chemistry of Materials* **2008**, *20* (3), 1041-1048. DOI: 10.1021/cm701959e.
- (111) Horn, F.; Jackson, R. General mass action kinetics. *Archive for Rational Mechanics and Analysis* **1972**, *47* (2), 81-116. DOI: 10.1007/BF00251225.
- (112) Gassara, F.; Brar, S. K.; Verma, M.; Tyagi, R. D. Bisphenol A degradation in water by ligninolytic enzymes. *Chemosphere* **2013**, *92* (10), 1356-1360. DOI: 10.1016/j.chemosphere.2013.02.071 PubMed.
- (113) Peeples, W.; Rosen, M. K. Mechanistic dissection of increased enzymatic rate in a phase-separated compartment. *Nat Chem Biol* **2021**, *17* (6), 693-702. DOI: 10.1038/s41589-021-00801-x From NLM.
- (114) Gao, Y.; Roberts, C. C.; Toop, A.; Chang, C. E.; Wheeldon, I. Mechanisms of Enhanced Catalysis in Enzyme-DNA Nanostructures Revealed through Molecular Simulations and Experimental Analysis. *ChemBiochem* **2016**, *17* (15), 1430-1436. DOI: 10.1002/cbic.201600224 From NLM.

- (115) Yoshimoto, M.; Sato, M.; Yoshimoto, N.; Nakao, K. Liposomal Encapsulation of Yeast Alcohol Dehydrogenase with Cofactor for Stabilization of the Enzyme Structure and Activity. *Biotechnology Progress* **2008**, *24* (3), 576-582. DOI: <https://doi.org/10.1021/bp070392e>.
- (116) Dinu, M. V.; Dinu, I. A.; Saxer, S. S.; Meier, W.; Pielles, U.; Bruns, N. Stabilizing Enzymes within Polymersomes by Coencapsulation of Trehalose. *Biomacromolecules* **2021**, *22* (1), 134-145. DOI: 10.1021/acs.biomac.0c00824.
- (117) Liu, Y.; Du, J.; Yan, M.; Lau, M. Y.; Hu, J.; Han, H.; Yang, O. O.; Liang, S.; Wei, W.; Wang, H.; et al. Biomimetic enzyme nanocomplexes and their use as antidotes and preventive measures for alcohol intoxication. *Nature Nanotechnology* **2013**, *8* (3), 187-192. DOI: 10.1038/nnano.2012.264.
- (118) Nguyen, V.-T.; Kwon, Y. S.; Gu, M. B. Aptamer-based environmental biosensors for small molecule contaminants. *Current Opinion in Biotechnology* **2017**, *45*, 15-23. DOI: <https://doi.org/10.1016/j.copbio.2016.11.020>.
- (119) Golmohammadi, R.; Valegård, K.; Fridborg, K.; Liljas, L. The Refined Structure of Bacteriophage MS2 at 2.8 Å Resolution. *Journal of Molecular Biology* **1993**, *234* (3), 620-639. DOI: <https://doi.org/10.1006/jmbi.1993.1616>.
- (120) Wu, M.; Brown, W. L.; Stockley, P. G. Cell-Specific Delivery of Bacteriophage-Encapsulated Ricin A Chain. *Bioconjugate Chemistry* **1995**, *6* (5), 587-595. DOI: 10.1021/bc00035a013.
- (121) Ashley, C. E.; Carnes, E. C.; Phillips, G. K.; Durfee, P. N.; Buley, M. D.; Lino, C. A.; Padilla, D. P.; Phillips, B.; Carter, M. B.; Willman, C. L.; et al. Cell-Specific Delivery of Diverse Cargos by Bacteriophage MS2 Virus-like Particles. *ACS Nano* **2011**, *5* (7), 5729-5745. DOI: 10.1021/nn201397z.
- (122) Cargile, B. J.; McLuckey, S. A.; Stephenson, J. L. Identification of Bacteriophage MS2 Coat Protein from *E. coli* Lysates via Ion Trap Collisional Activation of Intact Protein Ions. *Analytical Chemistry* **2001**, *73* (6), 1277-1285. DOI: 10.1021/ac000725l.
- (123) Hooker, J. M.; Kovacs, E. W.; Francis, M. B. Interior Surface Modification of Bacteriophage MS2. *Journal of the American Chemical Society* **2004**, *126* (12), 3718-3719. DOI: 10.1021/ja031790q.
- (124) Kovacs, E. W.; Hooker, J. M.; Romanini, D. W.; Holder, P. G.; Berry, K. E.; Francis, M. B. Dual-Surface-Modified Bacteriophage MS2 as an Ideal Scaffold for a Viral Capsid-Based Drug Delivery System. *Bioconjugate Chemistry* **2007**, *18* (4), 1140-1147. DOI: 10.1021/bc070006e.
- (125) Sun, S.; Li, W.; Sun, Y.; Pan, Y.; Li, J. A new RNA vaccine platform based on MS2 virus-like particles produced in *Saccharomyces cerevisiae*. *Biochem Biophys Res Commun* **2011**, *407* (1), 124-128. DOI: 10.1016/j.bbrc.2011.02.122 From NLM.
- (126) Li, J.; Sun, Y.; Jia, T.; Zhang, R.; Zhang, K.; Wang, L. Messenger RNA vaccine based on recombinant MS2 virus-like particles against prostate cancer. *Int J Cancer* **2014**, *134* (7), 1683-1694. DOI: 10.1002/ijc.28482 PubMed.
- (127) Kökpınar, Ö.; Walter, J.-G.; Shoham, Y.; Stahl, F.; Scheper, T. Aptamer-based downstream processing of his-tagged proteins utilizing magnetic beads. *Biotechnology and Bioengineering* **2011**, *108* (10), 2371-2379. DOI: <https://doi.org/10.1002/bit.23191>.
- (128) Zhang, Y.; Tsitkov, S.; Hess, H. Complex dynamics in a two-enzyme reaction network with substrate competition. *Nature Catalysis* **2018**, *1* (4), 276-281. DOI: 10.1038/s41929-018-0053-1.
- (129) Höbartner, C.; Mittendorfer, H.; Breuker, K.; Micura, R. Triggering of RNA Secondary Structures by a Functionalized Nucleobase. *Angewandte Chemie International Edition* **2004**, *43* (30), 3922-3925. DOI: <https://doi.org/10.1002/anie.200460068>.

- (130) Govan, J. M.; Young, D. D.; Lusic, H.; Liu, Q.; Lively, M. O.; Deiters, A. Optochemical control of RNA interference in mammalian cells. *Nucleic Acids Res* **2013**, *41* (22), 10518-10528. DOI: 10.1093/nar/gkt806 From NLM.
- (131) Matsushita-Ishiodori, Y.; Ohtsuki, T. Photoinduced RNA Interference. *Accounts of Chemical Research* **2012**, *45* (7), 1039-1047. DOI: 10.1021/ar200227n.
- (132) Ikeda, M.; Kamimura, M.; Hayakawa, Y.; Shibata, A.; Kitade, Y. Reduction-Responsive Guanine Incorporated into G-Quadruplex-Forming DNA. *Chembiochem* **2016**, *17* (14), 1304-1307. DOI: 10.1002/cbic.201600164 From NLM.
- (133) Seeman, N. C.; Sleiman, H. F. DNA nanotechnology. *Nature Reviews Materials* **2017**, *3* (1), 17068. DOI: 10.1038/natrevmats.2017.68.
- (134) Guo, P. The emerging field of RNA nanotechnology. *Nature Nanotechnology* **2010**, *5* (12), 833-842. DOI: 10.1038/nnano.2010.231.
- (135) Wu, C.; Wan, S.; Hou, W.; Zhang, L.; Xu, J.; Cui, C.; Wang, Y.; Hu, J.; Tan, W. A survey of advancements in nucleic acid-based logic gates and computing for applications in biotechnology and biomedicine. *Chemical Communications* **2015**, *51* (18), 3723-3734, 10.1039/C4CC10047F. DOI: 10.1039/C4CC10047F.
- (136) Filonov, G. S.; Moon, J. D.; Svensen, N.; Jaffrey, S. R. Broccoli: Rapid Selection of an RNA Mimic of Green Fluorescent Protein by Fluorescence-Based Selection and Directed Evolution. *Journal of the American Chemical Society* **2014**, *136* (46), 16299-16308. DOI: 10.1021/ja508478x.
- (137) Santoro, S. W.; Joyce, G. F. A general purpose RNA-cleaving DNA enzyme. *Proceedings of the National Academy of Sciences* **1997**, *94* (9), 4262-4266. DOI: doi:10.1073/pnas.94.9.4262.
- (138) Morse, D. P.; Bass, B. L. Detection of inosine in messenger RNA by inosine-specific cleavage. *Biochemistry* **1997**, *36* (28), 8429-8434. DOI: 10.1021/bi9709607 From NLM.
- (139) Cattenez, P. B.; Taft, R. J.; Westhof, E.; Mattick, J. S. Transcriptome-wide identification of A > I RNA editing sites by inosine specific cleavage. *Rna* **2013**, *19* (2), 257-270. DOI: 10.1261/rna.036202.112 From NLM.
- (140) Miller, H. I.; Riggs, A. D.; Gill, G. N. Ribonuclease H (hybrid) in Escherichia coli. Identification and characterization. *J Biol Chem* **1973**, *248* (7), 2621-2624. From NLM.
- (141) Itaya, M.; Kondo, K. Molecular cloning of a ribonuclease H (RNase HI) gene from an extreme thermophile Thermus thermophilus HB8: a thermostable RNase H can functionally replace the Escherichia coli enzyme in vivo. *Nucleic Acids Res* **1991**, *19* (16), 4443-4449. DOI: 10.1093/nar/19.16.4443 From NLM.
- (142) Findly, D.; Herries, D. G.; Mathias, A. P.; Rabin, B. R.; Ross, C. A. The Active Site and Mechanism of Action of Bovine Pancreatic Ribonuclease. *Nature* **1961**, *190* (4778), 781-784. DOI: 10.1038/190781a0.
- (143) Fujimoto, M.; Kuninaka, A.; Yoshino, H. Substrate Specificity of Nuclease P1. *Agricultural and Biological Chemistry* **1974**, *38* (9), 1555-1561. DOI: 10.1080/00021369.1974.10861384 (accessed 8/15/2022).
- (144) Vanecko, S.; Laskowski, M., Sr. Studies of the specificity of deoxyribonuclease I. II. Hydrolysis of oligonucleotides carrying a monoesterified phosphate on carbon 3'. *J Biol Chem* **1961**, *236*, 1135-1140. From NLM.
- (145) Deutscher, M. P.; Marlor, C. W.; Zaniewski, R. Ribonuclease T: new exoribonuclease possibly involved in end-turnover of tRNA. *Proc Natl Acad Sci U S A* **1984**, *81* (14), 4290-4293. DOI: 10.1073/pnas.81.14.4290 From NLM.

- (146) Viswanathan, M.; Lanjuin, A.; Lovett, S. T. Identification of RNase T as a high-copy suppressor of the UV sensitivity associated with single-strand DNA exonuclease deficiency in *Escherichia coli*. *Genetics* **1999**, *151* (3), 929-934. DOI: 10.1093/genetics/151.3.929 From NLM.
- (147) Williams, E. J.; Sung, S. C.; Laskowski, M., Sr. Action of venom phosphodiesterase on deoxyribonucleic acid. *J Biol Chem* **1961**, *236*, 1130-1134. From NLM.
- (148) Jinek, M.; Chylinski, K.; Fonfara, I.; Hauer, M.; Doudna, J. A.; Charpentier, E. A Programmable Dual-RNA-Guided DNA Endonuclease in Adaptive Bacterial Immunity. *Science* **2012**, *337* (6096), 816-821. DOI: doi:10.1126/science.1225829.
- (149) Cong, L.; Ran, F. A.; Cox, D.; Lin, S.; Barretto, R.; Habib, N.; Hsu, P. D.; Wu, X.; Jiang, W.; Marraffini, L. A.; et al. Multiplex genome engineering using CRISPR/Cas systems. *Science* **2013**, *339* (6121), 819-823. DOI: 10.1126/science.1231143 From NLM.
- (150) Jost, M.; Santos, D. A.; Saunders, R. A.; Horlbeck, M. A.; Hawkins, J. S.; Scaria, S. M.; Norman, T. M.; Hussmann, J. A.; Liem, C. R.; Gross, C. A.; et al. Titrating gene expression using libraries of systematically attenuated CRISPR guide RNAs. *Nature Biotechnology* **2020**, *38* (3), 355-364. DOI: 10.1038/s41587-019-0387-5.
- (151) Yu, X.; Martin, P. G. P.; Michaels, S. D. BORDER proteins protect expression of neighboring genes by promoting 3' Pol II pausing in plants. *Nature Communications* **2019**, *10* (1), 4359. DOI: 10.1038/s41467-019-12328-w.
- (152) Castanotto, D.; Lin, M.; Kowolik, C.; Wang, L.; Ren, X. Q.; Soifer, H. S.; Koch, T.; Hansen, B. R.; Oerum, H.; Armstrong, B.; et al. A cytoplasmic pathway for gapmer antisense oligonucleotide-mediated gene silencing in mammalian cells. *Nucleic Acids Res* **2015**, *43* (19), 9350-9361. DOI: 10.1093/nar/gkv964 From NLM.
- (153) Liang, X. H.; Sun, H.; Nichols, J. G.; Crooke, S. T. RNase H1-Dependent Antisense Oligonucleotides Are Robustly Active in Directing RNA Cleavage in Both the Cytoplasm and the Nucleus. *Mol Ther* **2017**, *25* (9), 2075-2092. DOI: 10.1016/j.ymthe.2017.06.002 From NLM.
- (154) Lim, K. R. Q.; Maruyama, R.; Echigoya, Y.; Nguyen, Q.; Zhang, A.; Khawaja, H.; Sen Chandra, S.; Jones, T.; Jones, P.; Chen, Y. W.; et al. Inhibition of DUX4 expression with antisense LNA gapmers as a therapy for facioscapulohumeral muscular dystrophy. *Proc Natl Acad Sci U S A* **2020**, *117* (28), 16509-16515. DOI: 10.1073/pnas.1909649117 From NLM.
- (155) Petersen, M.; Wengel, J. LNA: a versatile tool for therapeutics and genomics. *Trends Biotechnol* **2003**, *21* (2), 74-81. DOI: 10.1016/s0167-7799(02)00038-0 From NLM.
- (156) Stein, C. A.; Hansen, J. B.; Lai, J.; Wu, S.; Voskresenskiy, A.; Høg, A.; Worm, J.; Hedtjörn, M.; Souleimanian, N.; Miller, P.; et al. Efficient gene silencing by delivery of locked nucleic acid antisense oligonucleotides, unassisted by transfection reagents. *Nucleic Acids Res* **2010**, *38* (1), e3. DOI: 10.1093/nar/gkp841 From NLM.
- (157) Tominaga, H.; Ishiyama, M.; Ohseto, F.; Sasamoto, K.; Hamamoto, T.; Suzuki, K.; Watanabe, M. A water-soluble tetrazolium salt useful for colorimetric cell viability assay. *Analytical Communications* **1999**, *36* (2), 47-50, 10.1039/A809656B. DOI: 10.1039/A809656B.
- (158) Zhang, S.; Chaput, J. C. Synthesis of Threose Nucleic Acid (TNA) Phosphoramidite Monomers and Oligonucleotide Polymers. *Current Protocols in Nucleic Acid Chemistry* **2012**, *50* (1), 4.51.51-54.51.26. DOI: <https://doi.org/10.1002/0471142700.nc0451s50>.
- (159) Manuel, B. A.; Karloff, D. B. Recruit and retain a diverse workforce. *Nature Reviews Chemistry* **2020**, *4* (9), 435-437. DOI: 10.1038/s41570-020-0214-z.



- (160) Schmidt-Dannert, C.; Arnold, F. H. Directed evolution of industrial enzymes. *Trends in Biotechnology* **1999**, *17* (4), 135-136. DOI: 10.1016/S0167-7799(98)01283-9 (accessed 2022/07/31).
- (161) Kenneth Gibbs, J. Diversity in STEM: what it is and why it matters. *Scientific American*. 2014; Vol. 2022.
- (162) AlShebli, B. K.; Rahwan, T.; Woon, W. L. The preeminence of ethnic diversity in scientific collaboration. *Nature Communications* **2018**, *9* (1), 5163. DOI: 10.1038/s41467-018-07634-8.
- (163) Hong, L.; Page, S. E. Groups of diverse problem solvers can outperform groups of high-ability problem solvers. *Proceedings of the National Academy of Sciences* **2004**, *101* (46), 16385-16389. DOI: doi:10.1073/pnas.0403723101.
- (164) Henry, M. A.; Shorter, S.; Charkoudian, L.; Heemstra, J. M.; Corwin, L. A. FAIL Is Not a Four-Letter Word: A Theoretical Framework for Exploring Undergraduate Students' Approaches to Academic Challenge and Responses to Failure in STEM Learning Environments. *CBE—Life Sciences Education* **2019**, *18* (1), ar11. DOI: 10.1187/cbe.18-06-0108.
- (165) Xu, Y. J. Attrition of Women in STEM: Examining Job/Major Congruence in the Career Choices of College Graduates. *Journal of Career Development* **2017**, *44* (1), 3-19. DOI: 10.1177/0894845316633787.
- (166) Toldson, I. A. Why Historically Black Colleges and Universities are Successful with Graduating Black Baccalaureate Students Who Subsequently Earn Doctorates in STEM (Editor's Commentary). *Journal of Negro Education* **2018**, *87* (2), 95-98.
- (167) Hofstra, B.; Kulkarni, V. V.; Munoz-Najar Galvez, S.; He, B.; Jurafsky, D.; McFarland, D. A. The Diversity&#x2013;Innovation Paradox in Science. *Proceedings of the National Academy of Sciences* **2020**, *117* (17), 9284-9291. DOI: doi:10.1073/pnas.1915378117.
- (168) Heather L. Ford, C. B., Margarita Azmitia, Karine Blaufuss, Petra Dekens. Women from some under-represented minorities are given too few talks at world's largest Earth-science conference. *Nature* **2019**, *576*, 32-35. DOI: <https://doi.org/10.1038/d41586-019-03688-w>.
- (169) Steele, C. M. *Whistling Vivaldi: How Stereotypes Affect Us and What We Can Do*; W. W. Norton & Company, 2011.